2022-07-28

Vaping Additives Affect Lateral Organization and Functionality of Lung Surfactant Model Systems

Van Bavel, Nicolas

UNIVERSITY OF CALGARY

Vaping Additives Affect Lateral Organization and Functionality of Lung Surfactant Model Systems

by

Nicolas Van Bavel

A THESIS

SUBMITTED TO THE FACULTY OF GRADUATE STUDIES

IN PARTIAL FULFILMENT OF THE REQUIREMENTS FOR THE

DEGREE OF MASTER OF SCIENCE

GRADUATE PROGRAM IN BIOLOGICAL SCIENCES

CALGARY, ALBERTA

JULY, 2022

Abstract

Recent use of THC-based vapes has led to an outbreak of respiratory health issues. While the pathology is unresolved, common symptoms point to dysfunction of the lung surfactant (LS). This is a lipid-protein monofilm situated at the air-water interface in alveolar sacs, which acts to lower surface tension, preventing lung collapse during respiration. Inhaled substances that reach the alveoli will encounter LS. Certain vape additives have been identified as potential causative agents, these being tetrahydrocannabinol and cannabidiol, commonly found in THC products, as well as vitamin E and its derivative vitamin E acetate. The lipophilic nature of these additives may allow them to partition into the monofilm, wherein they could interact with lipids to disrupt proper function.

The aim of this thesis was to use model surfactants to better understand the interactions between vaping additives and the primary lipid components of lung surfactant. These films were made up of phosphatidylcholines, phosphatidylglycerols, and cholesterol. Additionally, the clinical surfactant BLES was also used and compared to the model systems. BLES is used in surfactant replacement therapy, making it a good physiological counterpart to the simple model films studied. Surface activity of the films were measured using a Langmuir-Blodgett trough which allowed for compression and expansion of the films, mimicking respiration. Changes to the lateral organization of the films was conducted with Brewster angle microscopy. Visualization of BLES was also carried out with atomic force microscopy, which allowed for higher resolution images of the surfactant's molecular architecture. Vape additives were found to destabilize domain formations in most systems, often accompanied by fluidization of the film. The effects on BLES provided a unique insight into the mechanistic action of additive induced surfactant dysfunction. Crucial multilayer structures that form on the surface of the film during

compression were abolished in the presence of vitamin E acetate, reducing the surfactants ability to maintain a low surface tension. The Langmuir-Blodgett trough has demonstrated to be useful for studying *in vitro* interactions between lipids and vape additives. With further optimization, this method may be used to predict *in vivo* effects of vape additives.

Acknowledgements

Massive thank you to my supervisor Dr. Prenner for letting me pursue my passion in science by being a part of his lab. I'm very grateful for all the support and wisdom he has provided over the last two years and could not have achieved this without his contributions. I would also like to thank my parents Wes and Theresa Van Bavel for always supporting me and pushing me to pursue my goals. Another special thanks to my sister Marisa Van Bavel who has taken this journey before and helped me through my years as a graduate student. To all my friends and colleagues I have met, thank you for the fun times during this journey. Namely may great lab mates, Colin Unruh, Kevin Sule, Anna-Marie Lewrenz, and Patrick Lai. Thanks to my committee members and collaborates for all their guidance. Dr. Anikovskiy for allowing me to participate in many fun nanoscience projects and offering me a NANS TAship.. Dr. Loebenberg for his expertise throughout my project and assistance in a publication. Dr. Amrein for the BLES samples and access to AFM, as well as his great insights.

Table of Contents

List of Tables

List of Figures

List of Symbols, Abbreviations and Nomenclature

Vitamin E (Vit-E)

Vitamin E Acetate (Vit-EAc)

Tetrahydrocannabinol (THC)

Cannabidiol (CBD)

Centers for Disease and Control Prevention (CDC)

E-cigarette, or vaping, product use-associated lung injury (EVALI)

Lung Surfactant (LS)

Bovine lung extract surfactant (BLES)

Bronchoalveolar lavage (BAL)

α -tocopherol transport protein (α-TTP)

Phosphatidylcholines (PC)

Phosphatidylglycerols (PG)

Dipalmitoylphosphatidyl choline (DPPC)

Palmitoyloleoylphosphatidyl choline (POPC)

Palmitoyloleoylphosphatidyl glycerol(POPG)

Dipalmitoylphosphatidyl glycerol (DPPG)

Dimyristoylphosphatidyl choline (DMPC

Surfactant proteins (SP)

Liquid-expanded (LE)

Liquid-condensed (LC)

Liquid-ordered (Lo)

Hexagonal phase (H_{II})

Compressibility Modulus (Cm)

Brewster Angle Microscopy (BAM)

Langmuir-Blodgett (LB)

Atomic Force Microscopy (AFM)

1,6-Diphenyl-1,3,5-hexatriene (DPH)

Generalized Polarization (GP)

Chapter 1: Introduction

1.1 Overview

Vitamin E (Vit-E) is a biologically prevalent and essential molecule to humans, with an average blood plasma concentration of 28 uM and tissue concentrations ranging between 2 to 150 ug/g of tissue (4 to 350 nM/g of tissue) [1–3]. While it takes roles in a facet of cellular processes, ranging from protein interaction to genetic regulation, its most well understood, and arguably most important functionality, is the stabilization and protection of cell membranes [4–6].

The amphipathic nature of Vit-E (Figure 1) localizes it into the hydrophobic region in the lipid bilayer of cell membranes and subcellular organelles [7]. Within, Vit-E is active in stabilizing the membrane by forming complexes with components that have a tendency to destabilize the membrane, such as free fatty acids [7]. In addition to structural roles, Vit-E is also necessary as an antioxidant for protection against lipid peroxyl radicals.

This crucial vitamin's sudden appearance in e-cigarettes, or vapes, now poses unexpected health concerns. Users of vape products containing Vit-E, as well as a derivative in the form of Vit-E acetate and certain cannabinoids, have been afflicted with e-cigarette, or vaping, product use-associated lung injury (EVALI), a new class of lung illnesses characterized by acute damage to the alveoli. While the mechanism by which Vit-E inflicts EVALI is currently unknown, one plausible route is by means of disrupting the structure and function of lung surfactant (LS).

LS is a lipid-protein monolayer, present at the air-water interface in alveoli, and is responsible for maintaining stability of the alveolar sacs against collapse. The lipophilic nature of Vit-E that allows it to insert into cellular membranes may also result in partitioning into the LS, wherein, its presence can disrupt the lipid monolayer by altering packing surrounding lipids, thereby impeding functionality and potentially leading to lung collapse.

1.2 Nomenclature and structure:

The name Vit-E is an umbrella term for a class of 8 lipid soluble molecules consisting of a chromanol ring and isoprenoid tail. These molecules are subdivided into tocopherols tocotrienols, with the former exhibiting a fully saturated isoprenoid tail and the latter containing double bonds at the 3' 7' and 11' positions (Figure 1). Each group consists of an alpha (α), beta (β), gamma (γ), and delta (δ) form, based on the methylation of the chromanol ring (figure 1). These structural variations make Vit-E unique amongst vitamins, in that it does not have a single chemical structure. Despite this, Vit-E is most commonly used to refer to α-tocopherol, as this form is most prevalent in humans and exhibits the highest biological activity [7–9]. In blood plasma it accounts for ~85% of tocopherols however in Vit-E rich tissue such as the heart or liver, it may compose upwards of 97% of all tocopherols [7,10,11]. In fact, the National Institute of Health specifies that alpha tocopherol is the only Vit-E supplement required by humans to fulfill their Vit-E intake [12].

As would be expected, the structure of tocopherols is closely linked to their functional roles in biological systems. While all forms are able to insert into the membrane, due to their hydrophobic isoprenoid tail, certain forms are more adept in their primary role as an antioxidant. The α form dominates in this area, as it has been demonstrated to most readily donate its hydroxyl hydrogen to lipid radicals [13]. This enhancement of antioxidant function is due to the presence of methyl groups at the R_1 and R_2 positions, which aid in stability of the tocopheroxyl radical [4].

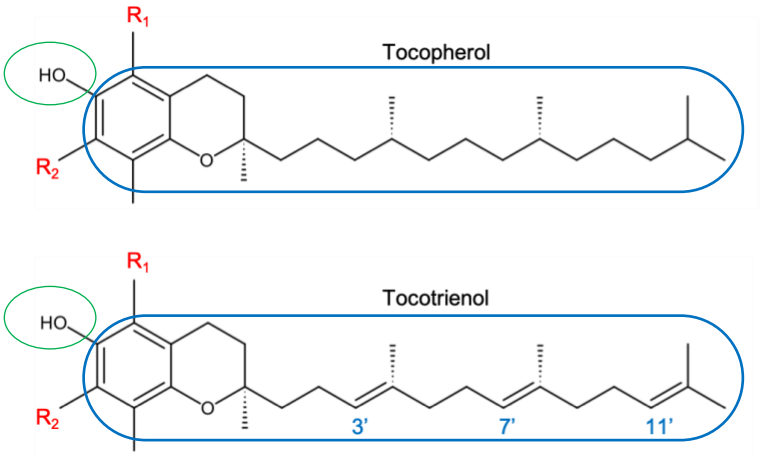

Position on chromanol ring	R_1	R_2
Alpha	CH_3	CH_3
Beta	CH_3	H
Gamma	H	CH_3
Delta	H	H

Figure 1. Chemical structure of vitamin E with hydrophilic (green) and hydrophobic (blue) regions denoted.

α-tocopherol also differs from the other forms in that it is solely recognized and distributed throughout the body by α-tocopherol transport protein (α-TTP) [14]. The functions and essential nature of α-tocopherol will be expanded upon in the next section.

1.3 Biological Importance

The importance of Vit-E was discovered nearly 100 years ago, when rats fed a diet of all the known vitamins failed to reproduce [15]. As Vit-E had not yet been discovered it was missing from the diet. Since then, many roles of Vit-E have been deduced by examining the symptoms of Vit-E deficiency. These range from regulation of cell proliferation, modulation of immune response, genetic regulation, participation in the electron transport chain, and most notably, as an antioxidant [4–6]. Vit-E deficiency in humans is linked to a rare genetic disorder whereby a mutation in the gene for α-TTP results in a non-functional product [16]. As the name suggests, α-TTP only recognizes α-tocopherol, and is responsible for isolating it from the other tocopherol forms absorbed by the liver. α-tocopherol is then incorporated into very low density lipoproteins which are released by the liver and distributed throughout the body [17]. Therefore, while an individual may still uptake the necessary amount of α-tocopherol from their diet, they will not be able to

transport it to the tissues in need. The term for this condition is ataxia with Vit-E deficiency, and is most notably characterized by neurodegeneration [18]. α-tocopherol is one of the predominant antioxidants in cell membranes, and its absence can quickly lead to high levels of lipid peroxyl radicals, whose propagation will disrupt membranes and induce cell death [19]. An interested reader may see the reviews by Wang & Quinn (1999), Azzi & Stocker (2000), and Traber & Atkinson (2007), if they wish to know more about the various functions of Vit-E [4,11,19]. Vit-E's presence and influence on the properties of cell membranes will be the focus of the next section, as this will be most relevant to how it may interact with LS.

1.4 Biophysical effects in membranes

Within cells, Vit-E is localized to the plasma membrane as well as the membranes of the mitochondria and other organelles [20,21]. As mentioned previously, this vitamin plays a crucial role as an antioxidant, preventing the propagation of lipid peroxidation. This is especially relevant in the mitochondria, as reactive oxygen species are readily formed during the process of cellular respiration [22]. The resulting tocopheroxyl radical is stabilized by electron delocalization in its chromanol ring and may be converted back to α-tocopherol through a redox cycle involving coenzyme Q as well as a hydrogen donor such as vitamin C (Figure 2) [11,23]. The powerful antioxidant ability of Vit-E, and its eventual recycling, allows for membranes to require as little as 1 molecule of Vit-E per 2000 of other lipids in order to prevent any disruption from free radical species [24]. In the membranes of organelles that are prone to oxygen radical exposure, the amount of Vit-E may be more. This is seen in mitochondria and lysosomes where the molar ratio of Vit-E to lipid is 1:935 and 1:68 respectively [24].This small amount of Vit-E also has other effects on cell membranes by altering the packing capabilities of surrounding lipids. α-tocopherol has been

reported to alter membrane microviscosity by rigidifying the membrane and decreasing mobility of neighbouring lipids [25].

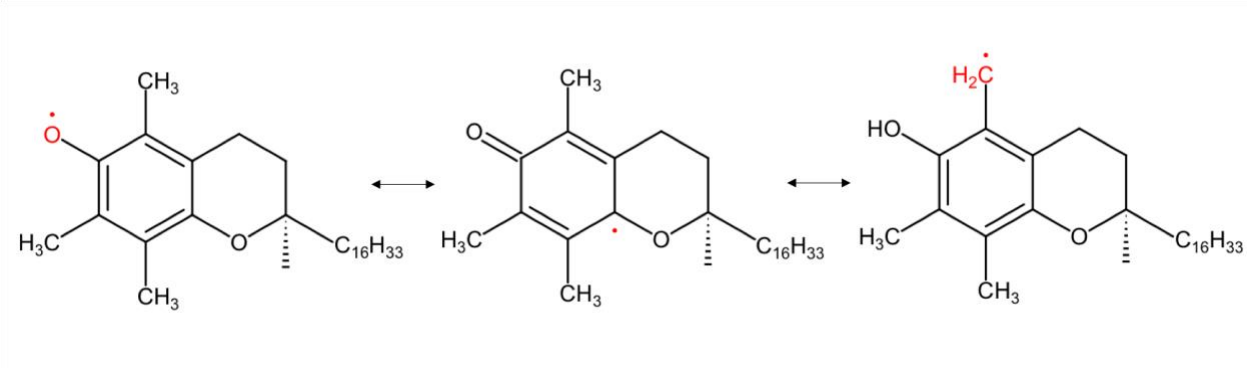

Figure 2. Resonance forms of the tocopheroxyl radical.

Its mode of interaction is similar to that of cholesterol, in that the rigid rings of these molecules interact with and reduces the mobility of lipid acyl chains [26]. Additionally, due to a similar membrane location, Vit-E may compete with cholesterol [33,57] or outcompete the sterol in some cases. However, α-tocopherols relatively low molar ratio to fatty acids (1:1000) and the larger presence of competing cholesterol suggests that it would affect only a small number of local lipids (7). From this information, it may also be assumed that α-tocopherol will display localized interaction with lipids of the LS, but may not have a significant effect on the film as a whole if deposited in relatively low concentrations. In plasma membranes, Interaction between polyunsaturated fatty acids and α-tocopherol is known and serves great biological importance [27]. In lipid systems containing high amounts of free fatty acids, α-tocopherol was able to inhibit the disordering effects of the fatty acids on phospholipid bilayers, by forming complexes through head group and acyl chain interactions [27]. In this way, Vit-E was demonstrated to protect the membrane against the hydrolytic products of phospholipase A, which possess detergent-like properties capable of disrupting lipid bilayers [7,25].

Nevertheless, other studies have demonstrated that bilayers composed of phospholipids are also influenced by the presence of Vit-E. The acyl chain packing of liposomes composed of dimyristoylphosphatidylcholine (DMPC) (Figure 3), were affected by α-tocopherol as well as α-tocopheryl acetate at concentrations as low as 5 mol% [25]. Differential scanning calorimetry of the gel to liquid crystalline transition demonstrated that 15 mol% α-tocopherol resulted in a broadening of the phase transition temperature range by 3 ºC and lowered both the transition temperature (Tm) and enthalpy by 1.2 ºC and 3.6 kcal/mol respectively. These measurements are consistent with the idea that α-tocopherol partitions into the gel-state and subsequently reduces tight packing of the lipids. The experiment was repeated with differing head groups (phosphatidylserine, phosphatidylglycerol, and phosphatidylethanolamine) which contain differing overall charges (Figure 3). Very similar changes in enthalpy and Tm were obtained for all head groups, suggesting that headgroup interactions between the phospholipids and tocopherols play an insignificant role, more likely the interaction occurs between the hydroxyl group of α-tocopherol and the phosphate oxygens of the phospholipid.

In membranes composed of the key phosphatidylcholines (dipalmitoylphosphatidyl choline; DPPC, and Palmitoyloleoylphosphatidyl choline; POPC), similar to that in LS, α-tocopherol was found to decrease lipid packing in the gel state and increase it in the liquid-crystalline state [28].

Two common fluorescence methods can be used to determine lipid packing. Those being 1,6-Diphenyl-1,3,5-hexatriene (DPH)-anisotropy, and Laurdan generalized polarization (GP) (Figure 4), which were used to elucidate the effects by α-tocopherol, and α-tocopheryl acetate, on membrane fluidity and changes in acyl chain order [28]. DPH is a fluorescent probe that partitions into the hydrophobic core of the lipid bilayer, and it is used to provide information about acyl chain

ordering. Likewise, the fluorescent probe Laurdan is also incorporated into the membrane and is used to determine membrane fluidity near the glycerol-phosphate backbone.

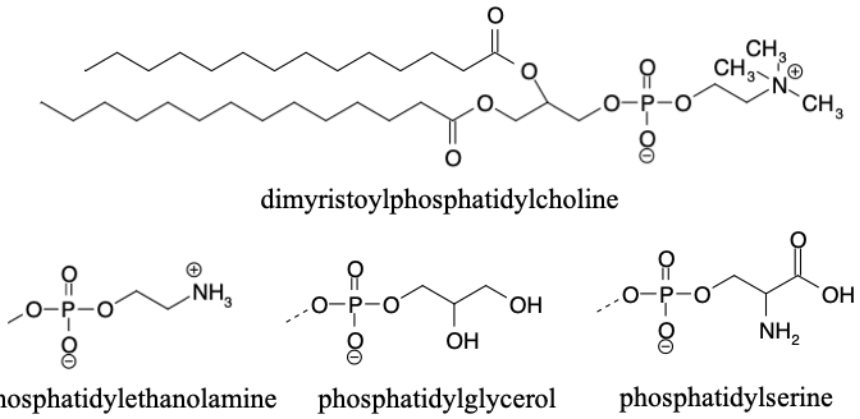

Figure 3. Structure of DMPC and the alternate headgroups PE, PG, and PS.

An increase in acyl chain order was observed for the DPPC/POPC liposome in the liquid-crystalline state, as indicated by an increase in florescence polarization values of DPH [28]. Additionally, in the gel phase, the fluorescence polarization value of DPH decreased, indicating that α-tocopherol decreases acyl chain order. Laurdan GP measurements also showed that α-tocopherol decreases the phase Tm of DPPC by ~2 ºC and broadens the transition range, very similar to the DMPC system. Interestingly, unlike α-tocopherol, the derivative α-tocopheryl acetate, had no effect on the phase transition from gel to liquid-crystalline in DPPC bilayers. One explanation is the reduced polarity of α-tocopheryl acetate, due to the additional methyl group, which localizes it to small aggregates in the hydrophobic core of the membrane, where it has little influence on lipid phase transitions [28]. These changes in chain ordering resemble the effect as cholesterol, which is unsurprising given their similar chemical structures (Figure 5). Both α tocopherol and cholesterol contain a large hydrophobic portion in the form of a rigid ring structure and single acyl chain, which allows for incorporation into the hydrophobic portion of the membrane and subsequently reduces the free motion of lipid molecules in the liquid-crystalline

phase [29]. Vit-E showed a stronger impact on DPPC membrane phase behavior than cholesterol whereby 2% exceeded the effect of 10% sterol [59].

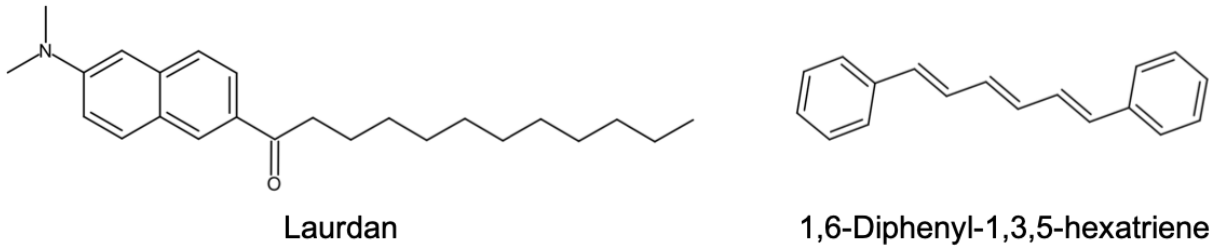

Figure 4: Chemical structures of Laurdan and DPH.

Cholesterol and α-tocopherol also influence structural features of lipid membranes by inducing local curvature [30,31]. This has been measured for DOPE membranes, where the addition of cholesterol relieved chain packing, and induced a transition to the inverse hexagonal phase (H_{II}) [30]. This phase is characterized by lipids forming tubes, whereby the polar regions are oriented towards the inside of the tube, while the tails point outside (Figure 6). These tubes are arranged in a hexagonal lattice, as the name suggests. Addition of cholesterol to DOPE decreased the H_{II} lattice spacing (see figure 6) in a concentration dependent manner, from 68 Å with 0 mol% cholesterol, to 63 Å at 30 mol% cholesterol [30]. This implies an increase in curvature of the lipid layer, a phenomenon necessary for modulating the activity of membrane-dependent enzymes and channel gating [32–34]. It has been reported that activity of Ca-ATPase in liposomes increased upon addition of cholesterol do to a direct interaction with PE that promoted a bilayer to hexagonal transition, decreasing membrane hydration and stability [35]. Likewise, α-tocopherol has been reported to induce negative curvature in DOPE monolayers, and also induce a transition to H_{II} [31]. The effects of α-tocopherol on the structure of the monolayer has been studied using X-ray diffraction. Based on previous research that illustrates α-tocopherol alters activity of membrane-

dependent enzymes by means other than direct binding [36–39], it was suggested that the vitamin must alter the lipid packing and local curvature in the membrane, that would directly influence enzymatic activity [31].

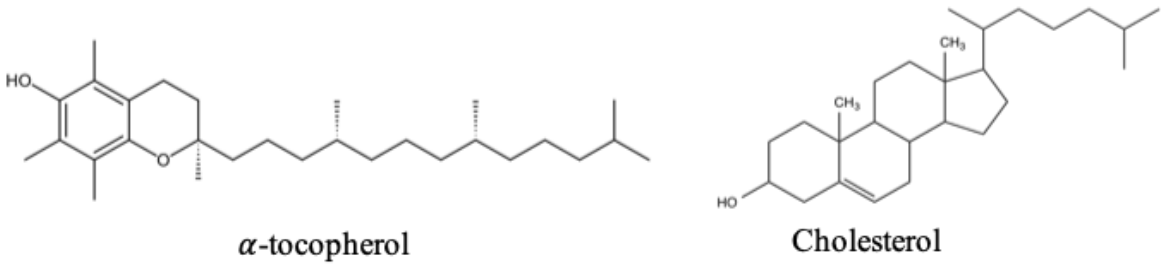

Figure 5. Chemical structures of α-tocopherol and cholesterol.

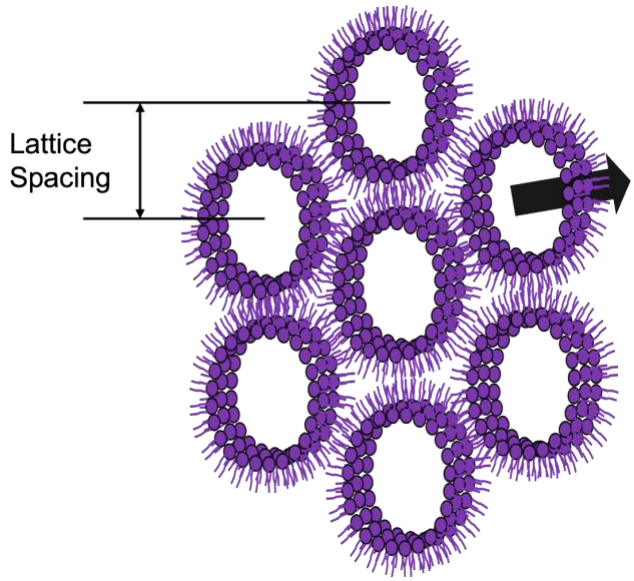

Figure 6. Schematic of the hexagonal phase (H_{II}).

Like for cholesterol, an increasing concentration of α-tocopherol in the DOPE monolayer reduces lattice spacing and increases curvature, however, to a greater extent. At 30 mol% α-tocopherol, the lattice spacing is reduced by 12 Å, as opposed to the decrease of 5 Å seen with 30 mol% cholesterol [31]. This significant change is the result of a smaller intrinsic radii of curvature, which is 13.7 Å for α-tocopherol and 22.8 Å for cholesterol. This means that the geometric shape of α-tocopherol allows for a negative curvature to spontaneously form in the membrane [30,31].

These results present interesting connotations in the context of LS. The changes to lipid packing and phase transitions discussed above may suggest that the physical properties of the LS will be similarly altered upon introduction of α-tocopherol. While these interactions are often necessary in cell membranes, and even offer beneficial stabilizing effects to the lipid structures, they may be detrimental for the structure and function of LS. Proper functionality is reliant on a well-defined lipid composition and packing behaviours. Packing defects in more heterogeous lipid mixtures will affect interactions with proteins [53] and induce changes of surface charge density and surface potentials. The increase in membrane curvature may also affect surfactant protein-lipid complexes and distrupt the protein assisted film folding during exhalation.

Alterations to this process by the presence of α-tocopherol may impede functionality, destabilizing the monolayer and triggering collapse of the film.

1.5 Appearance of Vitamin E in vaping

The use of electronic cigarettes, or vapes, has grown considerably in the recent decade, especially among adolescents, with one Canadian survey from 2018-19 reporting that 34% of students in grades 7-12 have tried vaping [39]. These devices heat an "e-liquid" solution comprised primarily of propylene glycol or vegetable glycerin, with the addition of flavorings and sometimes nicotine [40,41]. The growing popularity of vapes has produced many types of vape products, whereby some pose significant health risks. The presence of Vit-E and Vit-E acetate in THC products first came about in illicit markets for their cost effective use as thickening agents and to dilute the THC oil. In 2018 no products had Vit-E acetate, then an investigation in 2019 found that almost all of them did. Around the same time, there was a surge in cases of individuals suffering lung illnesses after reportedly vaping THC products. In 2019, the Centers for Disease and Control Prevention (CDC) classified these severe lung illnesses as e-cigarette, or vaping, product use-associated lung

injury (EVALI). The severity of EVALI ranges from throat irritation and coughing to pneumonia and in extreme cases death [41]. Generally, it is defined as an acute respiratory illness with damage to the alveoli [42]. The constituent chemicals causing EVALI have not been fully elucidated, however, current research has identified Vit-E acetate, THC, and CBD as potential agents [43]. Examination of bronchoalveolar-lavage fluid (fluid washed from the lungs) from patients with EVALI has provided insight into these causative agents [43]. In 48 of 51 (94%) patients inflicted with EVALI, Vit-E acetate was identified in the BAL fluid [32]. Conversely, in healthy individuals, this molecule was not present [43]. Likewise, THC was found in 94% of patients with EVALI, but was absent in healthy users [43]. This information calls attention to understanding the mechanism by which these agents adversely affect lungs, with hopes that future vape products will be manufactured in a safer manner.

1.6 Introduction to Lung Surfactant

One area of interest that warrants investigation in the context of EVALI is the LS present in alveolar sacs (Figure 7). An inhaled substance, travels through the trachea, large and small bronchioles, and may finally arrive at the alveoli, where gas exchange occurs. The interior of each alveolus is lined by an epithelial layer containing type I and type II pneumocytes, at the surface of this is a thin aqueous layer which is covered by a monomolecular film known as the lung surfactant (LS) [44]. The aqueous layer serves as a medium for the adsorption/desorption of material with the LS, such as lamellar bodies excreted by type II pneumocytes, whose adsorption onto the air-water interface forms the LS [45,46]. The LS itself is a lipid-protein monolayer, which is crucial for proper gas exchange and acts to prevent alveolar collapse by reducing the surface tension to near zero during expiration [43,46]. Around 80% of the lipids are phospholipids and about 10% are neutral lipids such as cholesterol (Figure 8) [47,48]. The major phospholipid in LS is

dipalmitoylphosphatidylcholine (DPPC) which constitutes 40 mol % of all the phosphatidylcholines found in the human LS, but can comprise up to 56 mol% in other species (Figure 7) [49]. DPPC functions to maintain the low surface tension during exhalation in the breathing cycles, as it is able to form a tightly packed rigid monolayer [50]. However, its high rigidity limits respreadability upon inhalation. To account for this, the LS surfactant also contains unsaturated phospholipid constituents, such as the zwitterionic palmitoyloleoylphosphatidylcholine (POPC) and the negatively charged palmitoyloleoylphosphatidylglycerol (POPG), which are responsible for maintaining the fluidity

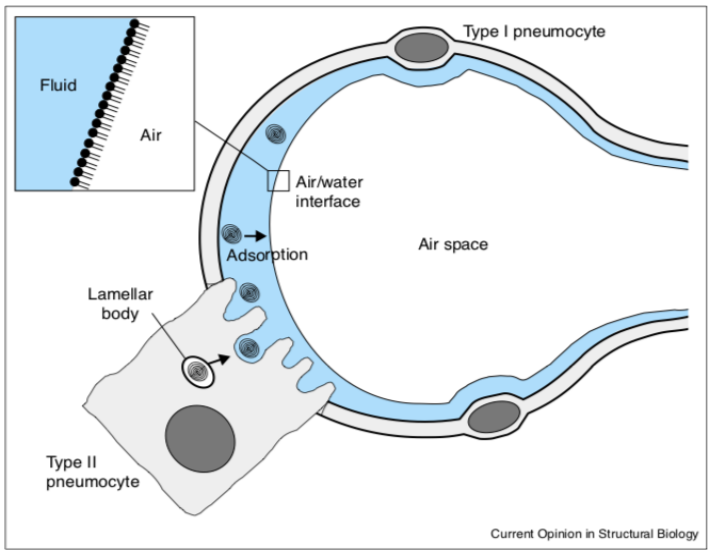

Figure 7. Schematic of the alveolar sac with the lung surfactant outlined. Piknova (2002).

of the monolayer due to their unsaturated nature (Figure 9) [49,51]. In addition to lipids, the LS contains about 10% protein, in the form of surfactant proteins A-D (SPs). SP B & C are hydrophobic proteins which incorporate into the monolayer and increase adsorption of lipids to the air-water interface [46]. During compression, SP-B/C promote the formation of multilayers on the surface of the interface. This allows for maintenance of low surface tensions, as the multilayers rapidly respread over the interface during inhalation. SP A & D are hydrophilic proteins and have

been shown to enhance the capabilities of SP C & B, as well as provide a degree of innate immune defense [46,52].

The LS will be the point of contact for inhaled vape constituents and given the lipid soluble nature of α-tocopherol, it is likely to partition into the monolayer. Patients with EVALI are also seen to have increased levels of lipid-laden macrophages (LLM). These result from impaired LS recycling and uptake of exogenous lipids [53]. They are considered a biomarker of EVALI and their presence further supports dysfunction of LS by the additives. Additionally, the uptake of vape additives by macrophages may provide insight into alternative pathologies of EVALI, as the fate if vape additives is unknown and it may be likely that there are additionally targets to the LS in the alveolar space [53].

To better elucidate the mechanism of EVALI, the effects of Vit-E, as well as Vit-EAc and the cannabinoids, on LS can be examined using a Langmuir Blodgett (LB) trough and Brewster angle microscopy (BAM).

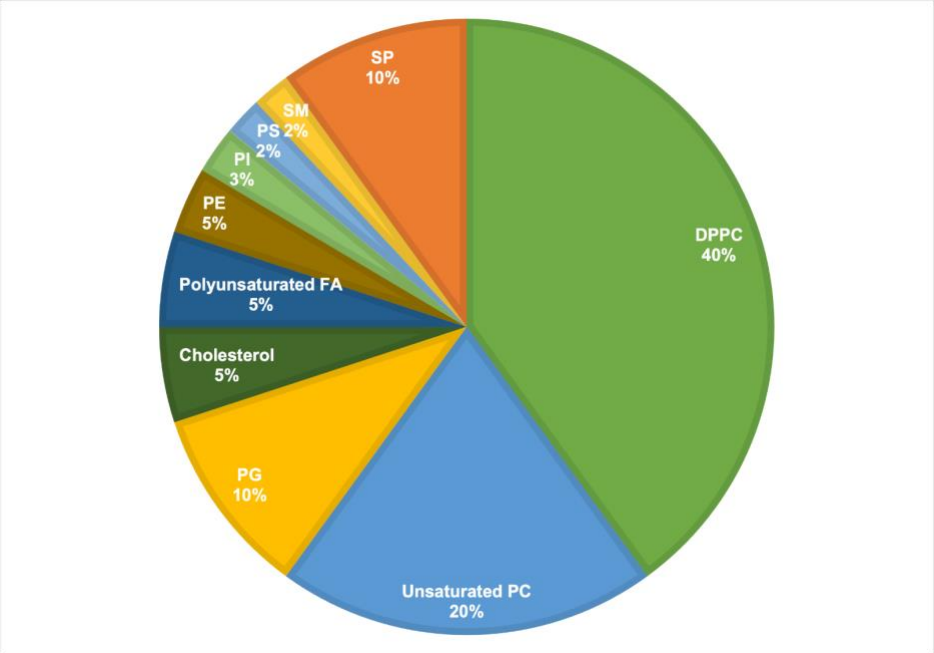

Figure 8. Composition of lipids and proteins in lung surfactant given in molar ratio. PC=phosphatidylcholine; PG=phosphatidylglycerol; FA=fatty acid; PE=phosphatidylethanolamine; PI=phosphatidylinositol; PS=phosphatidylserine; SM=sphingomyelin [47,48].

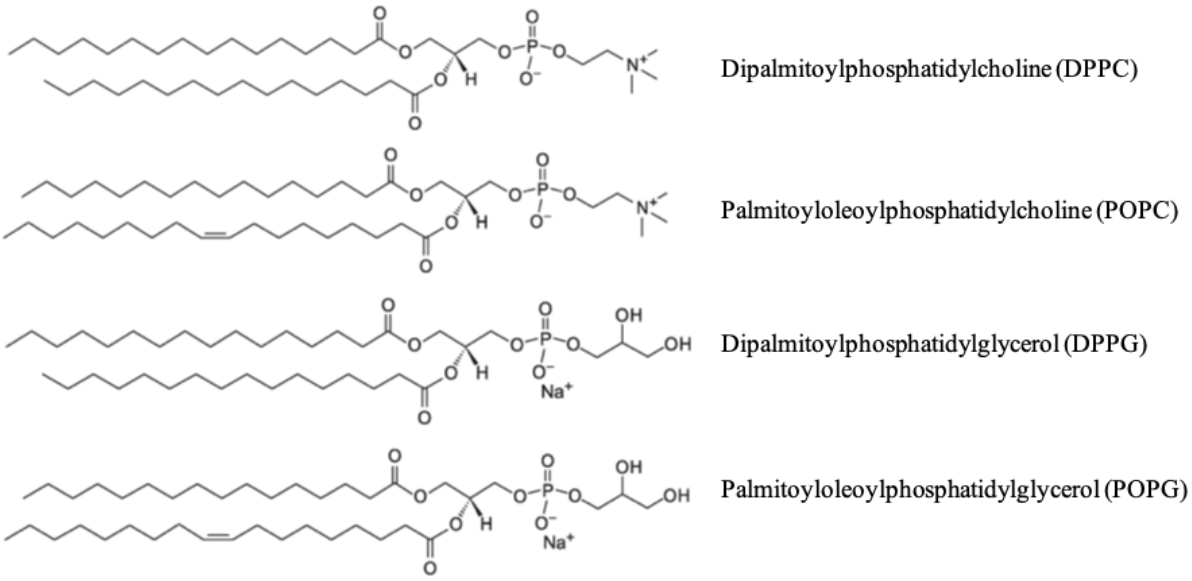

Figure 9. Structure of the most prevalent phospholipids in the lung surfactant.

1.7 Objectives

Vitamin E is a biologically vital molecule for our cells. Its lipid soluble nature allows it to insert into plasma membranes, where it acts to stabilize the bilayer and protect against oxidative stress. Its structural similarity to cholesterol has aided in understanding its mechanism of function. Like cholesterol it primarily acts to reduce the random motion of acyl chains, ordering lipid films. The biophysical data presented, shows that vitamin E readily partitions into DMPC, DOPE, and a variety of other phospholipids, wherein it may alter the biophysical aspects of the bilayer. Phase transition temperatures and enthalpies, as well as the overall packing of lipids are all influenced by the presence of vitamin E. Additionally, it has been demonstrated to induce curvature in lipid monolayers. While these effects are often beneficial to the stability of plasma membranes, and in some cases, proper function of relevant proteins, these dynamic changes to the LS are potentially dangerous.

Inhalation of vitamin E, and its derivative vitamin E acetate, through vaping may introduce these molecules into the lung surfactant. If the vitamins alter the packing of the LS or influence other biophysical properties, as seen with the lipid systems above, then the integrity of the LS may be compromised. Tight packing of the LS upon expiration is key to maintaining a low surface tension and protecting the alveoli against collapse. Likewise, the availability of lipids to spread out and enter a fluid state after inhalation, maintains the structure of the film. Vitamin E as been demonstrated to prevent both of these by fluidizing lipids in the gel state and rigidifying them in the liquid state. As such, it is imperative to study the impacts of vitamin E acetate on a biomimetic model of LS in a direct manner using a LB-trough and BAM. These methods will be expanded upon in the next chapter

Chapter 2: Materials and Methods

2.1 Lung Surfactant Model Systems

The most prominent PC and PG lipids in LS were chosen for the biomimetic model systems. These included DPPC, POPC, POPG, and DPPG (Table 1). Lipids were purchased from Avanti polar lipids as dry powders. Solutions of 1 mM lipids were prepared in 7:3 v/v chloroform:methanol (HPLC grade, EMD Millipore, Canada) and stored at -80 ºC. The molar ratio of lipids were 45:8:1:6 (DPPC:POPC:DPPG:POPG). Cholesterol was also introduced in some of the systems at 2% total lipid weight. All model systems used are laid out in table 2.

Table 1. Lipids used in lung surfactant model systems and their respective acyl chain lengths.

Lipid	**Chain Length**
Dipalmitoylphosphatidylcholine (DPPC)	16:0, 16:0
Palmitoyleoylphosphatidylcholine (POPC)	16:0, 18:1
Dipalmitoylphosphatidylglycerol (DPPG)	16:0, 16:0
Palmitoyleoylphosphatidylglycerol (POPG)	16:0, 18:1
Cholesterol (Chol)	N/A

Table 2. Molar ratio of lipids used in each model system.

Model	DPPC	POPC	DPPG	POPG	Chol
PC	45	8			
PG			1	6	
DPPC/POPG	4			1	
DPPC/POPG+Chol	4			1	+2%

Interactions with additives were first examined for individual lipid systems, followed by binary mixtures, and the addition of cholesterol. By assessing effects on increasingly complex

model systems, additive interactions with each component can be analyzed. This allows for a better understanding of the means by which additives may disrupt surfactant function. As touched on in Chapter 1, LS must be able to attain high surface pressures (low surface tension) during compression, and effectively respread afterwards. Exhalation reduces the surface area and induces high lateral pressure requiring the presence of rigid, tightly packed lipids to maintain film integrity. In contrast, increasing surface areas during inhalation requires fast respreading of LS, as provided by fluid lipids. To examine the effects of additives on a film that can support these two functions, a binary mixture of the predominant PC and PG lipids were used.

The major phospholipid of LS, DPPC, is primarily responsible for allowing the film to reach low surface tensions, as its fully saturated acyl chains allow for tight packing and zwitterionic headgroup does not produce a significant repulsive force between neighbouring phospholipids. The melting temperature of DPPC bilayers is 41 ºC, just above the physiological temperature of 37 ºC. Therefore, it is not entirely fluid which is necessary in order to achieve the LC state throughout compression. At 25ºC the monolayer still exhibits this important property with only minor changes to physical properties of the monolayer when compared to 37 ºC. Importantly, phase transitions of lipids in the film occur due to compression of the system, as opposed to temperature that is commonly seen in lipid bilayers. Therefore, even at unphysiological temperatures, relevant changes to the film state throughout compression can be measured accurately.

The primary PG lipid is the partially unsaturated anionic POPG. This phospholipid provides fluidity necessary for film respreadability, as it cannot densely pack due to headgroup charge repulsion and an unsaturated acyl chain. Lastly, cholesterol was incorporated into this mixture at a 2% weight ratio to the total phospholipid mass. At low amounts, cholesterol provides

key structural support for LS. Alongside DPPC, it enables LS to attain near zero surface tension. The structure of cholesterol is somewhat similar to that of the additives, containing fused cyclic rings and a relatively small hydrophilic component. This may promote interactions between the molecules and provide a reasonable basis for the means by which additives interfere with proper surfactant function.

To first understand the biophysical effects of vape additives on lipid monolayers, a constant concentration of 5 mol% was chosen. The concentration of certain additives, such as Vit-EAc, in vape products has been reported anywhere between 23-80% [54]. Therefore, a 5 mol% concentration may be on the low end, taking into consideration, multiple inhalations of the product. Nevertheless, this provides a starting ground for determining interactions between the additives and various surfactant model systems. It is recommended that future studies examine a range of concentrations on the model systems to better elucidate mechanistic actions of vape additives and determine, if any, concentration dependent effects on the film that may arise due to continued inhalation of vape products.

2.2 Langmuir-Blodgett Trough

To better elucidate the mechanism of EVALI, the effects of vitamin E, vitamin E acetate and the cannabinoids on LS were examined using a LB trough and Brewster angle microscopy (BAM). These methods have previously been used to study the biophysical effects of nanoparticles on model LS films [55]. The first LB film was demonstrated by Irving Langmuir who successfully transferred water-surface monolayers to a solid substrate. Katharine Blodgett later discovered that these monolayer films could be stacked to form multilayer films. Since then, the trough set-up has been used to form and study monolayer films. The term Langmuir monolayer refers to a one-molecule thick layer of insoluble organic material spread on an aqueous subphase. Which is a

simplified but functional descriptor of the manner in which lipids are situated at the air-water interface in alveolar sacs, forming LS. In reality, multilayers are present both on the surface and in the subphase, mediated by surfactant proteins, which provide robustness to the film and allow for quick lipid reinsertion during inhalation (Figure 9).

SP-C plays roles in lipid adsorption to the air-water interface and in monolayer-bilayer transitions. The alpha-helix structure and thioester-linked palmitoyl groups of SP-C support its transmembrane orientation in bilayers, whereas in monolayers, it is titled to maximize acyl-chain interactions with surrounding lipids [56,57]. The formation of these bilayers is an important structural feature in stabilizing the film against collapse [58]. As the film becomes increasingly rigid under compression, it may begin to buckle prior to collapse [59]. The stacked bilayers act to dampen the strain on the film and are cross-linked to the monolayer via SP-C, as free floating bilayers have been shown to be ineffective at stabilizing the film against collapse [60].

α-helices are also the main structural feature of SP-B. This protein interacts with lipid layers both at the interface and in the alveolar fluid phase, promoting surfactant adsorption and maintaining film stability [61]. SP-B has been shown to oligomerize into a ring structure with a hydrophobic cavity, which greatly increases lipid transfer to the interfacial film [62].

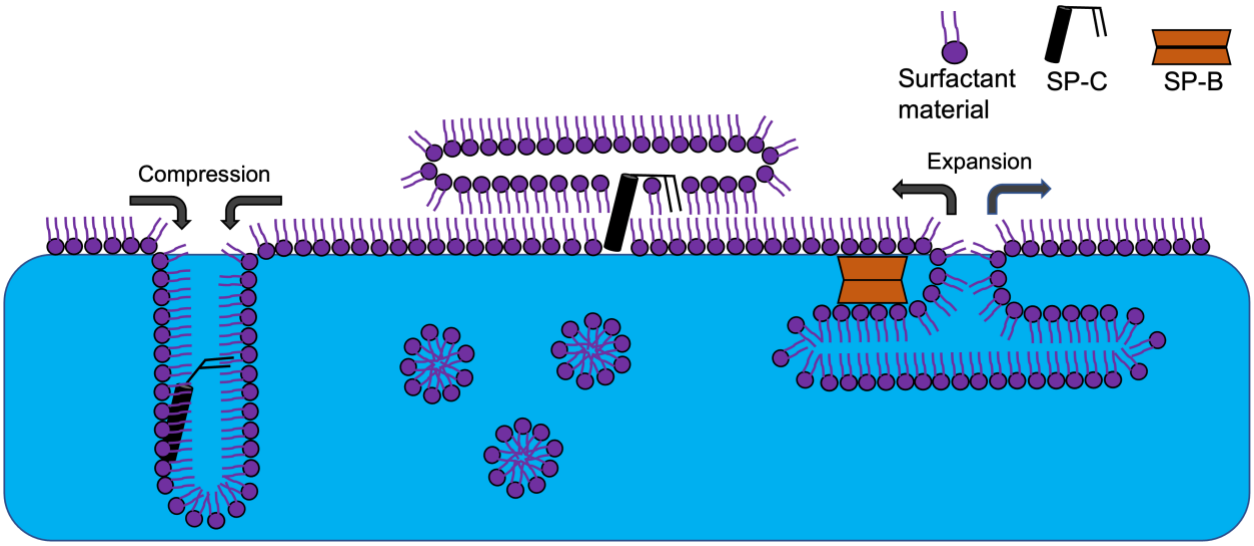

Figure 10. Schematic of lung surfactant formation

In the LB-trough setup, a monolayer may be compressed and expanded with Teflon barriers (Figure 10), altering the available surface area the material can occupy. During compression lipids are forced together and increased intramolecular interactions give rise to an increase in surface pressure. When the film is expanded, the surface pressure drops. The change in surface pressure can be recorded as a function of surface area, yielding surface pressure-area isotherms, which provides information on the phase state of lipids in the monolayer as well as overall stability. This will be expanded upon in section 2.4. Additional information can be extracted, such as compressibility by observing the rate of change of surface pressure as a function of surface area.

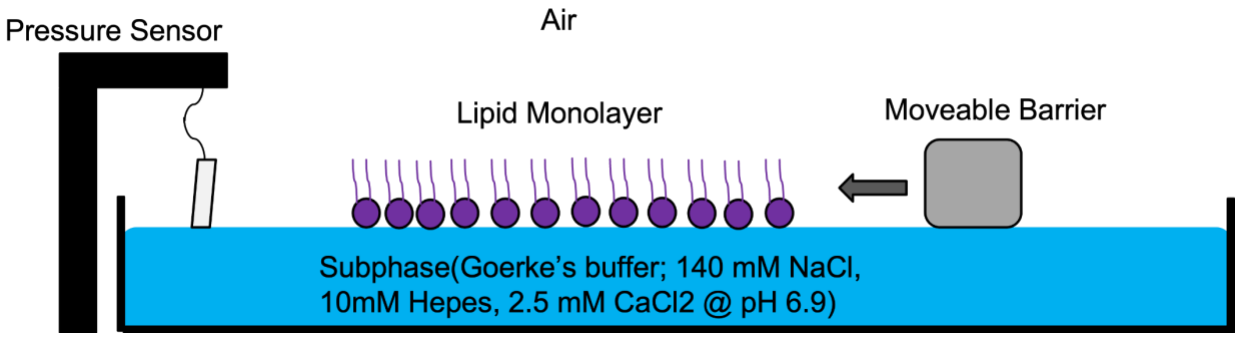

Figure 11. Schematic of LB-trough with a lipid monolayer deposited on an aqueous subphase.

Surface pressure is measured with a Wilhelmy plate wetted by the subphase and attached to a tensiometer. The total forces acting on the plate are, the weight of the plate and surface tension pulling it down, and buoyancy which opposes these forces. Force is measured by the tensiometer as the required force necessary to maintain static equilibrium of the plate. This is used to calculate surface tension using the Wilhelmy equation:

Equation 1:

$$\gamma = \frac{F}{2(w+d)\cos(\theta)}$$

Where γ is the surface tension, F is the sum of the forces acting on the plate, w is the width of the plate and d is its thickness. The contact angle for the plate is 0 assuming the plate is completely wetted, resulting in a value of 1 for $\cos(\theta)$. Therefore the equation can be simplified to:

Equation 2:

$$\gamma = \frac{F}{2(w+d)}$$

The LB-trough reports surface pressure rather than surface tension, which is given by the following equation:

Equation 3:

$$\prod = \gamma_0 - \gamma$$

In which $\prod$ is surface pressure, γ_0 is surface tension of pure subphase, and γ is the surface tension with a monolayer present.

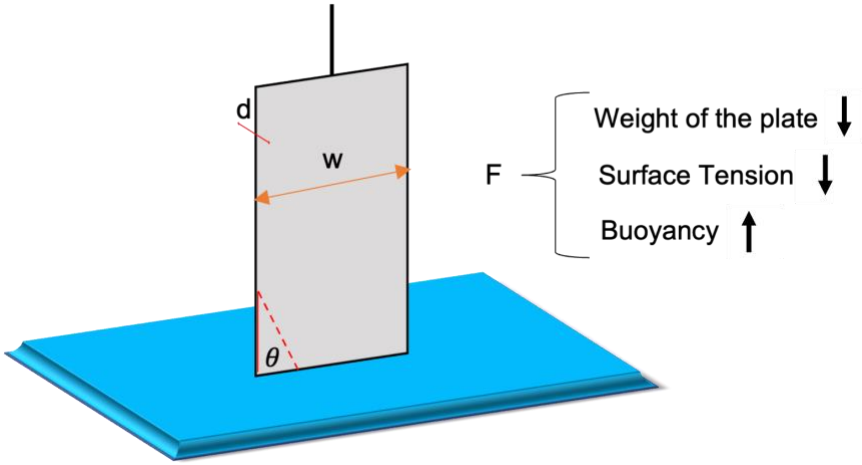

Figure 12. Schematic of a Wilhelmy plate situated on an aqueous subphase and the parameters used to calculate surface pressure.

While the LB-trough method allows for a means of producing biomimetic monolayers, it does suffer from a few shortcomings. Namely leakage of lipids from the trough. This is a particularly important consideration during high compression of rigid lipids like DPPC. As the film material forms a sheet-like structure and lipids may 'creep up' the walls of the trough, reducing the recorded surface pressure. This has been solved previously by saturating the walls of the trough with DPPC beforehand, thereby restricting film material from escaping and allowing for more accurate measurements. Alternatively, a captive bubble method may be used, which reproduces in situ behavior of LS films [63].

2.3 Experimental setup

A 22.5 x 10 cm Teflon Langmuir trough (Biolin, Stockport, U.K.) was used for the lipid monolayer setup. A 110 mL portion of Goerke's buffer (140 mM NaCl, 10 mM HEPES and 2.5 mM $CaCl_2$; pH 6.9) was used as the subphase, as this buffer mimics alveolar fluid. Lipids (~25 uL) were deposited at the air-water interface and a single Teflon barrier was used to compressed the monolayer at a rate of 96.9 cm^2/min while a Wilhelmy plate mounted on a pressure sensor

(Type PS) measured surface pressure. Isotherms were recorded at 25 ºC in triplicate to ensure reproducibility.

2.4 Isotherms and phase

As the film is compressed, lipids must reorient to accommodate the decreasing available surface area, and as a result undergo various phases throughout compression [104]. Changes in slope and inflections often denote phase changes, which provides information on the lateral organization of the lipids and importantly changes to their organization in the presence of additives.

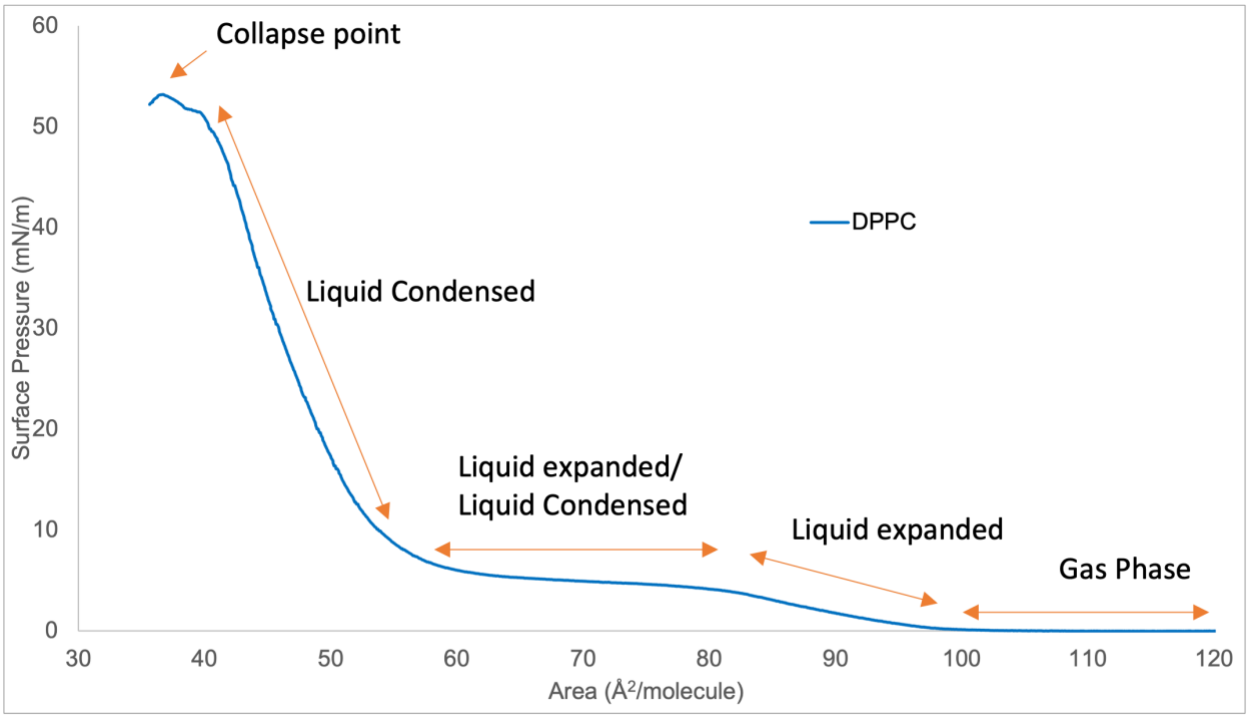

Figure 12. DPPC Surface pressure-area isotherm depicting various phases lipid monolayers may exhibit.

Initially, at high surface areas, the lipids are in the so-called gas phase in which there is a high degree of freedom and little to no interactions resulting in 0 surface tension. Upon compression, there is take-off point of lateral pressure where the lipids enter a liquid expanded phase (LE). Here, molecular interactions between lipids increase and the slope is relatively shallow. A plateau indicates a phase transition from the L_E to the liquid condensed phase (LC). Here, lipids undergo

reorientation of their acyl chains to accommodate neighboring lipids. Most lipids will directly transition from L_E to the L_C phase without a plateau. Afterwards, there is a steep increase in surface pressure as all the lipids are packed tightly together in the L_C phase with a high degree of acyl chain interactions. This continues to a collapse point, in which the film reaches a critical density and breaks down due to lack of available surface area. Lipids are either pushed out into the subphase or towards the air, resulting in a drop in surface pressure. This is used to compare stability of lipid films, with high attainable surface pressures indicating a more stable film. Changes to the slope of the isotherm upon addition of additives may indicate fluidizing or rigidifying effects. While shifts of the entire isotherm to the right correspond to incorporation of material, as more initial surface area is required. As lipids adopt the L_C phase, rigid domains become present on the film which can be visualized with Brewster angle microscopy or atomic force microscopy.

As the surface tension in alveoli must be maintained close to 0 mN/m, the range of surface pressure of the film is high, between 40 – 70 mN/m. Physiologically relevant surfactants like Infasurf and Bovine Lipid Extract Surfactant (BLES) can achieve this range of surface pressure [64] while the model lipid films fall below this. In this thesis, the effects of vape additive on model films was examined across surface pressures from 0 mN/m up to collapse. This provided a better biophysical understanding of additive induced changes to the films. Specific roles of lipids that make up complex surfactants like BLES, can be identified and their specific interactions with vape additives examined. Additionally, dysfunctional surfactant is unable to achieve low surface tensions, therefore, it was prudent to understand the effects of additives in the film at lower pressures that may be causing this loss of attainable surface pressure.

2.5 Compressibility

Compressibility refers to the ability of the film to be compressed to smaller areas. More fluid lipid states, seen in surface pressure-area isotherms as plateaus or shallow slopes, are highly compressible, as the film can under a large area change with minimal change to surface pressure. Compressibility at a given surface pressure can be calculated as the slope of the isotherm at a selected pressure [20]:

Equation 4:

$$k_\pi = (-1/A_\pi)(dA/d\pi)_\pi$$

Where A_π is the corresponding surface area at the given pressure, and $dA/d\pi$ is the slope at the selected pressure. The reciprocal of compressibility was then taken to yield the compressibility modulus, which is more readily comparable to bilayer values [21]

Equation 5:

$$C_m = k_\pi^{-1}$$

In contrast to compressibility high C_m values indicate a more rigid film. Comparison of C_m values between lipid films in the absence and presence of additives can provide additional information on changes to lipid lateral organization as a direct result of additive interactions.

2.6 Isocylces

Isocycling is another useful tool for assessing film functionality by generating isotherms over multiple compression and expansion cycles. Here, the film is compressed to a surface pressure just below the collapse point, as a collapsed film is unable to respread effectively, then expanded to low surface pressures. During respiration, some material is lost to the subphase as the film is squeezed during expiration. Lipids are readily reincorporated from reservoirs in the subphase and protein mediated processes. However, with the LB trough, this material cannot be reinserted on a

quick enough timescale. Consequently, the isotherm will shift to the left after each cycle. This shift in surface area can be used to compare relative material loss between lipid systems in the presence of additives, with larger shifts indicating more material loss.

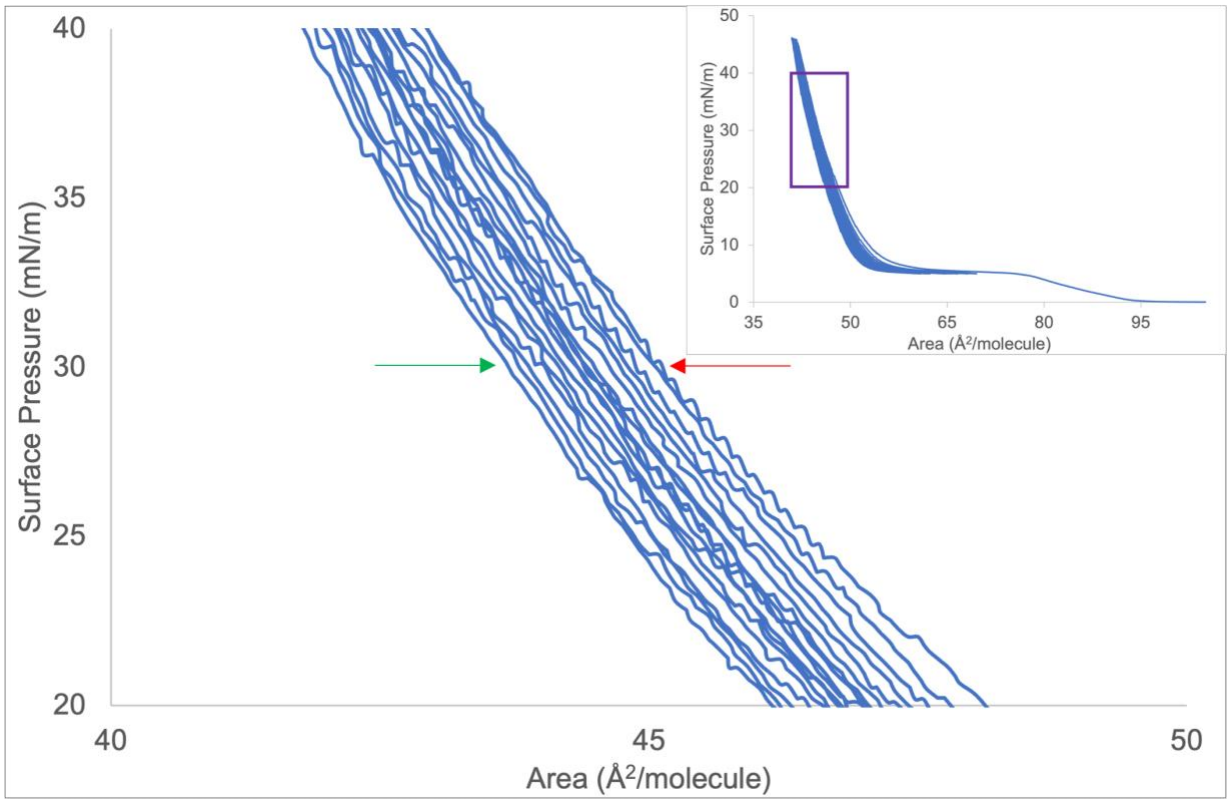

Figure 14. Surface pressure-area isotherm for DPPC after 10 compression-expansion cycles. Arrows indicate the shift in surface area at 30 mN/m from the 1st (red arrow) to the 10th (green arrow) cycle.

2.7 Brewster Angle Microscopy

Imaging of lipids on the LB trough was performed using an EP3 Brewster Angle microscope (Accurion, Germany) as shown in Figure 14. A Halyconics active vibration isolation table (Accurion, Germany) was used to dampen any vibrations which interfere with the imaging. EP3 V3.20 software was used to operate the microscope and acquire images at the air-water interface (Accurion, Germany).

Brewster angle microscopy is a well characterized tool for visualization of films on the surface of a subphase. It works by directing plane polarized light towards the air-water interface

at the so-called Brewster angle (~53.1° for water). At this angle, all of the incident light impacting the subphase will be refracted, while light hitting a film will be reflected into a camera (Figure 15). There is a change in the refractive index at the air-water interface by the addition of a lipid film, which allows for reflection [51]. Using this technique, qualitative information regarding lateral organization, phase separation, and domain formation can all be directly observed.

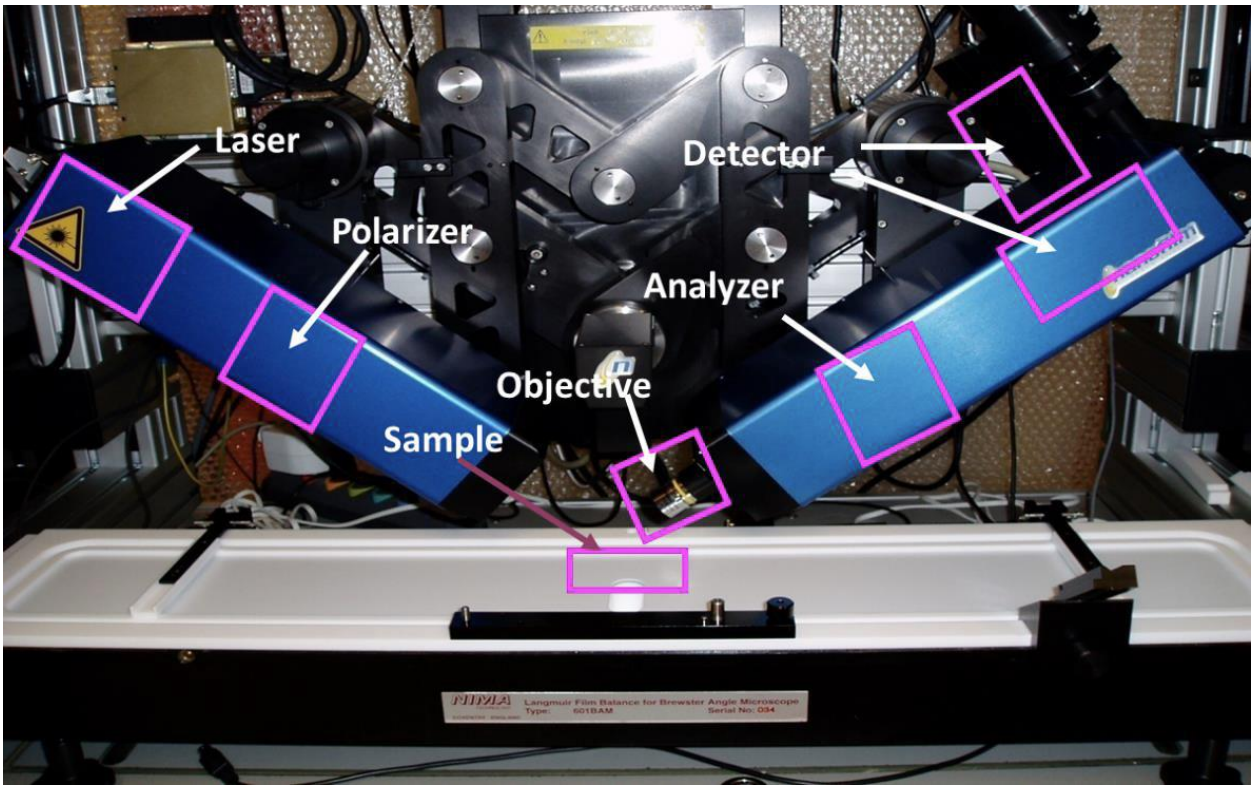

Figure 15. Brewster angle microscope situated above the LB trough with highlighted components used in film imaging.

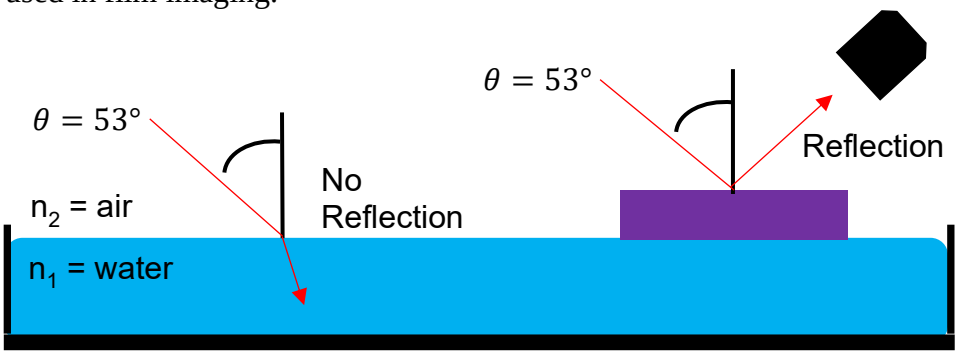

Figure 16. Schematic of the principle of Brewster angle microscopy. Incident light will refract when directed towards the subphase at the Brewster angle, but reflect into a camera when directed at a film.

Domain images without a lipid film present will appear as dark grey, while the presence of domains show up as bright clusters (Figure 16). The brightness of the clusters correspond to their height, as structures protruding from the film will be hit first by the laser. At high surface areas, no domains are present, but as the film is compressed and lipid interactions increase, domains begin to form. Domain formation occurs for multiple reasons: reorientation of lipids to maximize van der Waals interactions between acyl chains, hydrogen bonding between headgroups, and separation of rigid clusters from fluid phases. This generally occurs during phase transition, as lipids will pack tightly in the L_C phase, which protrude more from the subphase than the fluid L_E phase. Once all lipids adopt the L_C phase, the film coalesces into a homogenous light grey image on BAM.

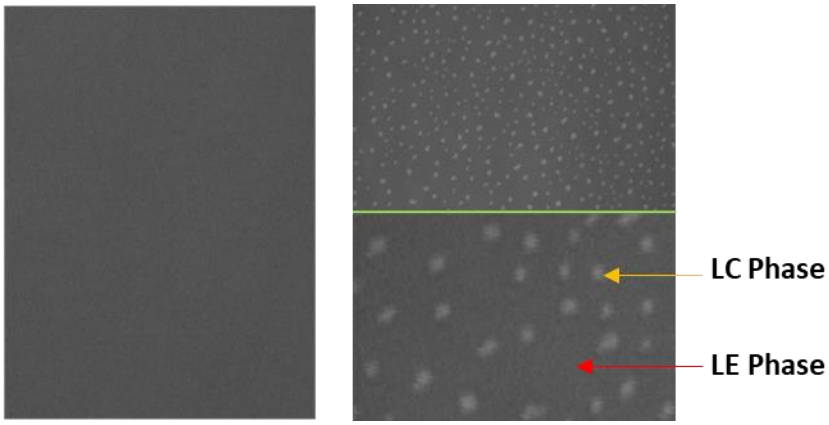

Figure 17: Brewster Angle microscopy images of subphase (left) and lipid film (right) showing the LC phase domains (yellow arrow) and LE phase (red arrow). A 4x magnification of the lipid film is shown below the green line.

2.8 Calculating Domain Thickness

The BAM images can be converted into pseudo 3D images, by attributing relative height to the intensity of reflected light. This allows for ease of comparison when assessing the lateral organization and domain architecture between lipid systems.

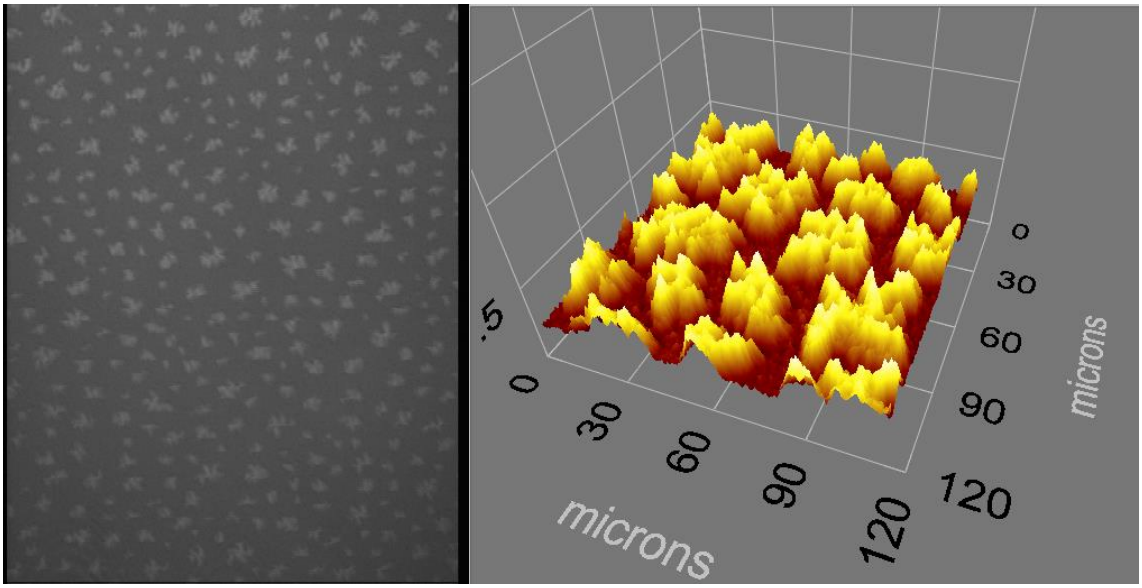

Figure 18. BAM image (left) and 3D reconstruction (right) of a DPPC film.

The gray scale in the BAM images provides information on reflectivity data, which along with the refractive indices of monolayer and subphase can be used to calculate domain thickness [65,66]

To estimate the thickness of the domains a calibration curve of the reflectivity vs the gray level of a BAM image of a clean subphase was recorded. This curve was used to convert the gray level to a reflected light intensity (Rp) from BAM images of the domains.

The refractive index of the monolayer was determined by measuring the reflectivity at angles between 52-56° and calculating the refractive index of the subphase (n_2) using equation 1. A plot of reflectivity against the calculated refractive index is used to find the refractive index of the monolayer (n) by fitting to equation 2. The refractive index of the monolayer (n) was estimated from the minimum value of the parabola.

Equation 6:

$$n_2 = tan(\theta_B)$$

Equation 7:

$$R_p(n_2) = \frac{an_2^4 - bn_2^4 + c}{dn_2^2 + e}$$

$$a = n^4 - 2n^2n_1^2 + n_1^4, b = 2n^6 - 4n^4n_1^2 + 2n^2n_1^4, c = n^8 - 2n^6n_1^2 + n^4n_1^4,$$
$$d = n^4, e = n^4n_1^2$$

The thickness of the liquid condensed domains were calculated from the reflectivity of the domains obtained the BAM images and calculated with equation 3. Using an approximation of n_1 =1, the previously determined n and n_2 =1.33 values.

Equation 8:

$$l = \frac{\sqrt{Rp}}{sin(2\theta_B - 90)}\left(\frac{\pi\sqrt{n_1^2 + n_2^2})(n_1^2 - n^2) \times (n_2^2 - n^2)}{\lambda(n_1^2 - n_2^2)n^2}\right)^{-1}$$

Together, these methods make use of the LB-trough and BAM to assess the biophysical aspects of lipid model systems at the air-water interface to determine the potential effects of vape additives on functionality.

Chapter 3: Vape Additives Properties and Interactions with Lipid Systems.

The lipophilic nature of the vape additives (Vit-E, Vit-EAc, THC, and CBD) allow them to partition into LS. The large-scale effects additives have on LS function will predominantly arise from interactions with the lipid components. To accurately analyze the results presented in this thesis and elucidate pathologies of EVALI, it is important to understand LS lipid-additive interactions. Vit-E plays a significant role in cell membranes as an antioxidant and lineactant, and as such, its interactions with lipids are better understood than the other additives. As Vit-E has been explored extensively in the first chapter, this chapter is devoted to exploring the interactions of Vit-EAc and the cannabinoids, so that their effects on LS systems may be better understood.

3.1 Vitamin E acetate

Vit-EAc is closely linked in structure with Vit-E, both contain a methylated phytyl tail and chromanol ring. However, Vit-EAc is esterified at the position of the hydroxyl group on the chromanol ring which disables antioxidative properties, makes it more thermostable, and reduces polarity. Vit-EAc is suspected of being the primary causative agent of EVALI [43], and while it shares many similar properties to Vit-E, the esterified derivative may induce unique effects on the monofilm. The decreased polarity of Vit-EAc, positions it slightly deeper in the hydrophobic core of lipid bilayers where it can interact and potentially interferes with the acyl chain motion of neighboring lipids [67]. NMR studies have concluded that the hydrophobic chain of Vit-EAc is packed in a loose manner, similar to liquid-crystalline packing of lipids. Distance between lipids in this phase is ~4.7 Å, as determined by X-ray scattering [68]. X-ray scattering has also given a distance of ~4.7 Å between the acyl chains of the lipids and Vit-EAc, while Vit-E packs tighter with a chain distance of 3.6 Å [67]. Vit-EAc is limited to hydrophobic interactions with lipids, while Vit-E exhibits hydrogen bonding between its hydroxyl group and the phosphate oxygens of

lipids. This extra interaction allows Vit-E to pack tighter in membranes and reduces its mobility compared to Vit-EAc [67,69]. Despite these differing interactions, both forms of the vitamin had comparable effects on DMPC membrane systems, characterized by a reduction in the enthalpy of gel-liquid crystalline phase transition by 3.6 kcal/mol and the T_m by 1.2 ºC [25]. However, in DPPC membrane systems only Vit-E was seen to affect phase transition, as Vit-EAc was theorized to cluster in small aggregates in the hydrophobic core of DPPC bilayers [28]. This suggests that the localization of Vit-EAc, and subsequent effects on membrane dynamics, are dependent on the chain lengths of lipid components in the membrane. In addition to disruption of acyl chain motion, Vit-EAc may also act as a lineactant. Lineactant activity reduces the line tension at phase boundaries, abolishing phase separation and decreasing the size of domains [70]. Molecular dynamic simulations have previously demonstrated that Vit-E localizes to the domain interface, where it acts to destabilize macrodomains [71]. Addition of 10 mol% Vit-E to giant unilamellar vesicles composed of DPPC/DOPC/cholesterol at a molar ratio of 27.5/37.5/25 respectively, eliminated phase separation and the presence of domains [72]. However, through additional analysis it was revealed that the film was not totally homogenous and still contained nanodomains [73]. Therefore, lineactant activity of Vit-E and Vit-EAc at the concentrations examined in this study are not expected to completely homogenize the film. Nevertheless, the mixing of lipid components in LS is detrimental to function, as the formation of a rigid film throughout expiration is dependent on DPPC and cholesterol organizing into a lipid ordered phase. Additionally, SP association between the film and lipid multilayers in the aqueous phase are critical for respreading during inhalation, and also require the presence of rigid domains for SP anchoring [52]. Lineactant activity also increases surface viscosity of LS, which affect dynamic processes during respiration, potentially causing hypoxemia [74]. This increase in surface viscosity is a direct result of film

homogenization and a subsequent decrease in the free area of lipids. Vit-EAc acting as a lineactant adversely affects LS function in a number of ways by reducing overall film robustness, interfering with SP-mediate action, and hampering dynamic processes that occur during expiration-inhalation cycles.

3.2 Tetrahydrocannabinol and Cannabidiol

The cannabinoids THC and CBD both exhibit aromatic rings and short side chains. CBD differs from THC in that it has free rotation around its rings and an additional hydroxyl group, while THC is characterized by a three fused ring structure (Figure 10)..

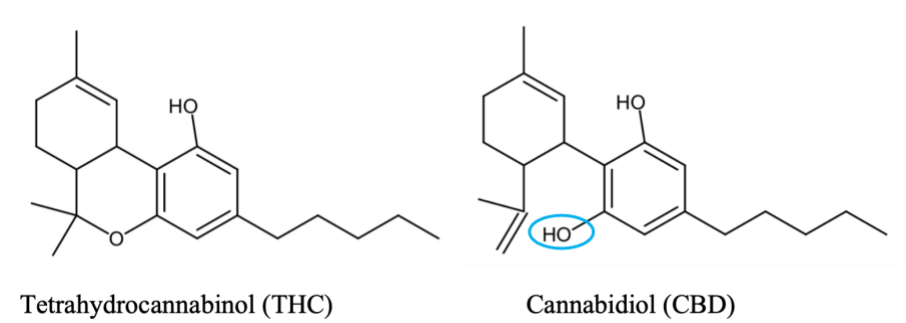

Figure 19. Structures of THC and CBD

The second hydroxyl group makes CBD slightly more polar than THC [75], and its increased mobility allows for better packing into lipid layers. Though it should be noted that the bulky ring structure of both cannabinoids and limited acyl chain interactions perturb membrane bilayers.

DPH anisotropy measurements demonstrated that both THC and CBD induce fluidization in the core of DMPC and DPPC bilayers, as well as PC-cholesterol vesicles [76]. Location of the cannabinoids at the head group region will space out lipids, allowing for more acyl chain movement, which was associated with an increase in DPH mobility [76]. Differential scanning calorimetry and solid-state ^{2}H-NMR found that the phenolic -OH group in THC allows it to interact

in the headgroup region, where it orients perpendicular to the bilayer chains, spacing out neighboring lipids [71]. Given the similar fluidizing effects seen with CBD, it is likely to orient in a similar manner.

The effects of THC have been further studied on DPPC/cholesterol bilayers using differential scanning calorimetry and solid-state NMR spectroscopy [77]. Again, THC acted to fluidize the system, but the study also identified THC interactions with cholesterol, which further increased fluidization of the bilayer. THC broadened the phase transition and introduced a new peak at 28.5ºC. This peak was previously discovered by incorporating THC within PC bilayers at molar concentrations >10%. However, when cholesterol was added to the system, the peak became apparent at 5 mol% THC. This suggests that cholesterol enhances the association between DPPC and THC. It is likely that the presence of cholesterol deeper in the core shifts THC 'up' where its hydroxyl group may interact with the phosphate of DPPC [77]. X-ray data and ^{13}C/MAS-NMR spectroscopy seem to confirm this by positioning THC at the headgroup region of DPPC where it is anchored by interactions with the phosphate group [78]. Similar interactions may occur between the cannabinoids and DPPC/cholesterol in LS, which will perturb packing and lead to the functional issues outlined previously.

A FT-IR study examining THC and Vit-EAc has found evidence that these two additives form a complex via hydrogen bonding [79]. Compared to control spectra for the additives, prevape mixtures and post vape condensate of Vit-EAc/THC displayed absorption stretching at wavenumbers corresponding to C=O, C-O, and OH groups. This suggests that THC hydrogen bonds to Vit-EAc at the hydroxyl and carbonyl groups respectively, shown in the schematic proposed by Lanzarotta et al. (2020) (Figure 19).. This was further confirmed by ^{13}C-NMR spectra, in which the Vit-EAc control displayed a carbonyl peak at 169.760 ppm, and expectedly, the THC

spectrum did not contain this. The prevape and postvape mixtures both had a carbonyl peak slightly shifted at 169.775 ppm. The shift is explained by deshielding of the carbonyl carbon as electron density is pulled away by the hydroxyl oxygen of THC. Given that CBD also contains hydroxyl groups, it may complex with Vit-EAc in a similar fashion, though direct evidence of this is currently unavailable.

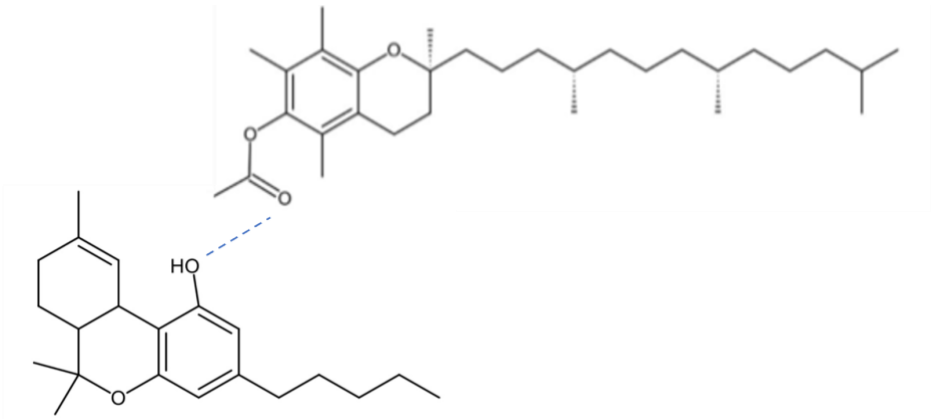

Figure 20. Proposed hydrogen bonding between THC and Vit-EAc.

The complexed forms of the cannabinoids with Vit-EAc may produce synergistic effects on lipid monofilms in regard to proper lipid packing. Localization of the additives could be altered, as Vit-EAc partitions at phase boundaries, it will bring the cannabinoids along with it which may destabilize domains further given the highly fluidizing effects of THC and CBD. Additionally, the same enhanced THC effect from cholesterol may now be applied for Vit-EAc. The vitamin localizes deeper in the hydrophobic core and will hold THC closer to the headgroup region, elevating its fluidizing effects on lipids. In this scenario, THC cannot anchor to phosphate groups as its hydroxyl is occupied by Vit-EAc, but the vitamin itself may act as an anchor due to hydrophobic interactions with neighboring lipid tails. CBD on the other hand has a free hydroxyl that can interact with nearby phosphates. The dual interaction of Vit-EAc and CBD with lipids may stabilize them in the film and further disrupt local packing.

3.3 Summary

The presence of additives in lipid films predominantly impact phase behavior and packing. Fluidization by the additives will primarily affect the film towards the end-state of expiration, as DPPC and cholesterol order into a rigid film. Here, additive induced spacing of the lipid components will destabilize the film and likely reduce the maximal attainable surface pressure. Disruption of phase transitions, that the vitamins have exhibited on PC model membranes, may interfere with proper lipid dynamics throughout compression. Namely, linactant function by the vitamins will act to mix the lipids, reducing domain sizes and increasing viscosity.

Chapter 4: Biophysical interactions of vape additives on simple lipid model systems

4.1 Surface pressure-area isotherms

To better understand the effects of vaping additives on biologically relevant surfactants, studies were first performed on simple lipid systems composed of the primary phospholipid classes found in LS. These being the zwitterionic PCs and anionic PGs [80]. Both groups exhibit a fully saturated lipid (DPPC and DPPG) and monounsaturated lipid (POPC and POPG). Model systems were composed of individual lipids and binary PC and PG films to determine interactions between the additives and lipids in terms of film packing and stability, and lateral film organization.

Vitamin E acetate was one of the first potential causative agents of EVALI identified, and its effects on simple model systems are shown below.

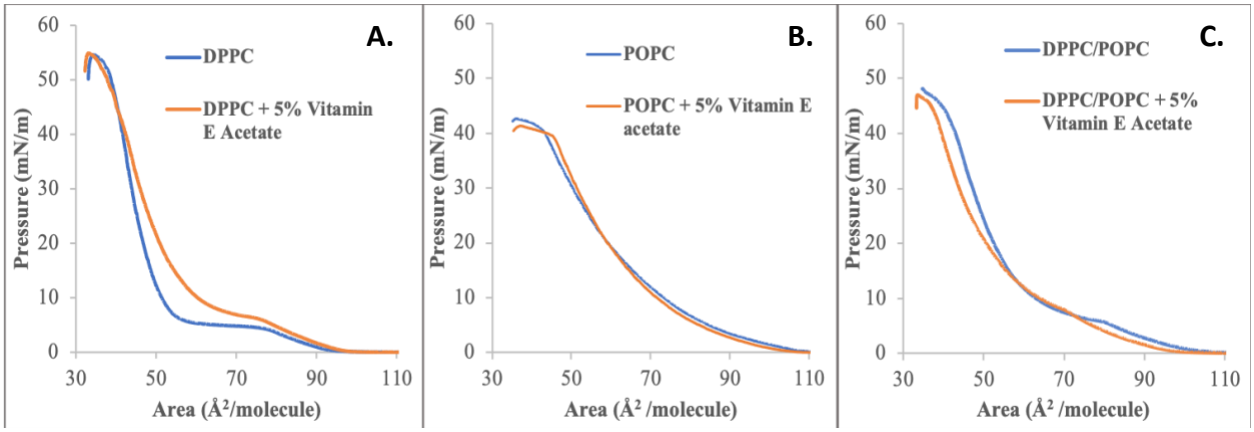

Figure 21. Surface pressure-area isotherms of PCs with 5 mol% Vit-EAc. **(A)** DPPC+Vit-EAc; **(B)** POPC+Vit-EAc; **(C)** DPPC/POPC (45:8)+Vit-EAc.

Pure DPPC films display a take-off pressure of ~93 Å^2/molecule, where lipids transition into the LE phase characterized by a gradual rise in surface pressure. The onset of a plateau at 6 mN/m is indicative of the phase coexistence region, in which DPPC is reordering into the LC phase. At 55 Å^2/molecule, surface pressure steeply increases as the DPPC is entirely in the LC phase, and the film is relatively incompressible. Upon further compression, the film reaches a collapse point at

39 Å^2/molecule and 55 mN/m. Here, the monolayer breaks down and material is either pushed out into the subphase or forms multilayers on the surface.

Addition of Vit-EAc prolongs the LE phase of DPPC and induces a less pronounced phase coexistence region between 80 and 55 Å^2/molecule. This fluidizing effect has been demonstrated in bilayer lipid, in which the ring group and methylated phytyl tail of Vit-EAc prevents tight packing of the saturated lipids.

The POPC isotherm exhibits a continuous LE phase throughout compression. The monounsaturated acyl chain of this lipid disallows for a condensed phase of the film. A slightly steeper slope of the isotherm is apparent in the presence of Vit-EAc, indicating a tighter packing of the POPC monolayer (Figure 20B). While Vit-EAc had an opposite effect on DPPC films, it may act to order acyl chains of lipids in the fluid phase, albeit not to a large extent.

The isotherm shape of a film containing both PC lipids was largely dominated by DPPC, with an initial LE phase that transitioned into the LC phase. Throughout phase transition, pressure gradually rose as the POPC component remains in the fluid phase during compression.

Vit-EAc in the presence of the binary PC system almost completely abolishes this region between 80 and 60 Å^2/molecule (Figure 20C). Furthermore, a continuous gradual slope was observed throughout the isotherm. Reduction of tight packing of DPPC by Vit-EAc outweighs its impact on enhanced POPC packing, resulting in an overall fluidization of the film. The slight reduction in collapse pressure indicates a destabilizing effect on the film, which was not seen for DPPC alone. DPPC is the primary lipid component of LS, and functions to achieve high surface pressures correlated to the low surface tension maintained in a functional surfactant. Vit-EAc hindering this may point to dysfunction of the film.

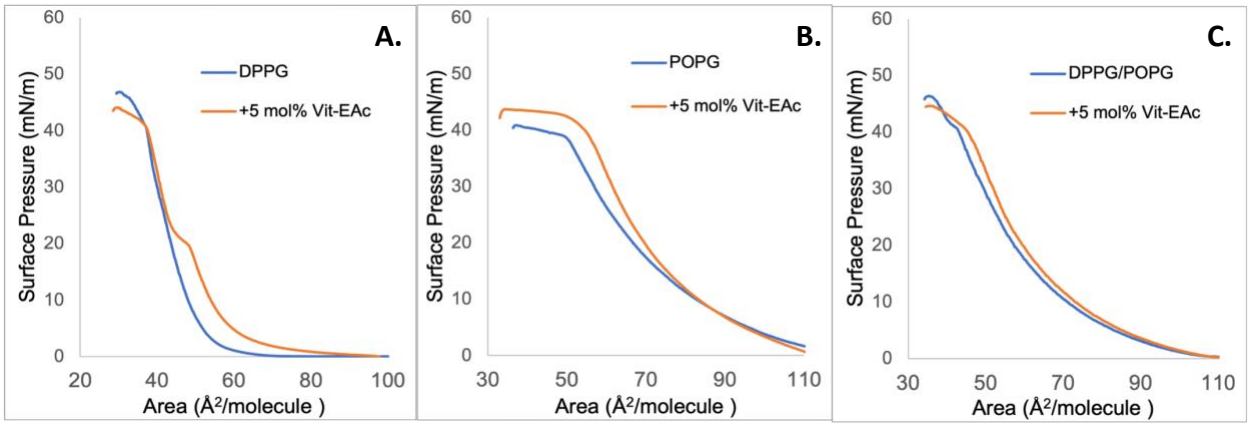

Figure 22. Surface pressure-area isotherms of PGs with 5 mol% Vit-EAc. **(A)** DPPG+Vit-EAc; **(B)** POPG+Vit-EAc; **(C)** DPPG/POPG (45:8)+Vit-EAc.

PG lipids are the second major class of phospholipids found in LS. They are present in smaller amounts than their PC counter parts but provide important function in film respreading during inhalation. POPG specifically produces a highly fluid film, through headgroup charge repulsion and its unsaturated nature.

DPPG quickly adopts a LC phase after the take-off point at 64 Å^2/molecule, leading to film collapse after a short compression duration at 48 mN/m. Vit-EAc shifts the take-off point to 88 Å^2/molecule, and the film undergoes prolonged compression before a steep rise in pressure at 60 Å^2/molecule, associated with the LC phase. The initial slow rise in pressure indicates that Vit-EAc interferes with proper packing of DPPG, restricting it from directly entering the LC phase. A shoulder is observed at 20 mN/m of pressure, followed by another steep increase in pressure. This deflection in the film may be a region of lipid reorganization in which material is squeezed out of the film. Given that DPPG cannot pack effectively in the presence of Vit-EAc, the additive is likely expelled at this point to accommodate the decreasing available area. The subsequent steep increase in pressure supports the idea that Vit-EAc is removed, and DPPG is able to pack tightly again. There is a slight reduction in collapse pressure from 48 mN/m to 44 mN/m, which may be a consequence of lost lipid material from the film.

Similar to POPC, POPG exhibits a LE phase throughout compression, with the onset of a plateau at 39 mN/m. The increased slope of the POPG isotherm with Vit-EAc lends more evidence to the idea that highly fluid films are rigidified in the presence of the additive.

The binary PG isotherm shape is largely influenced by POPG, given it is at a 6 to 1 molar ratio to DPPG. There is a steeper increase in pressure above 15 mN/m due to the DPPG component. Vit-EAc appears to have an overall rigidifying effect on this film, as there is a steeper increase in surface pressure above 5 mN/m compared to the control. The effect of the additive on a given film seems dependent on which lipid is present in higher amounts. Comparing to the binary PC film in which DPPC was at a higher ratio to POPC, Vit-EAc displayed a fluidizing effect.

In physiological surfactant, DPPC is the primary component, and as such it might be suspected that Vit-EAc induces an overall loss of film rigidity. This is accompanied with a decrease in film stability, as seen in by the reduction of collapse pressure for the binary systems.

A stable film able to maintain high surface pressures is a key characteristic of functional surfactant [81]. Vape additive effects on overall film stability was analyzed next by comparing the collapse pressure of each lipid and lipid-additive system.

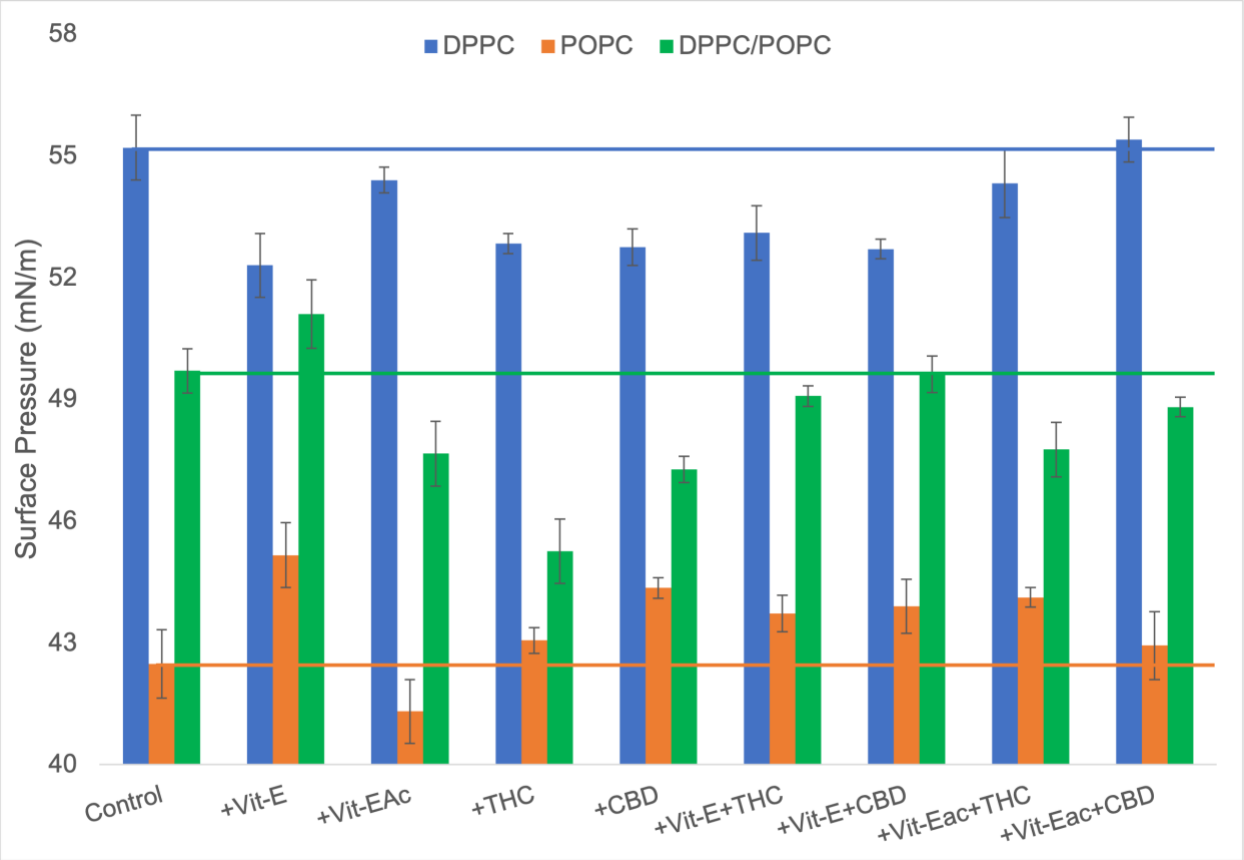

Figure 23. Collapse pressure of PC lipid films in single or double additive systems. Blue bars: DPPC-additive systems; Orange bars: POPC-additive systems; Green bars: DPPC/POPC-additive systems.

The presence of vape additives in DPPC films reduced collapse pressure, except in the double additive systems with Vit-EAc. Given the previous effects explored between additives and PC membranes, destabilization may be a direct result of disruption of proper lipid packing and film fluidization. Contrary to POPC films, which largely exhibited an increase in collapse pressure in the presence of the additives. Ordering of acyl chains via the additives appear to be responsible for increased stability.

The double PC system, containing mostly DPPC, tends to be less stable in the presence of the additives.

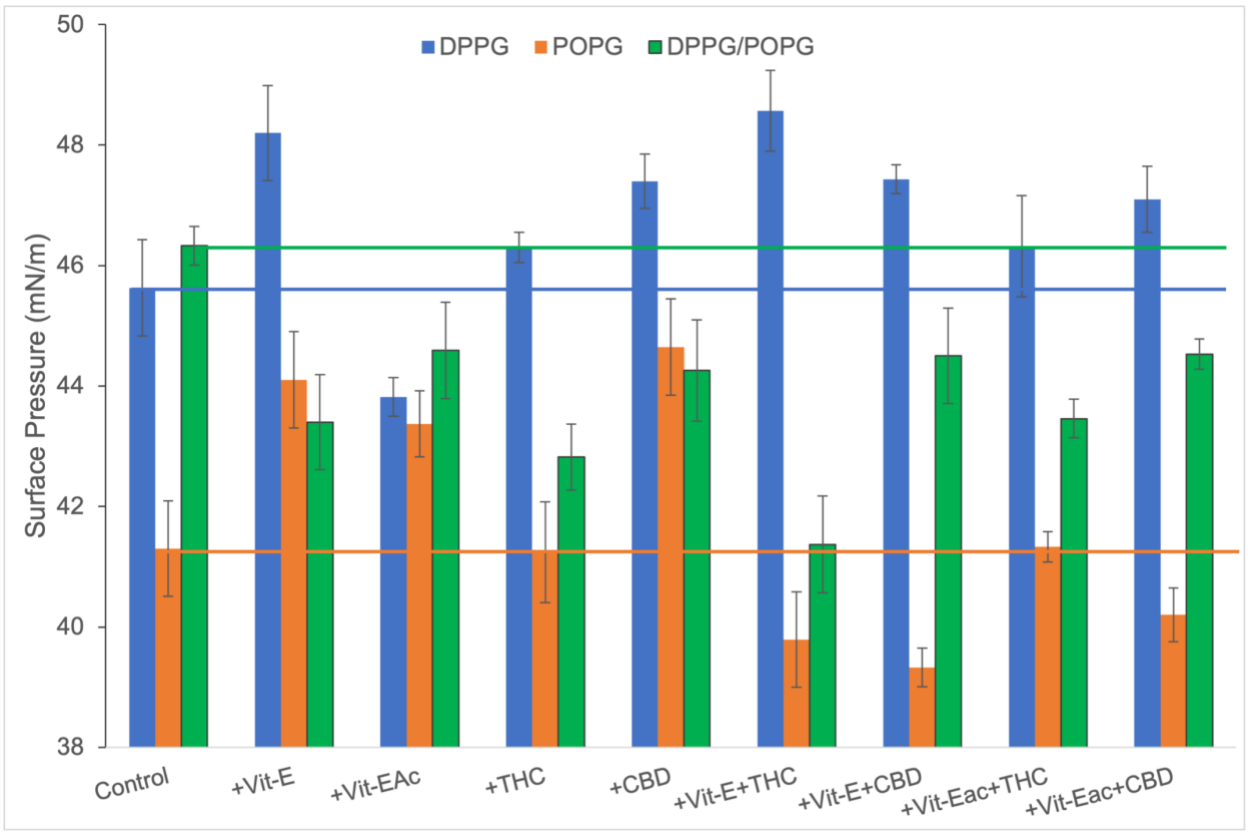

Figure 24. Collapse pressure of PG lipid films in single or double additive systems. Blue bars: DPPG additive systems; Orange bars: POPG-additive systems; Green bars: DPPG/POPG-additive systems.

Most of the DPPG-additive systems do not have a significant effect on film stability. Isotherms demonstrated that the additive may be expelled from the film, so while lipid organization is altered at low pressure, there is no lasting effect on film stability.

Similar to POPC, POPG is considerably more stable in the presence of most additive mixtures, given the ordering effect these additives seem to exhibit on unsaturated lipids. Despite the binary PG mixture containing largely POPG (6:1 POPG:DPPG), an overall decrease in film stability is seen. This effect may be further elucidated by BAM imaging, which also for effects on lateral organization to be determined that are not readily apparent from the isotherms alone

4.2 Brewster Angle Microscopy Images

BAM always for direct visualization of lateral film organization. Domain formation is unique for a given lipid film and provides useful information about the state the film is in. Changes to characteristic film organization by vape additives provide additional information regarding their effects on lipid organization that are not immediately evident from surface pressure-area isotherms alone.

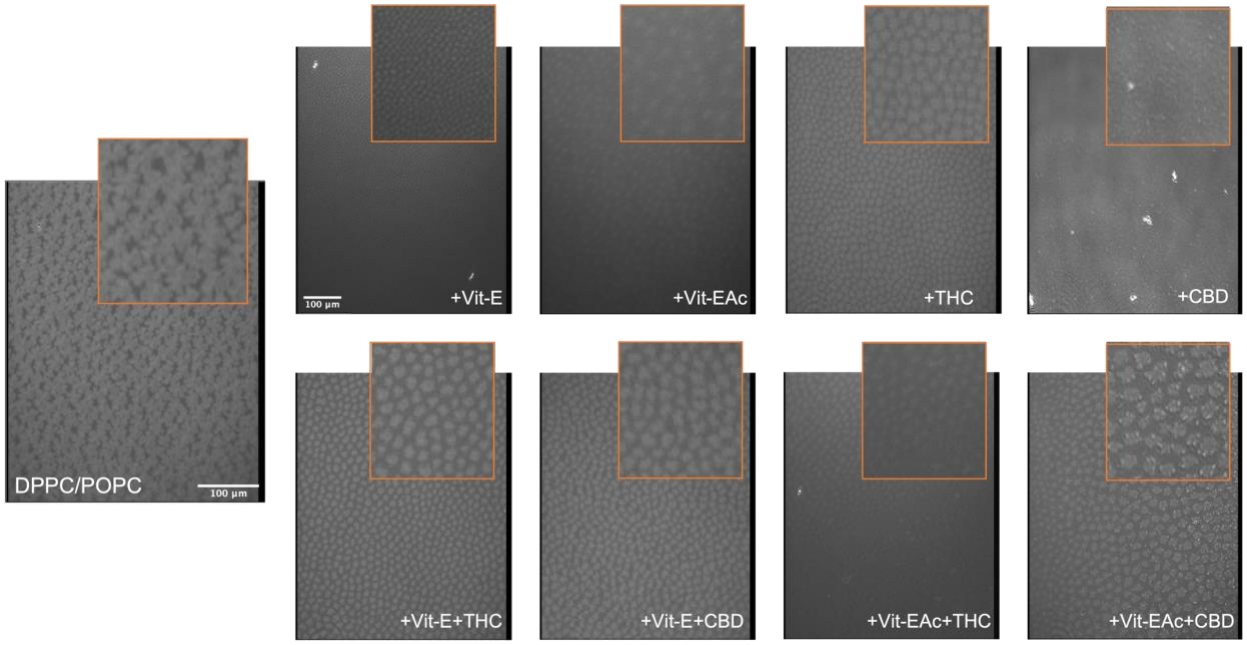

Figure 25. BAM images of POPC monofilm at 30 mN/m. Lipid-additive mixtures were made at a 95:5 molar ratio for single additive systems, and 95:2.5:2.5 molar ratio for double additive systems. Image dimensions are 418x519 microns and a 100 micron scale bar is shown in the control image. Inserts are 2x magnification.

Figure 24 shows the lateral domain formation of PC monolayers at 30 mN/m of pressure. Pure DPPC/POPC film shows almost complete coalescence of the LC phase, with small packets of LE phase. Lineactant activity of Vit-E is apparent by the formation of small circular domains. Addition of 5% Vit-EAc reduces the size of these domains as well and increases the space between them. This supports the notion that the lipids cannot pack tightly and that the film has become more fluid

THC also increases spacing between domains; however it does not significantly alter domain shape as it does not act as a lineactant. Instead, its fluidization of the film is apparent by the increase in LE phase. Interestingly, the presence of CBD resulted in a somewhat homogenous film, with a few large clusters of material dispersed throughout, as seen by the bright points in the image.

The double additive mixtures behave similarly with regards to domain formation. Favouring the formation of jagged domains in an orderly arrangement. The mixture containing Vit-EAc and CBD also displayed bright points on the edges of these domains. These protrusions may be due to Vit-EAc clustering at the domain boundaries.

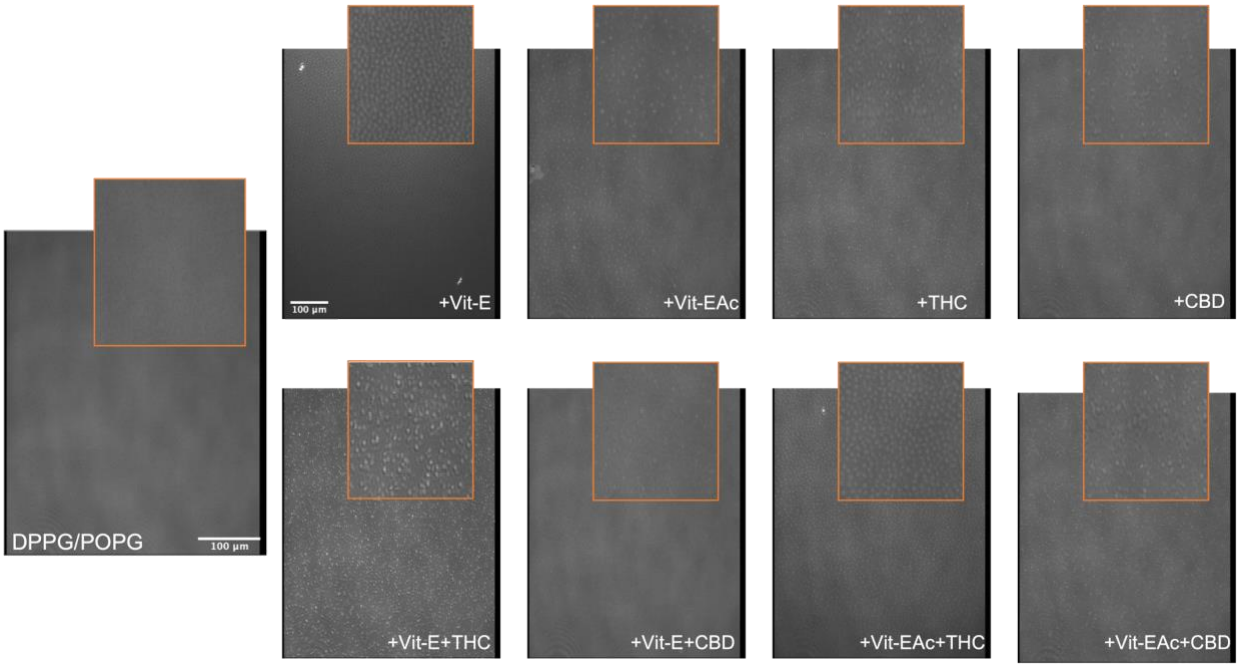

Figure 26. BAM images of POPG monofilm at 30 mN/m. Lipid-additive mixtures were made at a 95:5 molar ratio for single additive systems, and 95:2.5:2.5 molar ratio for double additive systems. Image dimensions are 418x519 microns and a 100 micron scale bar is shown in the control image. Inserts are 2x magnification.

DPPG/POPG pure films display a homogenous film at high surface pressures. The small portion of DPPG is mixed throughout the film and does not readily form LC domains. Addition of all

additives demixes the film. These systems display a heterogenous lateral organization, with Vit-E and Vit-EAc+THC resulting in significant domain formation domains. The other lipid-additive systems result in small clusters forming throughout the film, indicating packing defects. Vit-E+THC displays spikes, or protrusions, of the film as indicated by the brighter points in the BAM image. This system showed the most significant decrease in collapse pressure, at 41 mN/m compared to 46 mN/m of the control. Disruption of proper lipid packing and formation of additive-lipid clusters consequently destabilize the film.

Tight packing of the LS upon expiration is key to maintaining a low surface tension and protecting the alveoli against collapse. Likewise, the availability of lipids to spread out and enter a fluid state after inhalation maintains the structure of the film. Vitamin E has demonstrated to prevent both of these things by fluidizing lipids in the gel state and rigidifying them in the liquid state. Lipid-additive systems that result in protrusions from the film are accompanied by a notable decrease in collapse pressure.

Proper lipid packing is critical to a stable functional film. Here, it is seen that disruption of proper packing in binary lipid mixtures reduces stability of the film. This is visualized by alterations to domain formation and clustering of surfactant material. Previous works have shown good correlation between *in vitro* and *in vivo* results using this type of investigative approach [82]. The Langmuir-Blodgett trough with BAM together can aid in assessing the impact of vape additives on surfactant health before they are introduced to the market.

Chapter 5: Vaping additives negatively impact the stability and lateral film organization of lung surfactant model systems
(Published paper in Nanomedicine: https://doi.org/10.2217/nnm-2021-0398)

5.1 Background

The use of e-cigarettes or vapes has been a growing trend in North America as they were advertised as safer smoking alternatives. These devices heat an "e-liquid" solution comprised primarily of propylene glycol or vegetable glycerin containing flavorings and sometimes nicotine, into an inhalable aerosol [1]. Recreational vaping is commonplace amongst adolescents and young adults due to the variety of products and flavours [2], including cannabis-based vapes, which contain tetrahydrocannabinol (THC) and cannabidiol (CBD) oils. These cannabinoids have negative effect on adolescent neurodevelopment [3], but may also impede lung health. Indeed, increasing hospitalizations from lung illnesses related to cannabinoid vapes have been reported [4].

In 2019, the Centers for Disease Control and Prevention identified a new class of severe lung illnesses, known as e-cigarette, or vaping, product use-associated lung injury (EVALI) [5]. The bronchoalveolar lavage (BAL) fluid of afflicted individuals contained additives, which may lead to EVALI and were absent in healthy vape users. These include vitamin E acetate (Vit-EAc) and THC [5]. Moreover, other structurally related molecules (see Figure 1) such as vitamin E (Vit-E) and CBD may inflict comparable harm.

The mode of action of EVALI is still under investigation, however common symptoms like difficulty breathing or lung collapse point to a negative impact on lung surfactant (LS) [6]. The low vapor pressure of Vit-EAc and THC results in aerosol particles in the nanometer range (60-200 nm) [7]. Particles of this size deposit primarily in the alveolar space [8], where LS is located. LS contains lipids (90%) and proteins (10%) and forms a monofilm lining the alveoli [9]. Proper LS function requires this mixture to maintain stability during the breathing cycle and to prevent

alveolar collapse during exhalation [9]. Exhalation reduces the surface area and induces high lateral pressure requiring the presence of rigid, tightly packed lipids to maintain film integrity. The squeeze out mechanism suggests that fluid unsaturated lipids are removed during compression, whereas the supercompressibility model proposes that rapid compression results in some "super compressed" lipids that will not be squeezed out but promote low surface tension [10]. In contrast, increasing surface areas during inhalation requires fast respreading of LS, as provided by fluid lipids.

The most important lipid classes providing these two functions are phosphatidylcholines (PC) and phosphatidylglycerols (PG) [9]. The main component dipalmitoylphosphatidylcholine (DPPC) is a fully saturated phospholipid enabling tight packing and the formation of rigid structures. The second key lipid is palmitoyloleoyl phosphatidylglycerol (POPG), which contains an unsaturated bond promoting fluid monofilms for effective respreading. We have chosen a binary biomimetic model, as these lipids represent the two main lipid classes in LS and are suitable to study the impact of vaping additives on the key functions of LS. Other LS models have been used to characterize effects of vape additives [11,12] and investigated with biophysical methods [13-16].

The biophysical investigation used a Langmuir-Blodgett trough with monofilms spread at the air-water interface to assess lipid packing, film stability and elasticity. Compression and expansion cycles were used to mimic respiration. Finally, the lateral film organization was visualized by Brewster angle microscopy (BAM). These methods were used to determine changes in biophysical properties of LS in the nano- and micrometer size range upon addition of EVALI additives (Vit-E, Vit-EAc, THC, CBD).

5.2 Materials and Methods:

Materials: Dipalmitoylphosphatidylcholine and palmitoyloleoylphosphatidylglycerol were purchased from Avanti Polar Lipids Inc. (Alabaster, AL, USA). Vitamin E (Sigma Aldrich), Vitamin E acetate (Medisca, Richmond, BC, Canada), both tetrahydrocannabinol and cannabidiol were obtained from Cerilliant Corporation (Round Rock, TX, USA). ACS grade chloroform and methanol used to dissolve the lipids were purchased from EMD chemicals (Mississauga, ON, Canada). Sodium chloride and HEPES were obtained from Sigma Aldrich, and calcium chloride dihydrate from Thermofisher Scientific (Markham, ON, Canada).

Preparation of Goerke's buffer [17]: 140 mM NaCl, 10 mM HEPES, and 2.5 mM $CaCl_2 \cdot 2H_2O$ were dissolved in 1 L ultrapure water, pH adjusted to 6.9 and filtered using a 0.45μm Nalgene bottle top filter (Thermofisher Scientific).

Lipid/Additive Solutions: 1 mM DPPC and POPG were dissolved in chloroform:methanol (6:4 v/v and combined at a 4:1 molar ratio reflecting their biological abundance [18] for use on the Langmuir trough. 1 mM additive solution in methanol were mixed with the lipids. Combinations of lipids and additive for single additive samples were at a 95:5 molar ratio (lipid:additive), while double additive systems were mixed at molar ratios of 95:2.5:2.5 (lipid:additive1:additive2).

Surface Pressure-Area Isotherm: The surface pressure of the films at the air-water interface was recorded with a Wilhemy plate (Biolin, Manchester, UK) at 25 ºC. 110 mL of Goerke's buffer served as subphase in a 22.5 x 10 cm Teflon Langmuir trough. 25 μL of solution was deposited dropwise on the subphase surface at an initial area of 195 cm^2. Compression with a Teflon barrier at the max rate of 96.9 cm^2/min, but well below compression speed of lungs of 0.1 to 0.5 Hz [19], was carried out 10 minutes after film deposition, to ensure solvent evaporation. Experiments were recorded in triplicate using Nima 7.8 software (Biolin, UK) to ensure reproducibility.

Compressibility: Compressibility at a given surface pressure was calculated as the slope of the isotherm at selected pressures [20].

Equation S1:

$$k_\pi = (-1/A_\pi)(dA/d\pi)_\pi$$

Where A_π is the corresponding surface area at the given pressure, and $dA/d\pi$ is the slope at the selected pressure. The reciprocal of compressibility was then taken to yield the compressibility modulus, which is more readily comparable to bilayer values [21]

Equation S2:

$$C_m = k_\pi^{-1}$$

Brewster Angle Microscopy (BAM): BAM was performed using a Brewster angle microscope and EP3 software provided by Accurion (Göttingen, Germany). Briefly, BAM allows direct visualization of the lateral film organization [22] (details in supplemental). Lipid domain coverage (%) was analyzed using ImageJ (NIH, Bethesda, MA, USA)

3D Domain Visualization: 3D images of the films were obtained using the EP3 software. This signal intensity is translated into relative heights to generate a pseudo 3D image.

Film Thickness: The gray scale in the BAM images provides information on reflectivity data, which along with the refractive indices of monolayer and subphase can be used to calculate domain thickness [23,24].

To estimate the thickness of the domains a calibration curve of the reflectivity vs the gray level of a BAM image of a clean subphase was recorded. This curve was used to convert the gray level to a reflected light intensity (Rp) from BAM images of the domains.

The refractive index of the monolayer was determined by measuring the reflectivity at angles between 52-56° and calculating the refractive index of the subphase (n_2) using equation 1. A plot

of reflectivity against the calculated refractive index is used to find the refractive index of the monolayer (n) by fitting to equation 2. The refractive index of the monolayer (n) was estimated from the minimum value of the parabola.

Equation 1:

$$n_2 = tan(\theta_B)$$

Equation 2:

$$R_p(n_2) = \frac{an_2^4 - bn_2^4 + c}{dn_2^2 + e}$$

$$a = n^4 - 2n^2n_1^2 + n_1^4, b = 2n^6 - 4n^4n_1^2 + 2n^2n_1^4, c = n^8 - 2n^6n_1^2 + n^4n_1^4,$$
$$d = n^4, e = n^4n_1^2$$

The thickness of the liquid condensed domains were calculated from the reflectivity of the domains obtained the BAM images and calculated with equation 3. Using an approximation of n_1 =1, the previously determined n and n_2 =1.33 values.

Equation 3:

$$l = \frac{\sqrt{Rp}}{sin(2\theta_B - 90)}\left(\frac{\pi\sqrt{n_1^2 + n_2^2})(n_1^2 - n^2) \times (n_2^2 - n^2)}{\lambda(n_1^2 - n_2^2)n^2}\right)^{-1}$$

Statistics

Samples were repeated in triplicate and statistical differences from the samples treated with vitamins and cannabinoids analyzed using t-test.

Equation 4:

$$t = \frac{m - u}{s/\sqrt{n}}$$

Where m is the sample mean, u is the theoretical value, s is the standard deviation and n is the sample size. Each of the samples treated with vaping additives were compared to the controls to determine if they are significantly different ($p \leq 0.05$).

5.3 Results:

The lipophilic nature of these vape additives promotes their partitioning into lung surfactant and may lead to physical changes of the monolayer. Such effects may impact LS structure and function and consequently respiration. Thus, the presented biophysical investigation is important to understand potential mechanisms.

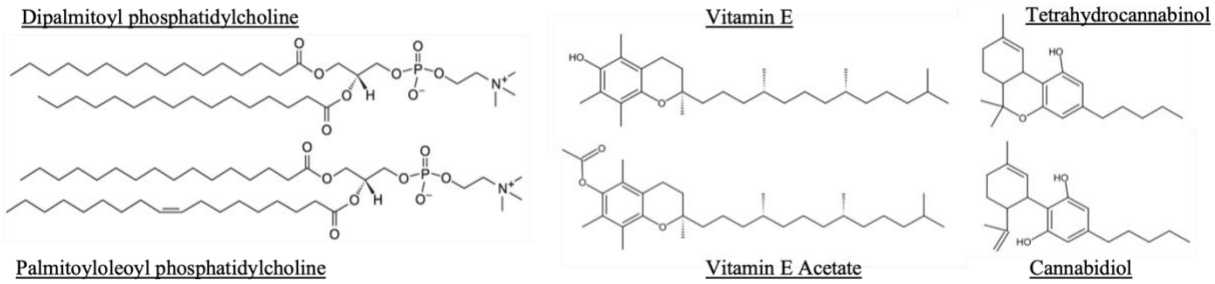

Figure 27. Structures of phospholipids and vape additives.

Surface pressure-area isotherms:

Figure 27 displays surface pressure-area isotherms of the individual lipid components with and without Vit-E, to better compare the isothermal changes in the lipid mixture. Vit-E shifts the characteristic LE/LC coexistence phase plateau of DPPC to higher pressures from 6 mN/m to 8 mN/m. The transition into the LC phase occurs at a higher pressure and starts earlier at 63 $Å^2$/molecule and 9 mN/m (vs 58 $Å^2$/molecule and 7 mN/m). The collapse pressure remains similar at ~51 mN/m. The characteristic long gentle slope range of POPG starting at 40 mN/m was eliminated by the presence of Vit-E. Moreover, the onset of surface pressure was observed at a larger take-off area of 117 $Å^2$/molecule. The isotherm has shifted to smaller areas, indicting better

packing and reached a slightly higher collapse pressure of 44 mN/m compared to 42 mN/m for pure POPG.

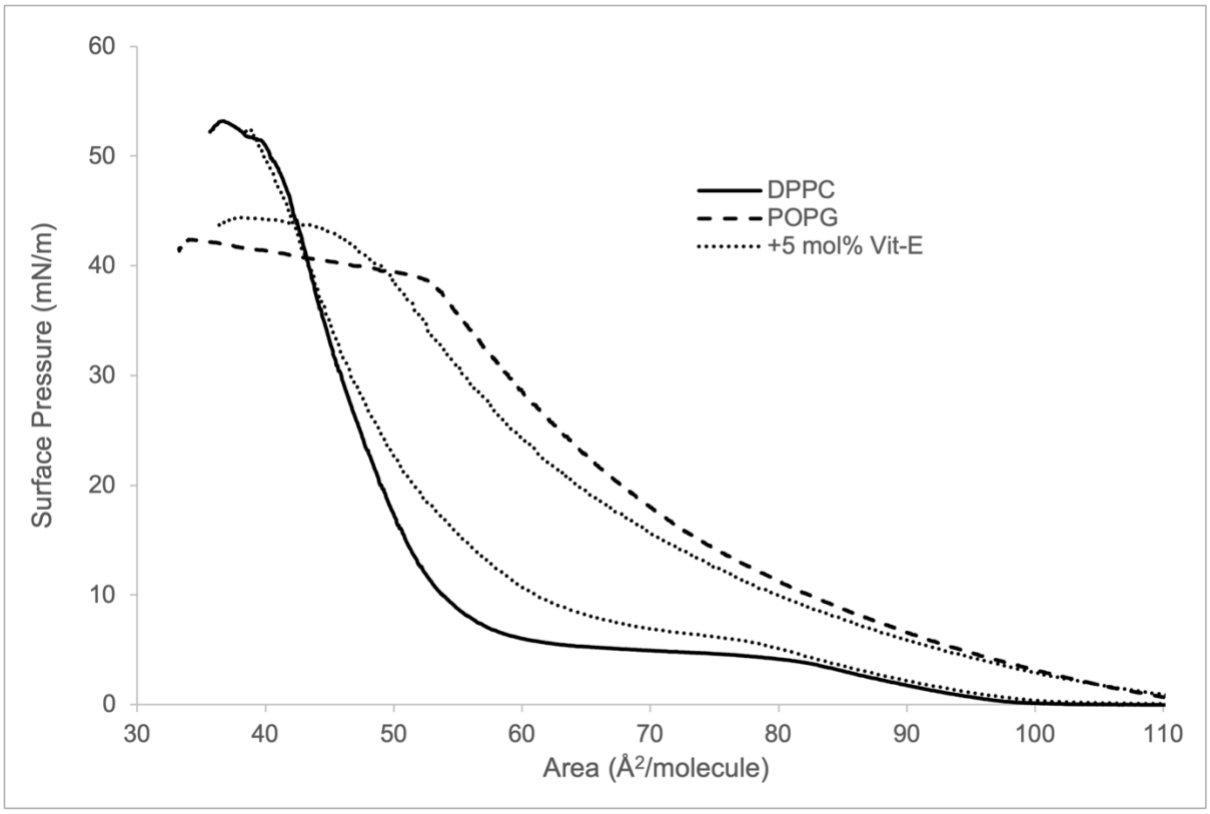

Figure 28. Surface pressure-area isotherms for DPPC and POPG lipid controls with Vit-E.

Figure 28 illustrates the surface pressure-area isotherms of the DPPC/DPPG=4/1 mol% LS model system with and without additives. DPPC/POPG monolayers exhibit various phases throughout compression, indicated by the isotherm shape (details in supplemental). The gas phase is observed at areas above 100 Å^2/molecule, where lipids have a high degree of freedom and a surface pressure of 0 mN/m. The take-off of lateral pressure at 100 Å^2/molecule indicates transition into the liquid-expanded (LE) phase, where lipids start interacting. A change in slope above 71 Å^2/molecule and a pressure of 9 mN/m, indicates a phase transition to the liquid-condensed (LC) phase. POPG transforms the distinct plateau region of DPPC at this pressure [25] to a more gradual transition into the LC phase. The slope increases again at ~55 Å^2/molecule and 16 mN/m, where the DPPC

component is almost exclusively in the LC phase, until the collapse pressure of ~51 mN/m, which is a measure of film stability. The addition of 5% Vit-E and Vit-EAc slightly shifted isotherms to larger areas indicating less packing. Both decrease the collapse pressure by 2.9 mN/m and 1.7 mN/m, slightly less for the more hydrophobic Vit-EAc. The cannabinoid systems result in smaller areas but a similar reduction of the collapse pressure as Vit-E.

All additive isotherms exhibit similar trends when compared to controls. To better compare multiple systems, bars graphs of area/molecules at distinct pressure values (10-40 mN/m) are shown in Figure 28A for single and Figure 28B for binary additions.

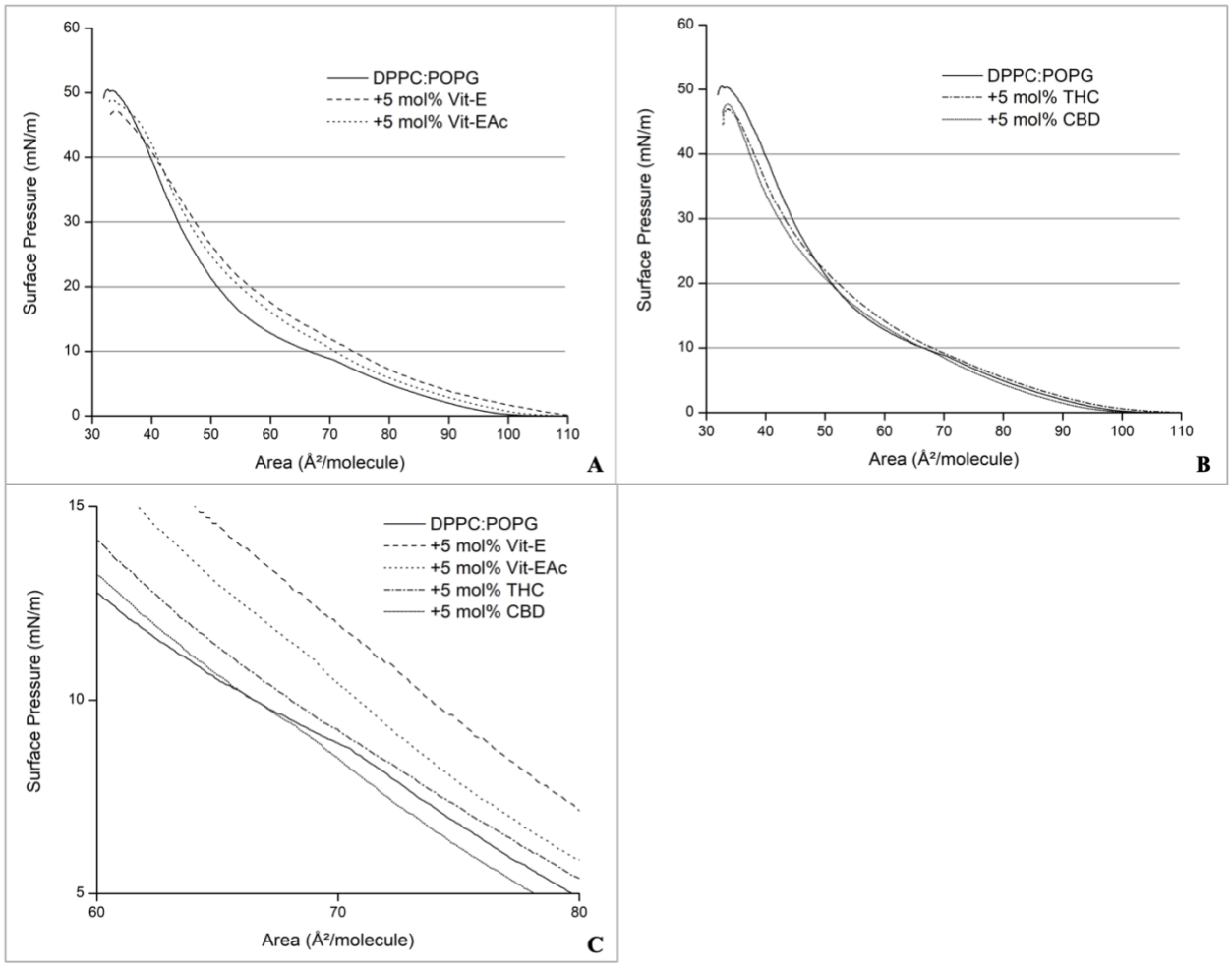

Figure 29. Surface pressure-area isotherms of DPPC:POPG (4:1 molar ratio). **(A)** With Vit-E and Vit-EAc. **(B)** With THC and CBD. **(C)** Enhanced image of shoulder present on isotherms between 5 and 15 mN/m.

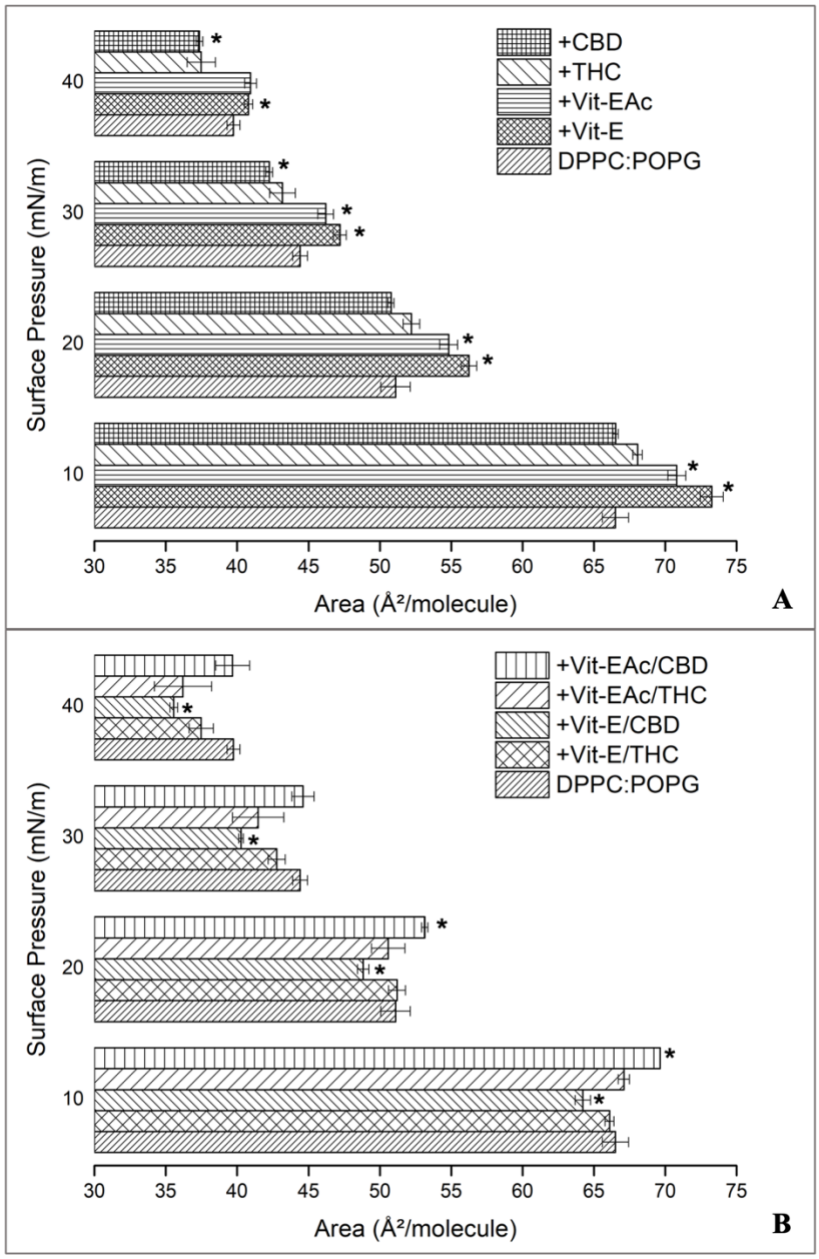

Figure 30. Surface area of the lipid system in the presence of additives at given surface pressures. **(A)** Single additive systems; molar ratio of 95:5 (lipid:additive) **(B)** Double additive systems; molar ratio of 95:2.5:2.5 (lipid:additive 1:additive 2). *Statistically significant differences from controls.

Table 3 Take-off area, collapse pressure, and compressibility moduli. *Statistically significant differences from controls

Lipid System	**Take-off Area (**Å^2/molecule)	**Collapse Pressure (mN/m)**	**Compressibility Modulus at 30 mN/m (mN/m)**
DPPC:POPG	99±0	50±0	99±2
+5% Vit-E	108±0 *	47±0*	71±1 *
+5% Vit-EAc	103±0 *	49±1 *	84±6 *
+5% THC	103±1 *	47±1*	80±1 *
+5% CBD	97±0 *	48±2*	77±1 *
+2.5% Vit-E + 2.5% THC	99±0	49±0 *	83±5 *
+2.5% Vit-E + 2.5% CBD	93±1 *	45±1 *	70±4 *
+2.5% Vit-EAc + 2.5% THC	100±1	47±0 *	81±6 *
+2.5% Vit-EAc + 2.5% CBD	100±0 *	49±1 *	84±1 *

The average of 3 isotherms of additives compared to LS controls (see Figure 29) shows that only Vit-E induced statistically relevant changes to larger areas. Binary 1:1 mixtures of Vit-E or Vit-EAc with one of the cannabinoids are presented in Figure 29B. Mixtures of the more hydrophobic Vit-EAc (compared to Vit-E) and CBD show the largest area increases at all pressures indicating reduced lipid packing, whereas Vit-E and THC mixtures are similar to controls. Interestingly, the equimolar mixture of Vit-E with the more polar CBD (compared to THC), shows a statistically relevant change to smaller areas indicating better lipid packing at all pressures.

Compressibility:

Surface area-pressure isotherms report on lipid packing and film stability, while the compressibility modulus (C_m) indicates how easily a film can be compressed, thus assessing film elasticity. Higher C_m value reflect films that resist compression, indicating tighter packed lipids. Values below 100 mN/m point to fluid and compressible films [26].

The reported pressure range during the respiratory cycles is between 40 and 70 mN/m [27]. Due to the simpler composition of the model system, the collapse pressure is lower than 70 mN/m, therefore a range of 10 to 40 mN/m was chosen to reflect similar phases to the biological system. Table 1 shows C_m values at 30 mN/m, within the selected range but well below the collapse pressure. Each additive system reduced C_m values compared to controls with a C_m of 99 mN/m. Vit-E had the strongest impact and reduced C_m by 28 mN/m, followed by CBD with 22 mN/m. THC and Vit-EAc were similar with 19 and 15 mN/m. For binary additives, Vit-E and CBD had the strongest effect and reduced Cm by 29 mN/m, whereas all others showed comparable reductions of ~17 mN/m.

Isocycles:

In addition to single compression isotherms, expansion-compression cycles report changes over time to better mimic the breathing cycle. Films were compressed to pressures well below the collapse point, and then expanded to pressure above 5 mN/m, thus maintaining well-established monofilms. If material is lost over time, film compression to smaller areas is needed to achieve the same pressure. The extent of the shift is proportional to the material lost from the interface. While the composition of the lost material is not known, it is reasonable to assume, based on squeeze out theory and the fact that the calculated slope values showed a progressive increase (+0.35), that the fluid components (i.e. POPG and the additives) will be removed first.

Figure 30A shows an enhanced image of 10 cycles of DPPC:POPG area-pressure isotherms of recorded between 5 and 40 mN/m. To assess if an equilibrium was reached in Figure 30, the isocycles were extended to 20 cycles (Figure 30A insert). The shift in area after 10 cycles was ~2.8 $Å^2$/molecule and higher after 20 cycles at 5.9 $Å^2$/molecule. Panel B describes material loss as area changes between the 1st (solid arrow) and 10th cycle (dotted arrow) at 20 mN/m. The control was the most stable system with an area shift of 2.8 $Å^2$/molecule (Figure 30B). All additives increased this shift, indicating enhanced material loss. The cannabinoids had the strongest impact with shifts of 5.1 $Å^2$/molecule for CBD and 3.7 $Å^2$/molecule for THC. In contrast, Vit-E and Vit-EAc, displayed the smallest changes of 3.0 and 3.4 $Å^2$/molecule, respectively. In double additive systems, Vit-E and Vit-EAc exhibited larger shifts with THC, 4.5 and 4.4 $Å^2$/molecule, than with CBD (4.0 and 3.8 $Å^2$/molecule)

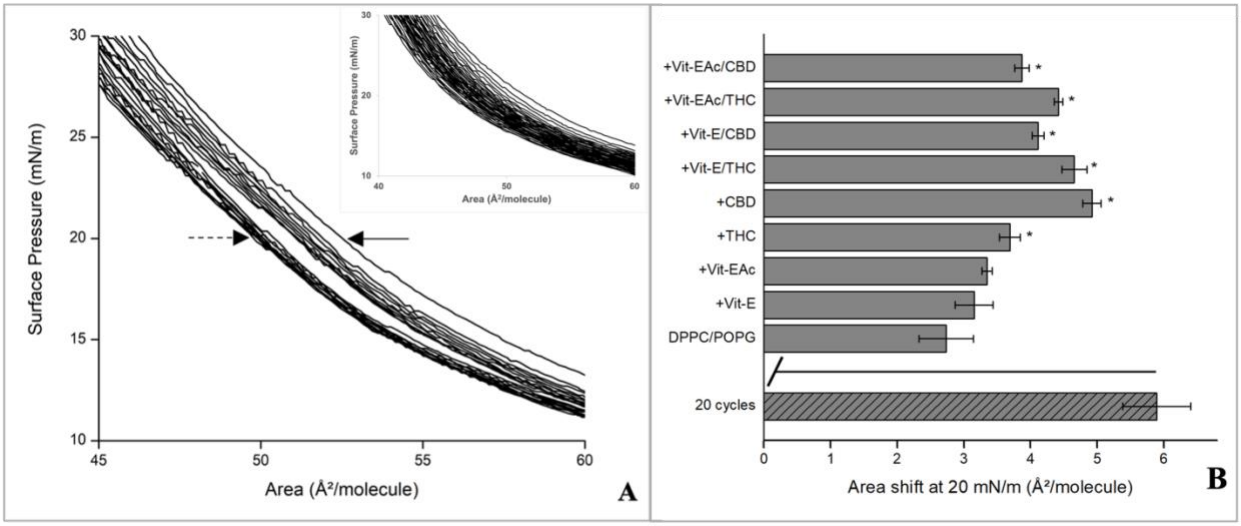

Figure 31. A: Surface pressure-area isotherm for 10 isocycles of DPPC:POPG between max and min surface pressures of 40 mN/m and 5 mN/m (an enhanced region between 30 and 10 mN/m is shown). Arrows indicate surface area shift at 20 mN/m between the 1st (solid arrow) and 10th (dotted arrow) cycle. Insert shows 20 cycles of DPPC:POPG between the same pressures. **B**: Shift in surface area for all systems at 20 mN/m after 10 compression/expansion cycles. Dashed bar indicates area shift for control after 20 cycles. *Statistically significant differences from controls.

BAM Images:

BAM adds complementary information by visualizing changes to the lateral film organization. Upon compression, lipids pack tighter and saturated lipids like DPPC exhibit domain formation in the LE-LC phase coexistence and the LC phase [28], while unsaturated POPG remains in the LE phase throughout compression. BAM images were taken at 25 mN/m, after transition into the LC phase and midrange of the isocycles, to assess changes in domain structure at higher pressure but well below the film collapse pressure.

As expected, DPPC/POPG controls displayed characteristic DPPC domains. The branched domains slowly grow in size, however, POPG prevents the film from homogenizing into a complete LC phase at high pressures (Figure 31A) as seen for DPPC alone [28].

The overall domain shapes are comparable, thus only more striking changes will be discussed. Vit-EAc (Figure 31C) exhibits initially circular domains that grow in size and form an ordered arrangment. The single cannabinoid additions show limited changes to domain shapes and organization. The mixture of Vit-E with THC exhibits less defined and small circular domains with a bright signal suggesting a structure protruding from the film (solid arrow) (Figure 31F) while the overall film organization suggests demixing with large areas of LE phase (dashed arrow) and intermitant domain clusters. Vit-EAc and THC combined (compare panels C and D) exhibit domains that are similar to THC in terms of shape (Figure 31H) whereas domains in CBD containing mixtures are much less defined than both single additions (Figure 31I).

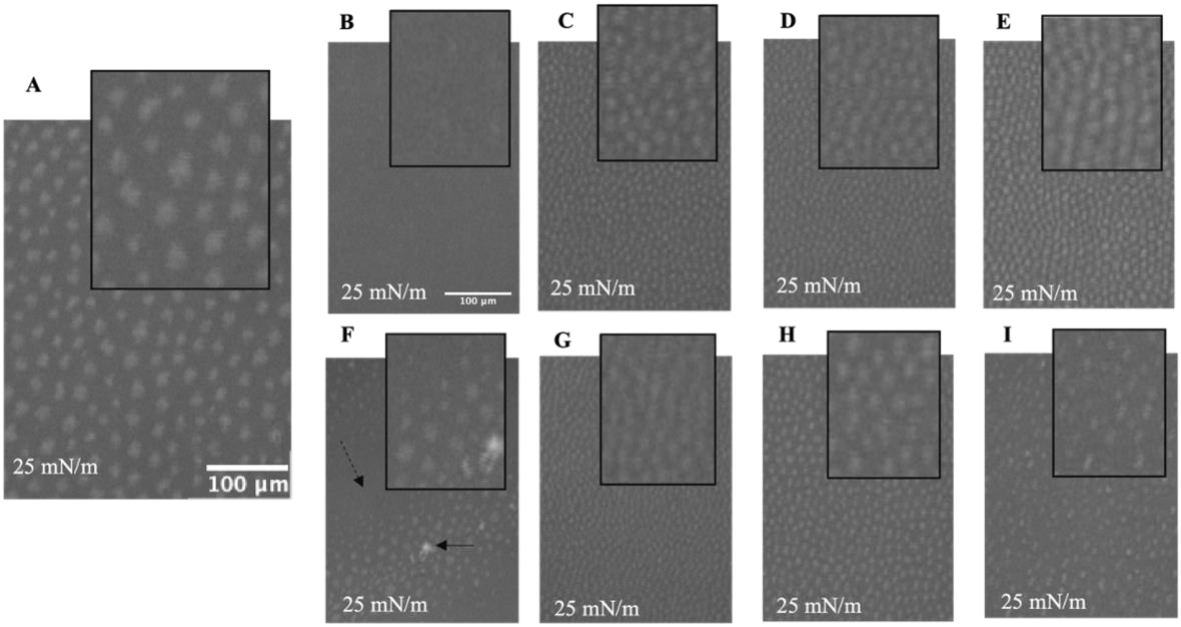

Figure 32. BAM images of lipid systems at 25 mN/m surface pressure. **(A)** DPPC:POPG (4:1). **(B)** Lipids:Vitamin E (95:5). **(C)** Lipids:Vitamin E acetate (95:5) **(D)** Lipids:THC (95:5) **(E)** Lipids:CBD (95:5). **(F)** Lipids:Vitamin E:THC (95:2.5:2.5). **(G)** Lipids:Vitamin E:CBD (95:2.5:2.5). **(H)** Lipids:Vitamin E acetate:THC (95:2.5:2.5). **(I)** Lipids:Vitamin E acetate:CBD (95:2.5:2.5).

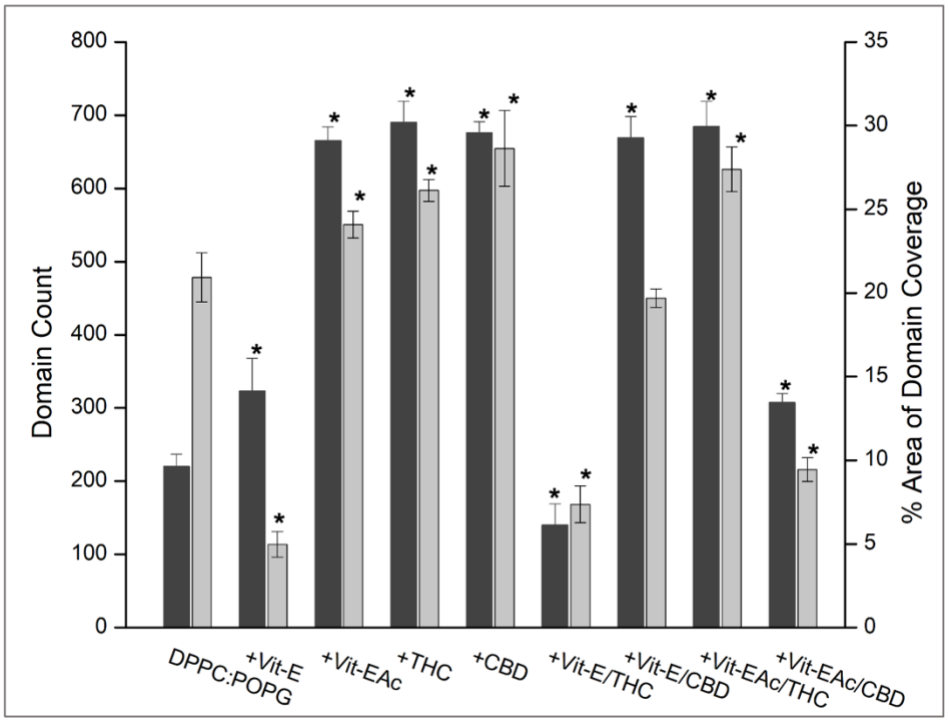

Figure 33. Number of domains (dark grey) and area% domain coverage (light grey) of each lipid system at 25 mN/m Data was extracted from BAM images with ImageJ. Images with dimensions 133x162 μm were used for analysis. n=3. *Statistically significant differences from control.

Domain formation was signficantly reduced by Vit-E with a concomittant increase of domain frequency. In contrast, Vit-EAc favoured the formation of many smaller domains which covered a larger area%. The cannabinoids led to numerous tightly packed domains with the highest counts and more uniform sizes. The mixture of Vit-E and THC resulted in overall better mixing throughout the film, with clusters of domains that varied in size but closely resembled the shape of DPPC/POPG (domain coverage compared to controls 21.1±1.6 vs 20.9±1.5)

3D analysis of the BAM images more clearly shows changes in lateral organization between control and additive samples. Vit-E and Vit-EAc not only reduced domain areas, but also reduced domain height, as seen by lower signal intensities (Figure 33 B, C).

The 3D images reveal numerous packed domains in systems containing Vit-EAc, THC, and CBD (Figure 33 C, D, E) with a stronger shift to more fluid LE regions with Vit-E+THC (Figure 33 F). Mixtures of either vitamins with CBD display nonuniform domain sizes, which was less evident in 2D BAM images.

These intensities were used to estimate LC domain thicknesses, following previously published methods [23]. Vit-E and Vit-EAc displayed large decreases in thickness with changes of >0.1 nm (Figure 34). THC alone, and in presence of the vitamins resulted in no significant change to domain thickness. CBD on the other hand, increased thickness by 0.09 nm and double additive systems with CBD resulted in significant reduction of domain thickness by 0.1 nm and 0.07 nm, with Vit-E and Vit-EAc, respectively.

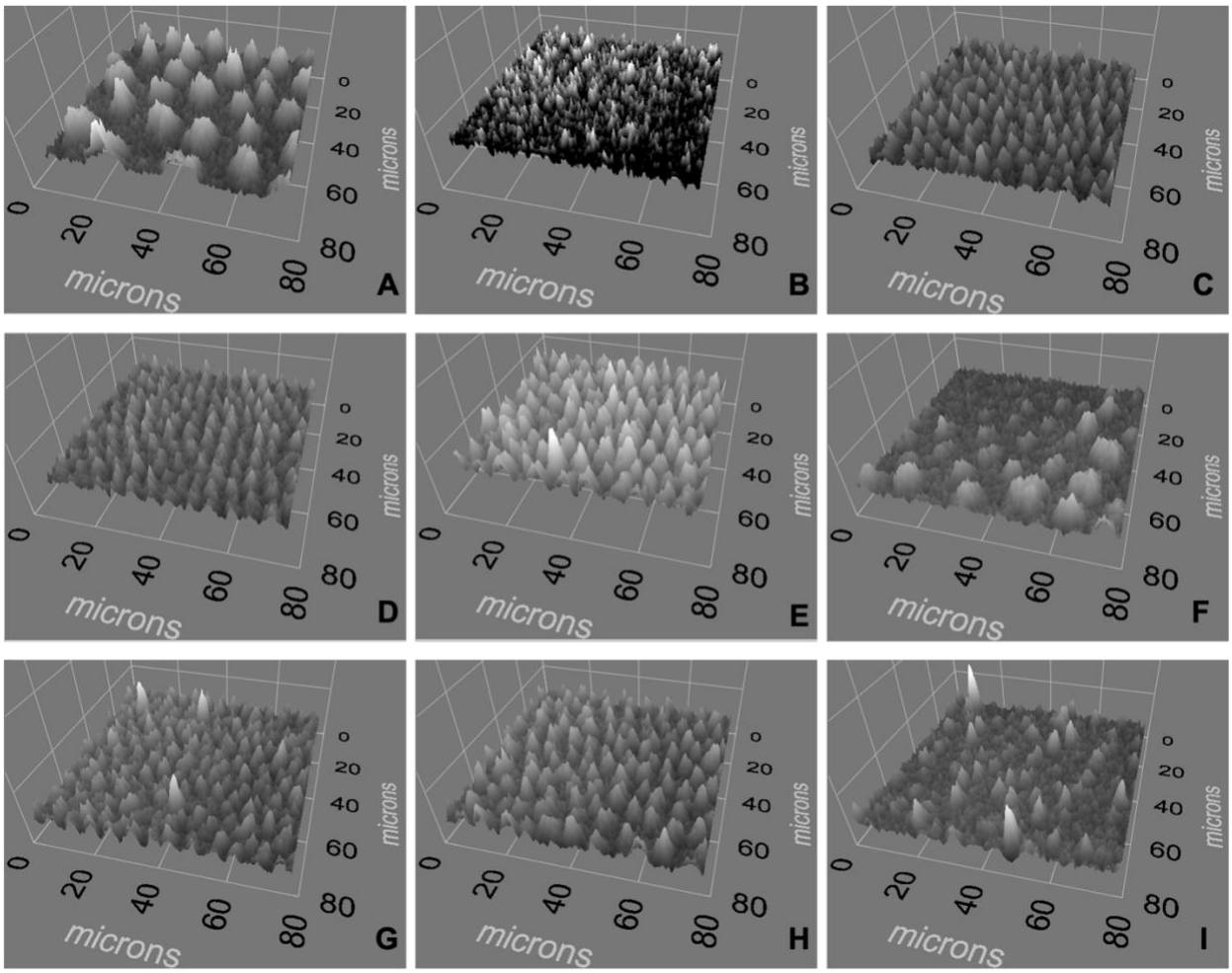

Figure 34. 3D representation of the lateral organization at 25 mN/m. **(A)** DPPC:POPG (4:1). **(B)** Lipids:Vitamin E (95:5). **(C)** Lipids:Vitamin E acetate (95:5) **(D)** Lipids:THC (95:5) **(E)** Lipids:CBD (95:5). **(F)** Lipids:Vitamin E:THC (95:2.5:2.5). **(G)** Lipids:Vitamin E:CBD (95:2.5:2.5). **(H)** Lipids:Vitamin E acetate:THC (95:2.5:2.5). **(I)** Lipids:Vitamin E acetate:CBD (95:2.5:2.5).

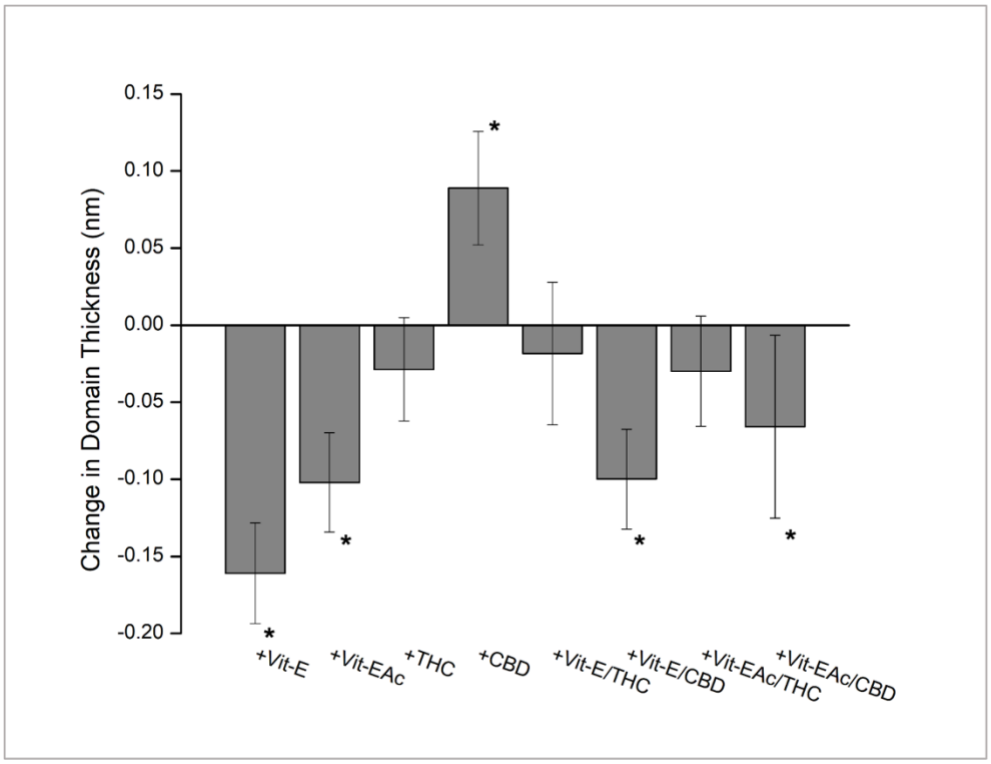

Figure 35. Change in thickness of DPPC:POPG (4:1) domains in the presence of additives. *Statistically significant differences from controls

5.4 Discussion:

A complimentary set of biophysical methods suitable to study biologically relevant lung surfactant models were used, including area-pressure isotherms [21] and Brewster angle microscopy [29]. Utilizing this approach, we have demonstrated a correlation of *in vitro* and *in vivo* results on the fatal outcome of coated versus uncoated nanoparticles in mice [30].

The rigid DPPC dominates the overall shape of the isotherms. The addition of 5 mol% additive is a conservative concentration compared to values reported in vaping fluids of 23-80% [31] But significant changes in all aspects as discussed below were observed.

Both, Vit-E and Vit-EAc, result in somewhat larger molecular areas (+6.8 and +4.4 $Å^2$/molecule) (Figures 28,29), larger lift off areas, predominantly for Vit-E (Table 1), and slightly reduced collapse pressures (-2.9 and -1.8 mN/m), suggesting less tightly packed and moderately destabilized films. In contrast, cannabinoids somewhat improved packing, as reflected by

comparable lift-off areas (Table 1) and smaller molecular areas throughout compression, while the moderately reduced collapse pressure was maintained (Figures 28 and 29).

Comprehensive reviews described the membrane behavior of Vit-E [32,33] and report its localization at the bilayer interface [34]. The Vit-E and Vit-EAc results align with previous differential scanning calorimetry reports for bilayers of saturated dimyristoyl PC (14 versus 16 carbons in DPPC). Both reduced the phase transition temperature from gel to liquid-crystal phase, broadened the peak and reduced the enthalpy [35,36]. It is believed that methyl substituents on the phytyl chain of Vit-E restrict it from forming a conformation similar to all-trans chains of lipids in the gel state [36]. This feature localizes Vit-E to more fluid states of the membrane [33,35], however, it has been observed by fluorescence measurements to perturb acyl chain packing of lipids in either the liquid-crystalline or gel state [36]. This suggests the potential for a negative impact on LS packing at all stages of compression. Moreover, Vitamin E has been reported to decrease mobility in the liquid-crystalline phase but decrease order in the gel phase, while Vit-E-ac had much less effects [37]. Finally, Vit-E has been reported to be a linactant [38], which is relevant for the discussion of BAM images below. In the single systems, results were independent of the lipid headgroup, suggesting interactions between the hydroxyl group of Vit-E and phosphate or carbonyls groups of the phospholipids [33,39]. The acetate group makes the Vit-E derivative somewhat less polar resulting in a deeper membrane location [37,39]. The trends observed here are similar but weaker compared to Vit-E, which agrees with DSC [36] and fluorescence results [37].

The addition of the bulkier rings of the cannabinoids exhibited comparable take off areas for CBD and a moderate increase for THC (Table 1). Both isotherms more closely followed the control curve, with slightly larger areas for THC (Figures 28,29). Moreover, the isotherm kink

around 8 mN/m due to LE-LC phase coexistence is basically abolished (Figure 28C) suggesting more homogeneous packing. Above 20 mN/m these isotherms exhibit smaller molecular areas (Figure 28,29A) indicating better lipid packing, although the moderate collapse pressure reduction was similar to the vitamins (Table 1). Considering the low amount of additives, the observed changes are moderate but relevant.

DSC data for 5% THC in DPPC reported broader peaks and reduced transition temperatures reflecting significant changes of the membrane phase behavior and unique peaks at higher concentrations were attributed to complex formation between THC and DPPC [40]. Insertion of CBD below the headgroups that affected membranes elasticity was reported as well [41]. Insertion below the headgroup and hydrophobic interactions between cannabinoid rings and lipid acyl chains would explain the reduced molecular areas, while at higher pressures, these rings could prevent best packing thereby moderately reducing the collapse pressure.

Interestingly, area increases for double additions were the strongest for Vit-EAc and CBD, followed by their binary mixture and single additions relative to controls (Figure 29B). Complexes between Vit-EAc and THC based on hydrogen bonds between the carbonyl oxygen of the vitamin and the hydroxyl group of the cannabinoid were reported [42] (Figure 19). CBD has two hydroxyl groups and may be able to form such H-bonds, potentially to a larger extent than THC (Figure 18). Indeed, Vit-EAc and CBD have a lower take off area than other mixtures (Table 1). In contrast, cannabinoid mixtures with Vit-E show comparable take-off areas (Table 1) but smaller area changes for both cannabinoids (Figure 4). The biggest collapse pressure reduction, indicating film destabilization, was seen for Vit-E and CBD, followed by Vit-EAc and THC. CBD possess free rotation around one of its cyclic rings, which could affect interactions with other molecules and lipid packing in the film.

Compressibility Modulus:

Compressibility moduli are a measure for film elasticity indicating the ease of film compression [20]. C_m values >100 mN/m indicate rigid LC phases, whereas values <100 mN/m suggest fluid LE phases [26]. This method has been used to determine elasticity in mixtures of sphingo- and phospholipids [21,43] and it was suitable to study the impact of vape additives on LS model LS. Controls had C_m values of 99±2 mN/m, which is close to the transition to LC phases and all additives reduced C_m. Addition of 5 mol% Vit-E changed the C_m value the most (72±1 mN/m; Table 1) presumably due to hydrogen bonding with the phospholipids (see above) and contributions of hydrophobic interactions with the acyl chains. These interactions stabilize Vit-E within the monolayer, however due to its shape, chain length, and methylated phytyl tail, it is unable to be accommodated by neighboring phospholipids, reducing compressibility. 5 mol% CBD and its binary mixture with Vit-E displayed reduced C_m, values of 77±1 and 70±4 mN/m (Table 1). CBD has two hydroxyl groups for hydrogen bonding, and unlike THC, free rotation around one of its aromatic rings, which may explain the difference to THC (Figure 18). Conversely, CBD in the presence of Vit-EAc only displays a C_m value of 84±1 mN/m, potentially due to the reduced H-bonding ability of the acetate.

Native LS contains more rigid components like cholesterol and saturated lipids (e.g. dipalmitoylphosphatidyl glycerol) [44]. Better-packed lipids are more prone to packing alterations than fluid systems.

The observed changes document potential negative effect of additives on LS. This concern is confirmed in the BAM section below.

Isocycles:

In addition to altered film rigidity, increased loss of film material would compromise LS stability and function. Material is lost naturally from the interface during breathing cycles but is recycled via processes involving surfactant proteins [9], and the release of lipids from type II pneumocytes for reincorporation into LS [9]. The observed shifts to smaller areas upon cycling are illustrated in Figure 30A,B. A normal breathing process would be 10-20 cycles per min [45] and thus changes over 10 cycles shown here are concerning. LS is a highly dynamic system undergoing rapid compression and expansion. The Langmuir trough cannot match physiological compression speeds and DPPC/POPG cannot be compressed beyond 50 mN/m to avoid irreversible film collapse. Nevertheless, the observed trends reflect biophysical changes in these films.

Vit-E and Vit-EAc contributed less to material loss than the cannabinoids (Figure 30B). Their smaller ring size and extended side chain will allow better interactions with the lipid side chains and thus reduce material loss, whereas cannabinoids have bulkier rings and very short side chains, which will negatively affect lipid packing and enhance potential for material loss.
This may contribute to the moderate reduction in collapse pressure (Table 1). CBD has the strongest overall effect, while THC exhibited stronger effects than the vitamins.

CBD is slightly more polar than THC due to its two hydroxyl groups [46] and could be more readily squeezed out into the subphase. CBD complexes with vitamins show more loss than the vitamins alone, but less than CBD alone. The above mentioned complex may form via hydrogen bonding, in a similar way described for THC with Vit-EAc, promoting retention in the monolayer [42]. The strong effect of CBD + Vit-EAc may be related to its structure as mentioned

previously. In contrast, THC complexes with vitamins exhibit more material loss than the individual components.

The fact that these complexes promote material loss over 10 cycles is concerning and could contribute to the negative health impacts observed in EVALI [47].

BAM Images:

The negative additive impact on the LS model clearly altered the lateral film organzation. Interestingly, the isotherms exhibited less changes than the BAM images. Similar observations have been reported for interactions of biocompatible nanoparticles with model LS [48].

Domains represent more rigid film regions, and their formation is influenced by chain length mismatch between lipids, various lipid types or differences in curvature [49]. The partly unsaturated and fluid POPG interacts with DPPC and reduces domain sizes by lowering line tension around their boundaries [50].

A similar effect is observed for Vit-EAc containing samples. All additives reduced the domain size and generally led to more circular shapes. Lipid domain sizes are governed by line tension [50], while shape and morphology are dominated by the orientation of molecular dipoles [51].

Molecular dynamics simulations show Vit-E partitioning into domain boundaries and the resulting lower line tension reduces domain sizes [52]. For more details on various mechanism of nanodomain formation and stabilization see DiPasquale et al. [38] and references within. The cannabinoids show more domains at higher pressures compared to controls. Moreover, binary mixtures containing Vit-E and Vit-EAc display more effects, dominated by the vitamins, but to a lesser extent for the acetate. Stronger interactions between vitamins and cannabinoids based on hydrogen bonding and the interfacial location of the vitamins are potential explanations.

The 3D images provide a more intuitive illistration of the additive impact on domain formation, size and size distribution and frequency (Figure 33). The relatively even domain distribution for controls is strongly reduced by Vit-E, and to a lesser extent Vit-EAc. The deeper membrane localization of Vit-EAc [39] has a stronger potential to affect hydrophobic interactions.

Cannabinoids results in more domains, while their binary mixtures are dominated by the vitamins, again due to smaller rings, longer side chain and better packing of the latter. Binary additions exhibit stronger effects than each of the single additions, except in the case of changes to domain size and thickness, presumably due to hydrogen bonding between vitamins and cannabinoids which enables them to act synergistically in a stable complex. The double additive system with Vit-E and THC lead to less domain formation, suggesting improved lipid mixing , while CBD in the presence of either vitamin displayed less uniform domains (Figure 33G,I). Vit-EAc and cannabinoid mixtures can also form H-bonds [42] but presumabley to a lesser extent and the cannabinoids dominate the systems.

Other studies show that Vit-E, Vit-EAc and an oxidized derivative also impact the LS compressibility modulus [11]. Other vaping additives such as propylene glycol and glycerol are able to deposit onto surfactant and alter DPPC molecules orientation at the interface [12]. While minor changes were observed for interfacial properties, organization of the multilayers were altered upon exposure of clinical surfactant to e cigarete vapor [53]. Moreover, a decreases in surface pressure for LS models was also reported [54]. Vaping solutions found to cause EVALI contained Vit-EAc ranging from 22-88% [31], suggsting that higher doses may be deposited into the lungs. It has been hypothesized that Vit-EAc may act as a linactant by reducing line tension between domains [55]. Our data indicate less line tension leading to smaller domains but to a lesser

extent than the known linactant Vit-E [52]. The highly ordered phases are critical for anchoring surfactant proteins B and C to facilitate monolayer folding and respreading upon inhalation.

Potential implications of vape additives on lung surfactant *in vitro* and *in vivo:*

Packing defects in more heterogeous lipid mixtures will affect interactions with proteins [56] and induce changes of surface charge density and surface potentials. While these data present a comprehensive set of biophysical data on the impact of vitamin and cannabinoid additives on major LS lipids, it is important to briefly refer to a minor component, the sterol cholesterol. Cholesterol is tightly controlled at 5-10% w/w of phospholipids [17] and is critical for maintaining low surface tensions [57], the formation of multilayers during exhalation [58] and it exhibits strong interaction with DPPC domains, which are important to withstand high lateral compression [59]. The structural similarity between vitamins and cholesterol suggests that their effects on LS may be related, as both rings and side chains will anchor them into the monolayer. Due to a similar membrane location, Vit-E may compete with cholesterol [35,60] or outcompete the sterol in some cases. Vit-E showed a stronger impact on DPPC membrane phase behavior than cholesterol whereby 2% exceeded the effect of 10% sterol [60]. Finally, Vit-E induced stronger curvature in membranes than cholesterol [61], which may affect the complex protein assisted film folding during exhalation. The importance of cholesterol in lung surfactant function warrants further investigation in future studies.

EVALI is commonly associated with respiratory symptoms of coughing, chest pain, and shortness of breath [47], in extreme cases pulmonary edema with hypoxemia and partial lung collapse [6]. The presented biophysical changes to LS may contribute to a compromised LS function.

5.3 Conclusion:

The observed changes agree with previous biophysical data on the impact of vitamins and cannabinoids on membranes like DPPC obtained by surface tension measurements, DSC, neutron scattering, fluorescence and infrared spectroscopy [36,37,62,63].

Changes to the dynamic ability of surfactant to be both, highly compressible and fluid enough for rapid respreading, can have a large impact on respiratory functions. The vaping additives exhibited the capability to reduce compressibility, collapse pressure, interfere with lipid organization and induce potential loss of material upon cycling. Vit-E displayed the largest effects on domain formation and size, while mixtures with cannabinoids greatly reduced domain uniformity and promoted demixing in some cases. These biophysical changes may contribute to the reduced respiratory function in EVALI and these results provide insight into a potential mechanism of vaping additives based on their interference of the proper lipid function.

5.4 References

(1) Eissenberg, T.; McRobbie, H. Electronic Cigarettes: Review of Use, Content, Safety, Effects on Smokers, and Ptential for Harm and Benefit. *Physiol. Behav.* 2018, **176** (5), 139–148. https://doi.org/10.1111/add.12659.Electronic.

(2) Pepper, J. K.; Lee, Y. O.; Watson, K. A.; Kim, A. E.; Nonnemaker, J. M.; Farrelly, M. C. Risk Factors for Youth E-Cigarette "Vape Trick" Behavior. *J. Adolesc. Heal.* 2017, **61** (5), 599–605. https://doi.org/10.1016/j.jadohealth.2017.05.010.

(3) Jacobus, J.; Tapert, S. Effects of Cannabis on the Adolescent Brain. *Curr. Pharm. Des.* 2014, **20** (13), 2186–2193. https://doi.org/10.2174/13816128113199990426.

(4) Center of Disease Control, Accessed Sept^{27th} 2021, URL: https://www.cdc.gov/tobacco/basic_information/e-cigarettes/severe-lung-disease.html https://doi.org/10.1016/j.cis.2014.03.009.

(5) Blount, B. C.; Karwowski, M. P.; Shields, P. G.; Morel-Espinosa, M.; Valentin-Blasini, L.; Gardner, M.; et al. Vitamin E Acetate in Bronchoalveolar-Lavage Fluid Associated with EVALI. *N. Engl. J. Med.* 2020, **382** (8), 697–705. https://doi.org/10.1056/nejmoa1916433.

**** paper of considerable interest: This paper illustrates the problem of EVALI, symptoms and list potential causes**

(6) Christiani, D. C. Vaping-Induced Acute Lung Injury. *N. Engl. J. Med.* **2020**, *382* (10), 960–962. https://doi.org/10.1056/nejme2000860.

(7) Mikheev, V. B.; Klupinski, T. P.; Ivanov, A.; Lucas, E. A.; Strozier, E. D.; Fix, C. Particle Size Distribution and Chemical Composition of Aerosolized Vitamin E Acetate. *Aerosol Sci. Technol.* 2020, **54** (9), 993–998. https://doi.org/10.1080/02786826.2020.1783431.

(8) Tsuda, A.; Henry, F. S.; Butler, J. P. Particle Transport and Deposition: Basic Physics of Particle Kinetics. *Compr. Physiol.* 2013, **3** (4), 1437–1471. https://doi.org/10.1002/cphy.c100085.

(9) Dziura, M.; Mansour, B.; Dipasquale, M.; Chandrasekera, P. C.; Gauld, J. W.; Marquardt, D. Simulated Breathing: Application of Molecular Dynamics Simulations to Pulmonary Lung Surfactant. *Symmetry (Basel).* **2021**, *13* (7), 1–19. https://doi.org/10.3390/sym13071259.

(10) Rugonyi, S.; Biswas, S. C.; Hall, S. B. The Biophysical Function of Pulmonary Surfactant. *Respir. Physiol. Neurobiol.* **2008**, *163* (1–3), 244–255. https://doi.org/10.1016/j.resp.2008.05.018.

**** paper of considerable interest: This is one of the key papers explaining the biophysical role of lung surfactant**

(11) Dipasquale, M.; Gbadamosi, O.; Nguyen, M. H. L.; Castillo, S. R.; Rickeard, B. W.; Kelley, E. G.; Nagao, M.; Marquardt, D. A Mechanical Mechanism for Vitamin E Acetate in E-Cigarette/Vaping-Associated Lung Injury. *Chem. Res. Toxicol.* **2020**, *33* (9), 2432–2440. https://doi.org/10.1021/acs.chemrestox.0c00212.

**** paper of considerable interest: This work provides insight into mechanism for the impact of Vitamin E acetate on lung surfactant model systems**

(12) Hayeck, N.; Zoghzoghi, C.; Karam, E.; Salman, R.; Karaoghlanian, N.; Shihadeh, A.; Eissenberg, T.; Zein El Dine, S.; Saliba, N. A. Carrier Solvents of Electronic Nicotine Delivery Systems Alter Pulmonary Surfactant. *Chem. Res. Toxicol.* **2021**, *34* (6), 1572–1577. https://doi.org/10.1021/acs.chemrestox.0c00528.

(13) Guzmán, E.; Santini, E. Lung Surfactant-Particles at Fluid Interfaces for Toxicity Assessments. *Curr. Opin. Colloid Interface Sci.* **2019**, *39*, 24–39. https://doi.org/10.1016/j.cocis.2019.01.003.
(14) Sosnowski, T. R.; Kubski, P.; Wojciechowski, K. New Experimental Model of Pulmonary Surfactant for Biophysical Studies. *Colloids Surfaces A Physicochem. Eng. Asp.* **2017**, *519*, 27–33. https://doi.org/10.1016/j.colsurfa.2016.06.044
(15) Sosnowski, T. R.; Podgórski, A. Assessment of the Pulmonary Toxicity of Inhaled Gases and Particles with Physicochemical Methods. *Int. J. Occup. Saf. Ergon.* 1999, **5** (3), 431–447. https://doi.org/10.1080/10803548.1999.11076430.
(16) Guzmán, E.; Santini, E.; Ferrari, M.; Liggieri, L.; Ravera, F. Interaction of Particles with Langmuir Monolayers of 1,2-Dipalmitoyl-Sn-Glycero-3-Phosphocholine: A Matter of Chemistry? *Coatings* 2020, **10** (5). https://doi.org/10.3390/COATINGS10050469.
(17) Leonenko, Z.; Finot, E.; Vassiliev, V.; Amrein, M. Effect of Cholesterol on the Physical Properties of Pulmonary Surfactant Films: Atomic Force Measurements Study. *Ultramicroscopy* 2006, **106** (8–9), 687–694. https://doi.org/10.1016/j.ultramic.2006.02.007.
(18) Bernhard, W.; Haagsman, H. P.; Tschernig, T.; Poets, C. F.; Postle, A. D.; Van Eijk, M. E.; Von Der Hardt, H. Conductive Airway Surfactant: Surface-Tension Function, Biochemical Composition, and Possible Alveolar Origin. *Am. J. Respir. Cell Mol. Biol.* 1997, **17** (1), 41–50. https://doi.org/10.1165/ajrcmb.17.1.2594.
(19) Gómez-Gil, L.; Schürch, D.; Goormaghtigh, E.; Pérez-Gil, J. Pulmonary Surfactant Protein SP-C Counteracts the Deleterious Effects of Cholesterol on the Activity of Surfactant Films under Physiologically Relevant Compression-Expansion Dynamics. *Biophys. J.* **2009**, *97* (10), 2736–2745. https://doi.org/10.1016/j.bpj.2009.08.045.
(20) Vollhardt, D.; Fainerman, V. B. Progress in Characterization of Langmuir Monolayers by Consideration of Compressibility. *Adv. Colloid Interface Sci.* 2006, **127** (2), 83–97. https://doi.org/10.1016/j.cis.2006.11.006. (14)
(21) Broniatowski, M.; Flasiński, M.; Dynarowicz-ŁĄtka, P.; Majewski, J. Grazing Incidence Diffraction and X-Ray Reflectivity Studies of the Interactions of Inorganic Mercury Salts with Membrane Lipids in Langmuir Monolayers at the Air/Water Interface. *J. Phys. Chem. B* 2010, **114** (29), 9474–9484. https://doi.org/10.1021/jp101668n.
(22) Hönig, D.; Möbius, D. Direct Visualization of Monolayers at the Air-Water Interface by Brewster Angle Microscopy. *J. Phys. Chem.* 1991, **95** (12), 4590–4592. https://doi.org/10.1021/j100165a003.
(23) Pusterla, J. M.; Malfatti-Gasperini, A. A.; Puentes-Martinez, X. E.; Cavalcanti, L. P.; Oliveira, R. G. Refractive Index and Thickness Determination in Langmuir Monolayers of Myelin Lipids. *Biochim. Biophys. Acta - Biomembr.* 2017, **1859** (5), 924–930. https://doi.org/10.1016/j.bbamem.2017.02.005.
(24) Winsel, K.; Hönig, D.; Lunkenheimer, K.; Geggel, K.; Witt, C. Quantitative Brewster Angle Microscopy of the Surface Film of Human Broncho-Alveolar Lavage Fluid. *Eur. Biophys. J.* 2003, **32** (6), 544–552. https://doi.org/10.1007/s00249-003-0290-2.
(25) Diamant, H.; Witten, T. A.; Ege, C.; Gopal, A.; Lee, K. Y. C. Topography and Instability of Monolayers near Domain Boundaries. *Phys. Rev. E - Stat. Physics, Plasmas, Fluids, Relat. Interdiscip. Top.* 2001, **63** (6), 1–17. https://doi.org/10.1103/PhysRevE.63.061602.

(26) Davies, J. T.; Rideal, E. K. Interfacial Phenomena. *Dev. Solid Oral Dos. Forms Pharm. Theory Pract. Second Ed.* 1961, Chapter 5, 217–281. https://doi.org/10.1016/B978-0-12-206056-4.50009-6

(27) Piknova, B.; Schram, V.; Hall, S. B. Pulmonary Surfactant: Phase Behavior and Function. *Curr. Opin. Struct. Biol.* 2002, **12** (4), 487–494. https://doi.org/10.1016/S0959-440X(02)00352-4.

(28) McConlogue, C. W.; Vanderlick, T. K. A Close Look at Domain Formation in DPPC Monolayers. *Langmuir* 1997, **13** (26), 7158–7164. https://doi.org/10.1021/la970898e.

(29) Daear, W.; Mahadeo, M.; Prenner, E. J. Applications of Brewster Angle Microscopy from Biological Materials to Biological Systems. *Biochim. Biophys. Acta - Biomembr.* 2017, **1859** (10), 1749–1766. https://doi.org/10.1016/j.bbamem.2017.06.016.

(30) Al-Hallak, M. H. D. K.; Azarmi, S.; Sun, C.; Lai, P.; Prenner, E. J.; Roa, W. H.; Löbenberg, R. Pulmonary Toxicity of Polysorbate-80-Coated Inhalable Nanoparticles; In Vitro and in Vivo Evaluation. *AAPS J.* 2010, **12** (3), 294–299. https://doi.org/10.1208/s12248-010-9190-4.

*** paper of interest: This work shows the use of the methods used in this work to assess the impact of coated versus uncoated nanoparticles in mice. The results direct correlation between in vitro and in vivo results.**

(31) U.S. Food and Drug Administration. Lung Injuries Associated with Use of Vaping Products, Accessed Dec21st 2021. URL: https://www.fda.gov/news-events/public-health-focus/lung-injuries-associated-use-vaping-products

(32) Atkinson, J.; Harroun, T.; Wassall, S. R.; Stillwell, W.; Katsaras, J. The Location and Behavior of α-Tocopherol in Membranes. *Mol. Nutr. Food Res.* 2010, **54** (5), 641–651. https://doi.org/10.1002/mnfr.200900439.

(33) Atkinson, J.; Epand, R. F.; Epand, R. M. Tocopherols and Tocotrienols in Membranes: A Critical Review. *Free Radic. Biol. Med.* 2008, **44** (5), 739–764. https://doi.org/10.1016/j.freeradbiomed.2007.11.010.

(34) Marquardt, D.; Williams, J. A.; Kuc, N.; Wassall, S. R.; Katsaras, J.; Harroun, T. A. Tocopherol Activity Correlates with Its Location in a Membrane: A New Perspective on the Antioxidant Vitamin E. *J. Am. Chem. Soc.* **2013**, 7523–7533.

(35) Wang, X.; Quinn, P. J. The Location and Function of Vitamin E in Membranes (Review). *Mol. Membr. Biol.* 2000, **17** (3), 143–156. https://doi.org/10.1080/09687680010000311.

(36) Massey, J. B.; She, H. S.; Pownall, H. J. Interaction of Vitamin E with Saturated Phospholipid Bilayers. *Biochem. Biophys. Res. Commun.* 1982, **106** (3), 842–847. https://doi.org/10.1016/0006-291X(82)91787-9.

(37) Massey, J. B. Interfacial Properties of Phosphatidylcholine Bilayers Containing Vitamin E Derivatives. *Chem. Phys. Lipids* 2001, **109** (2), 157–174. https://doi.org/10.1016/S0009-3084(00)00216-4.

(38) DiPasquale M, Nguyen MHL, Rickeard BW, *et al.* The antioxidant vitamin E as a membrane raft modulator: Tocopherols do not abolish lipid domains. *Biochim. Biophys. Acta - Biomembr*. 2020, **1862** (8), 183189. https://doi.org/10.1016/j.bbamem.2020.183189.

(39) Gomez-Fernandez, J. C.; Villalain, J.; Aranda, F. J.; Oritz, A.; Micol, V.; Coutinho, A.; et al. Localization of A-Tocopherol in Membranes. *Annals of the New York Academy of Sciences*. 1989, **570** (1), 109–120. https://doi.org/10.1111/j.1749-6632.1989.tb14912.x

(40) Mavromoustakos, T.; Theodoropoulou, E.; Papahatjis, D. Studies on the Thermotropic Effects of Cannabinoids on phosphatidylcholine bilayers using differential scanning calorimetry and small angle X-ray diffraction. *Biochim Biophys Acta.* 1996, **1281** (2), 235–244. doi: 10.1016/0005-2736(96)00027-2.

*** paper of interest: This work provides experimental data on the impact of THC on membrane biophysics. There are limited published data on this topic.**

(41) Hillard, C. J.; Harris, R. A.; Bloom, A. S. Effects of the Cannabinoids on Physical Properties of Brain Membranes and Phospholipid Vesicles: Fluorescence Studies. *J. Pharmacol. Exp. Ther.* 1985, **232** (3), 579–588.

(42) Lanzarotta, A.; Falconer, T. M.; Flurer, R.; Wilson, R. A. Hydrogen Bonding between Tetrahydrocannabinol and Vitamin E Acetate in Unvaped, Aerosolized, and Condensed Aerosol e-Liquids. *Anal. Chem.* 2020, **92** (3), 2374–2378. https://doi.org/10.1021/acs.analchem.9b05536.

**** paper of considerable interest: This work provides experimental evidende for h-bonding between additives, which could explain the enhanced effects observed in this work.**

(43) Ali, S.; Brockman, H. L.; Brown, R. E. Structural Determinants of Miscibility in Surface Films of Galactosylceramide and Phosphatidylcholine: Effect of Unsaturation in the Galactosylceramide Acyl Chain. *Biochemistry* 1991, **30** (47), 11198–11205. https://doi.org/10.1021/bi00111a002.

(44) Postle, A. D.; Heeley, E. L.; Wilton, D. C. A Comparison of the Molecular Species Compositions of Mammalian Lung Surfactant Phospholipids. *Comp. Biochem. Physiol. - A Mol. Integr. Physiol.* 2001, **129** (1), 65–73. https://doi.org/10.1016/S1095-6433(01)00306-3.

(45) Braun, S. R. Respiratory Rate and Pattern. *Clin. Methods Hist. Phys. Lab. Exam. Third Ed.* 1990. Chapter 43, 226-230.

(46) Wongwailikhit, K.; Jiratchaya, J. Comparison of the Two Common Solvents for THC and CBD Extractions. *Proc. 7th World Congr. Mech. Chem. Mater. Eng.* 2021, 1–7. https://doi.org/10.11159/iccpe21.115.

(47) Chadi, N.; Minato, C.; Stanwick, R. Cannabis Vaping: Understanding the Health Risks of a Rapidly Emerging Trend. *Paediatr. Child Health (Oxford).* 2020, **25**, S16–S20. https://doi.org/10.1093/pch/pxaa016.

(48) Daear, W.; Lai, P.; Anikovskiy, M.; Prenner, E. J. Differential Interactions of Gelatin Nanoparticles with the Major Lipids of Model Lung Surfactant: Changes in the Lateral Membrane Organization. *J. Phys. Chem. B.* 2015, **119**. 5356–5366.

(49) García-Sáez, A. J.; Chiantia, S.; Schwille, P. Effect of Line Tension on the Lateral Organization of Lipid Membranes. *J. Biol. Chem.* 2007, **282** (46), 33537–33544. https://doi.org/10.1074/jbc.M706162200.

(50) Benvegnu, D.; McConnell, H. Line Tension between Liquid Domains in Lipid Monolayers. *J. Phys. Chem.* 1992, **96**, 6820–6824.

(51) McConnell, H.M., de Koker, R., 1996. Equilibrium thermodynamics of lipid monolayer domains. *Langmuir*. 1996, **12** (20), 4897–4904.

(52) Muddana, H. S.; Chiang, H. H.; Butler, P. J. Tuning Membrane Phase Separation Using Nonlipid Amphiphiles. *Biophys. J.* 2012, **102** (3), 489–497. https://doi.org/10.1016/j.bpj.2011.12.033.

(53) Przybyla, R. J.; Wright, J.; Parthiban, R.; Nazemidashtarjandi, S.; Kaya, S.; Farnoud, A. M. Electronic Cigarette Vapor Alters the Lateral Structure but Not Tensiometric

Properties of Calf Lung Surfactant. *Respir. Res.* **2017**, *18* (1), 1–13. https://doi.org/10.1186/s12931-017-0676-9.
(54) Davies, M. J.; Leach, A. G.; Fullwood, D.; Mistry, D.; Hope, A. The PH Dependent Interaction between Nicotine and Simulated Pulmonary Surfactant Monolayers with Associated Molecular Modelling. *Surf. Interface Anal.* **2017**, *49* (9), 919–927. https://doi.org/10.1002/sia.6244.
(55) Lee, H. Vitamin E Acetate as Linactant in the Pathophysiology of EVALI. *Med. Hypothesis* **2020**, *144*. 110182. doi: 10.1016/j.mehy.2020.110182
**** paper of considerable interest: This work provides a comprehensive analysis of the potential effects of vitamin E acetate, including but not limited to the biophysical implications on lung surfactant.**
(56) Lee, A. G. Lipid-Protein Interactions in Biological Membranes: A Structural Perspective. *Viochim Biophys Acta.* 2003, **1612** (1), 1-40. https://doi.org/10.1016/S0005-2736(03)00056-7.
(57) Leonenko, Z.; Gill, S.; Baoukina, S.; Monticelli, L.; Doehner, J.; Gunasekara, L.; Felderer, F.; Rodenstein, M.; Eng, L. M.; Amrein, M. An Elevated Level of Cholesterol Impairs Self-Assembly of Pulmonary Surfactant into a Functional Film. *Biophys. J.* 2007, **93** (2), 674–683. https://doi.org/10.1529/biophysj.107.106310.
(58) Gunasekara, L.; Schürch, S.; Schoel, W. M.; Nag, K.; Leonenko, Z.; Haufs, M.; Amrein, M. Pulmonary Surfactant Function Is Abolished by an Elevated Proportion of Cholesterol. *Biochim. Biophys. Acta - Mol. Cell Biol. Lipids* 2005, **1737** (1), 27–35. https://doi.org/10.1016/j.bbalip.2005.09.002.
(59) Yu, S. H.; Possmayer, F. Interaction of Pulmonary Surfactant Protein A with Dipalmitoylphosphatidylcholine and Cholesterol at the Air/Water Interface. *J. Lipid Res.* 1998, **39** (3), 555–568. https://doi.org/10.1016/s0022-2275(20)33294-6.
(60) Stillwell, W.; Dallman, T.; Dumaual, A. C.; Thomas Crump, F.; Jenski, L. J. Cholesterol versus α-Tocopherol: Effects on Properties of Bilayers Made from Heteroacid Phosphatidylcholines. *Biochemistry* 1996, **35** (41), 13353–13362. https://doi.org/10.1021/bi961058m.
*** paper of interest: This work compares the effects of vitamin E with cholesterol, which may be important for the impact of additives on lung surfactant.**
(61) Bradford, A.; Atkinson, J.; Fuller, N.; Rand, R. P. The Effect of Vitamin E on the Structure of Membrane Lipid Assemblies. *J. Lipid Res.* 2003, **44** (10), 1940–1945. https://doi.org/10.1194/jlr.M300146-JLR200.
(62) Villalain, J.; Aranda, F. J.; Gomez-Fernandez, J. C. Calorimetric and Infrared Spectroscopic Studies of the Interaction of α -tocopherol and α -tocopheryl Acetate with Phospholipid Vesicles. *Eur. J. Biochem.* 1986, **158** (1), 141–147. https://doi.org/10.1111/j.1432-1033.1986.tb09731.x.
(63) Marquardt, D.; Kučerka, N.; Katsaras, J.; Harroun, T. A. α-Tocopherols Location in Membranes Is Not Affected by Their Composition. *Langmuir* 2015, **31** (15), 4464–4472. https://doi.org/10.1021/la502605c.

Chapter 6:Addition of Cholesterol to the Complex System:

6.1 Cholesterol in Lung Surfactant

Cholesterol has a contentious role in LS health. In cell membranes it is known to aid in packing to lower permeability, and regulate fluidity and diffusion rates [83,84]. In LS, it may perform similar roles by regulating the packing of lipids throughout respiration. According to the squeeze-out model of LS, unsaturated lipids are expelled during expiration, enriching the film with DPPC and cholesterol that enable low surface tensions to be reached [85,86]. DPPC alone is the only major LS phospholipid able to achieve relatively low surface tensions, however, in a pure film it suffers from slow adsorption rates to the air-water interface and is prone to irreversibly collapse when over-compressed or mechanically disturbed [85,87]. Cholesterol induces the formation of a liquid ordered (Lo) phase with DPPC. This enables the film to withstand higher lateral compression as well as have increased adsorption to the interface [88,89]. These effects are due to increased lipid mobility in the presence of cholesterol, as tightly packed lipids are spaced-out upon introduction of the planar molecule. Cholesterol comprises 2-10% by mass of the total lipids in LS, and thus its content must be highly regulated. Elevated amounts of the sterol are commonly found in cases of acute lung injury, suggesting surfactant dysfunction [90]. One way in which cholesterol may impede function is by rigidifying the fluid phases of the film. Force measurements between the film surface and an AFM tip reveal that bovine lung extract surfactant (BLES) films have higher fluidity at 5 mass% cholesterol compared to 20 mass% [91]. Cholesterol preferentially partitions into the condensed phases of saturated lipids, however, under excess amounts, cholesterol may be forced into the fluid phases of the film. Here, it increases acyl chain order of unsaturated lipids and reduces overall molecular area [92]. This is the so-called condensation effect, which may account

for surfactant dysfunction, as increased film rigidity suppresses protein adsorption and prevents the film from being able to withstand high lateral compression [91].

Additionally, surface tension measurements of BLES films demonstrated that cholesterol content ≥20 mass% restricted films from reaching values below 16 mN/m [93]. In a physiological sense, this level of surface tension does not support a structurally stable alveolus which can lead to issues associated with acute lung injury [94]. Instead, a continuous region of high compressibility was adopted, which maintained high surface tensions at low areas.

At proper levels, cholesterol is critical for forming small, slightly fluid domains with DPPC, which aid in SP adsorption and increase stability, allowing for low surface tensions to be attained. Elevated cholesterol content is strongly associated with surfactant dysfunction, as the rigidified film is unable to maintain low surface tensions.

6.2 Surface pressure-area isotherms and Isocycling

In this system, cholesterol has been added at a 2% weight ratio to the lipids. The complex monofilm now contains the two most important classes of lipids, that being a saturated PC and monounsaturated PG, alongside the biologically relevant sterol, cholesterol.

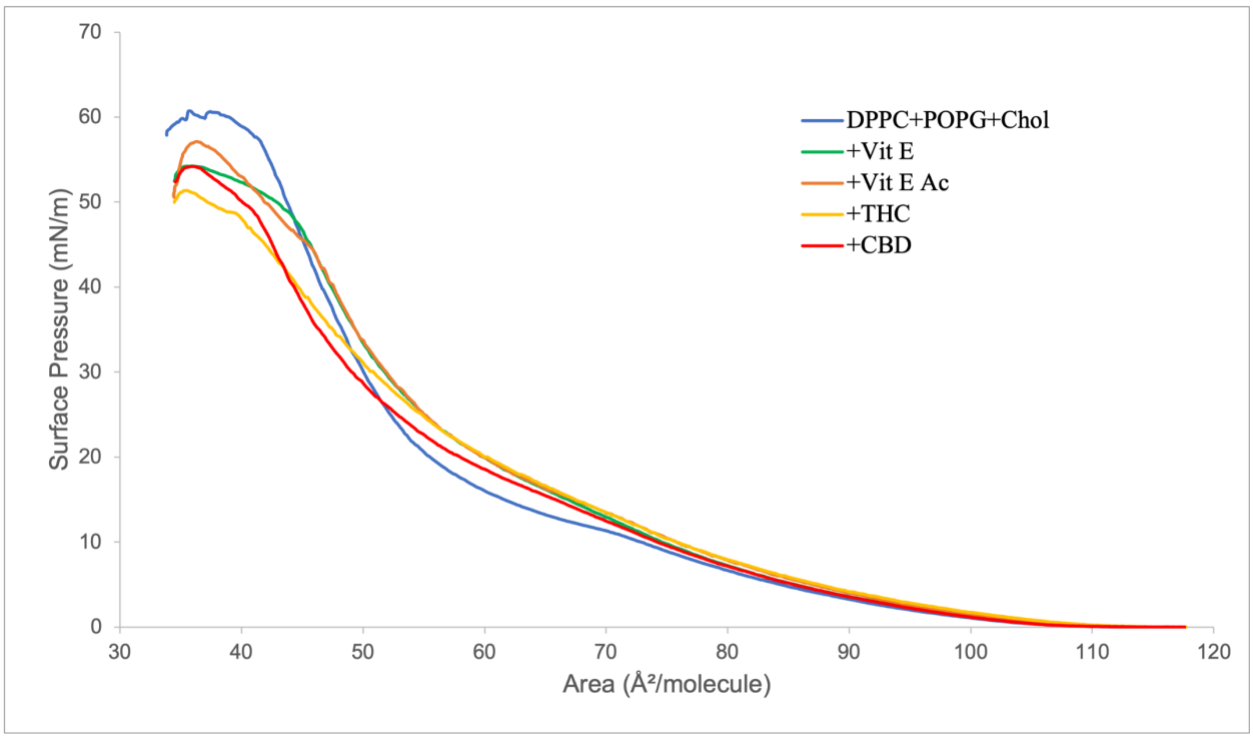

Figure 36. Surface pressure-area isotherms for DPPC:POPG+cholesterol (4:1+2%) in the presence of 5 mol% of Vit-E, Vit-EAc, THC, or CBD.

The control system (blue line) displayed a transition from the gas to LE phase, as indicated by the onset of surface pressure, at 108 $Å^2$/molecule. The slow rise in surface pressure proceeds until 72 $Å^2$/molecule and 11 mN/m, at which point there is a deflection as the DPPC component enters LE/LC phase coexistence. As with other multi component systems containing DPPC, this transition is not a flat plateau due to LE phase preference of the unsaturated lipids. The surface pressure begins to increase more sharply at 56 $Å^2$/molecule and 20 mN/m, continuing upwards to an inevitable collapse point, at 61 mN/m and 37 $Å^2$/molecule for this system.

Comparing the DPPC:POPG isotherms with and without cholesterol, the film is more stable in the presence of cholesterol, as evidenced by the increased collapse pressure (51 to 61 mN/m). This supports the idea that cholesterol plays an important role in lipid organization under high compression which acts to enhance film stability. Cholesterol is reported to form Lo lipid clusters with DPPC and that effect is likely seen here [135].

There is a slight shift to larger areas upon the addition of 5 mol% of Vit-E or Vit-EAc. This was also seen without cholesterol and was attributed to reduced packing. However, the shift seen here is <4 $Å^2$/molecule, suggesting that cholesterol regulation of lipid packing offsets much of this effect by the vitamins. The deflection point has shifted to 13-15 mN/m for all additive systems with a more gradual transition phase transition from LE to LC. This again demonstrates the fluidizing effects of the additives.

THC alone has interesting effects on the isotherm. It displays the largest shift in take-off area at, reducing packing most of all the single additives. It also displays the highest compressibility above 30 mN/m, and results in the lowest collapse pressure. This heightened effect by THC on the film compared to the other additives appears to be a direct result of cholesterol in the system. Formation of complexes between THC and DPPC have been reported based on DSC data [40]. Changes to membrane phase behavior were observed, which include reduced phase transition temperatures, broader peaks and unique peaks. As discussed in chapter 3, cholesterol aids in anchoring THC to the polar phosphate region of DPPC bilayers. Here it has little mobility and the changes seen to packing behavior may be attributed to the bulky rings of THC, which reduce the transition from LE to LC phase and increase compressibility at higher surface pressures. This interference with proper packing also results in the most destabilized film, as seen by the collapse pressure of 50 mN/m, compared to 61 mN/m for the control. CBD and Vit-E reduce collapse pressure to comparable amounts of 55 mN/m. The free rotation around the cyclic rings of CBD increase its mobility within the film. This allows for increased packing of neighboring lipids compared to THC, which accounts for the reduced compressibility and higher collapse pressure. Vit-E and Vit-EAc pack more favorably than the cannabinoids, due to their phytyl chain

interactions with lipid acyl tails. However, the methyl substituents still prevent best packing, increasing compressibility and reducing collapse pressure.

A shoulder between 48 and 51 mN/m is also present in all additive systems, followed by an area of high compressibility. This may be due to a loss of material from the film. Given that the control isotherm did not display this shoulder, it is unlikely that this is from leakage of the LB-trough, but rather an additive mediated loss. The increase in compressibility beyond this point suggests that it is not the additives that are being ejected, but rather the DPPC component which is crucial for achieving high surface pressures. Alternatively, it is possible that DPPC-cholesterol domains are being broken down at this point, and cholesterol is homogenized throughout the film, leading to a reduction in attainable surface pressure.

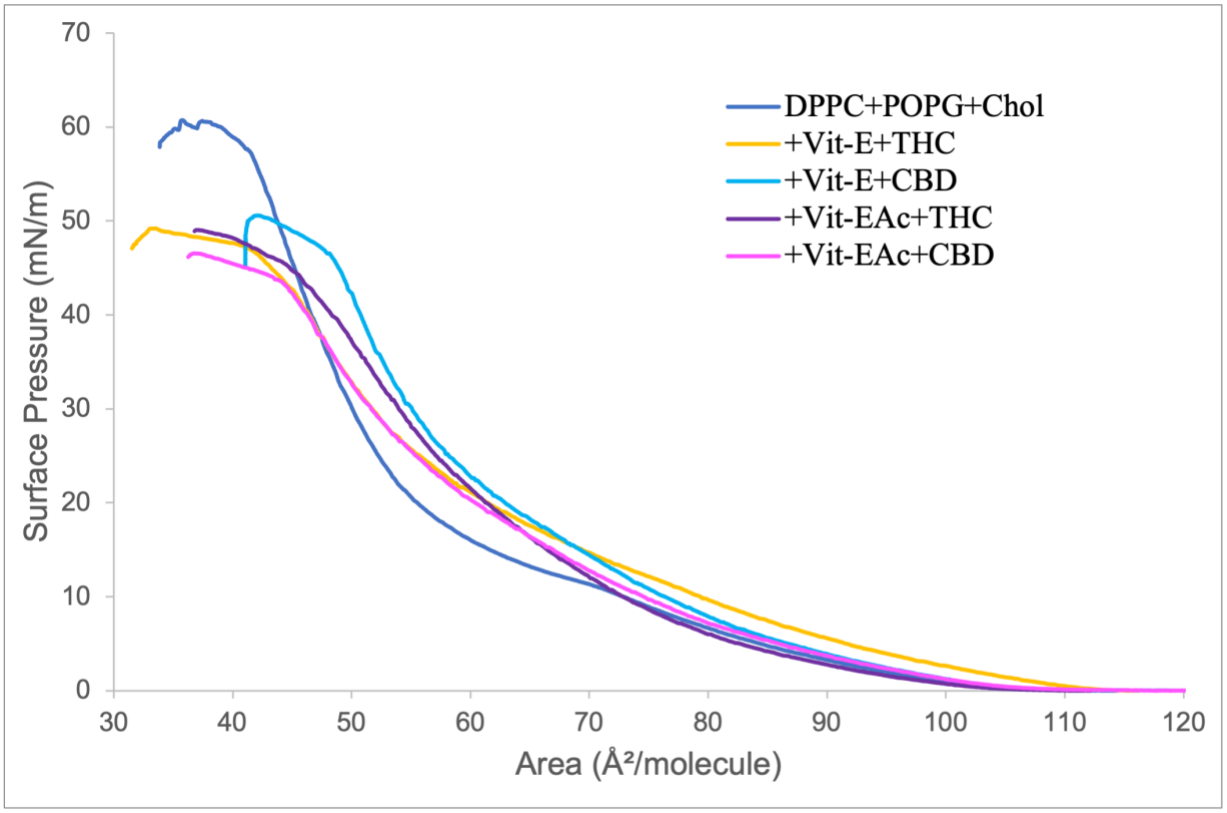

Figure 37. Surface pressure-area isotherms for DPPC:POPG+cholesterol (4:1+2%) in the presence of 2.5:2.5 mol% of Vit-E+THC or CBD and Vit-EAc+THC, or CBD.

The mixtures of vape additives show more pronounced effects on the phase transition region of the isotherm. Reduction of the isotherm kink indicates a more homogenous packing, most prominent with the mixture of Vit-EAc and THC. Complexation between the additives might account for this, as the Vit-E+THC result in a significant isotherm shift to the right, with a take-off area of 110 $Å^2$/molecule, compared to the control of 104 $Å^2$/molecule. Collapse pressures are also more significantly reduced by the additive mixtures compared to single systems, with surface pressures ≤50 mN/m. Again, a shoulder becomes apparent at 44-48 mN/m in all additive systems just before the collapse point. The change in slope here may be due to either loss of material, or increased mixing of cholesterol.

These results confirm that multiple additives acting on the film produce more significant effects in terms of lipid packing capabilities and stability, even when applied at the same total concentration of 5 mol%. Given the low concentrations used in these systems of 2.5 mol% of each additive, this is seriously concerning for LS health, that is potentially exposed to these additives at significantly higher concentrations, given that vaping products may contain up to 88% of Vit-EAc [95].

Isocycles:

Isocycling was also performed 10 times for these systems in the same manner as DPPC:POPG to determine the fate of the system over multiple respiratory cycles . Compression to surface pressures of 40 mN/m was followed by expansion to 5 mN/m and the shift in surface area was recorded at 20 mN/m as a means of determining relative material loss from the film. Recall that as material is lost from the film, the isotherm will shift to lower areas.

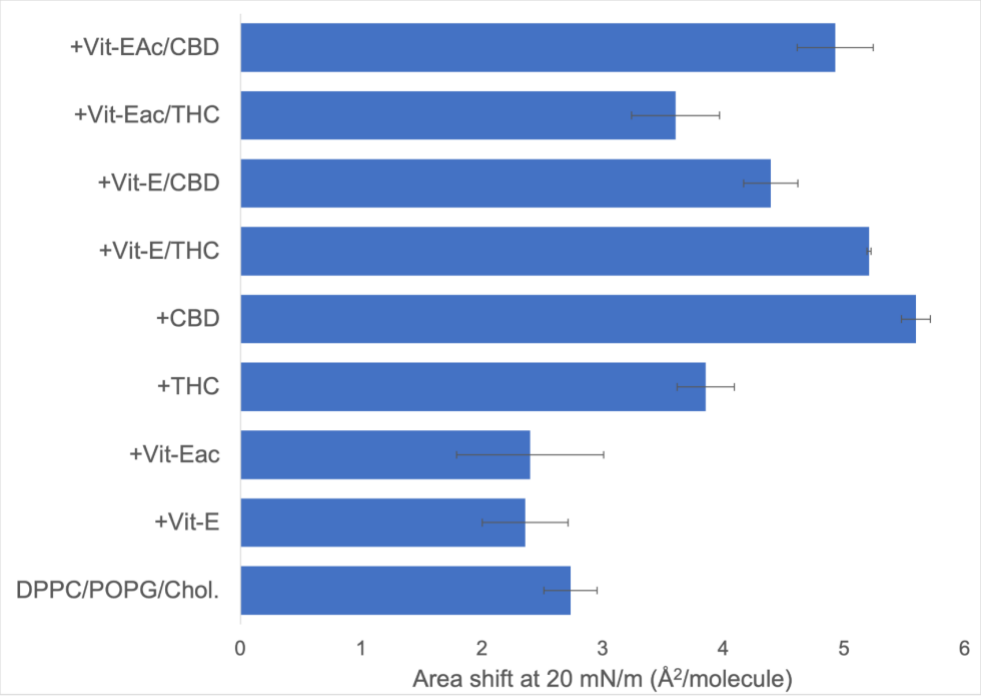

Figure 38. Shift in surface area at 20 mN/m after isocycling 10 times between high and low surface pressures of 40 and 5 mN/m.

Similar trends are seen here when compared to cholesterol free controls. The vitamins do not induce significant material loss, while CBD displays the largest shift in area. Again, the vitamins have more favorable interactions with the lipids due to smaller ring size and extended side chains which will not perturb the film to the same extent. Vit-E+THC showed the next highest increase in material loss. There is indication of this from the isotherm shift to the right (Figure 36), which suggested the film reduced packing capabilities, and was therefore at a greater potential for material loss during compression. Vit-EAc+THC showed less material loss here than in the system without cholesterol. The aforementioned interactions with cholesterol, which increases THC stability in the headgroup region, may account for this. Disruption of lipid packing will occur near the hydrophilic heads via THC, and the hydrophobic core via Vit-EAc. The double effect accounts for the packing defects seen in the isotherm but also for slightly less material loss as the additives are anchored by multiple interactions to the lipids.

6.3 Brewster angle microscopy images

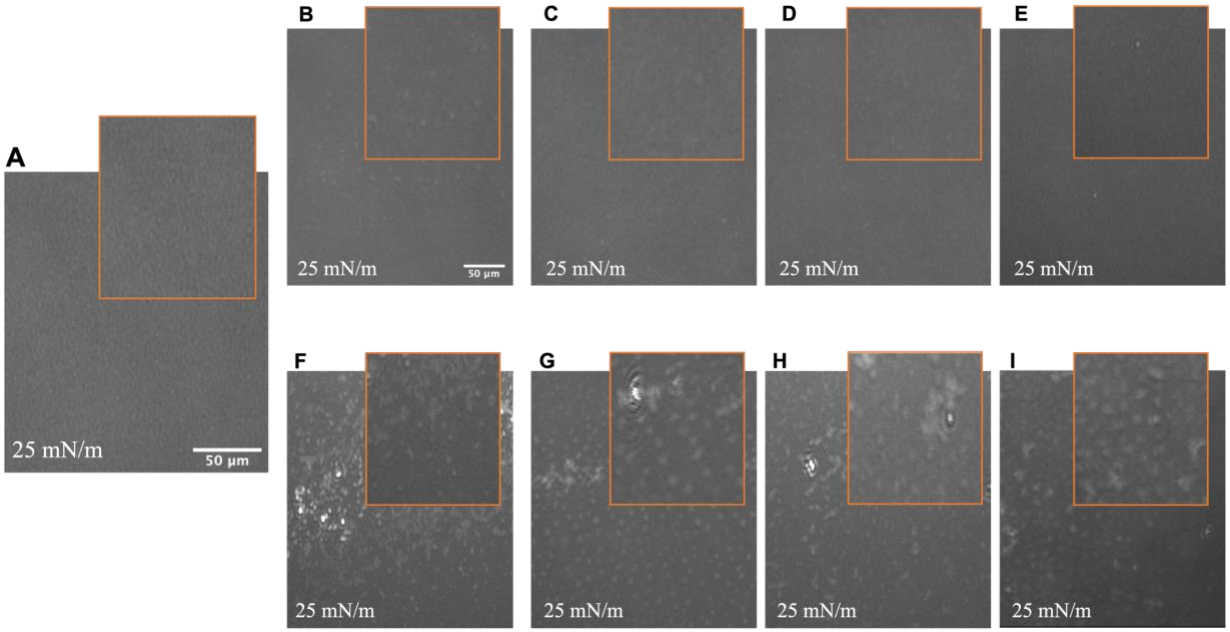

Figure 39. BAM images of lipid systems at 25 mN/m surface pressure. (A) DPPC:POPG+cholesterol (4:1+2%). (B) Lipids:Vit-E (95:5). (C) Lipids:Vit-EAc(95:5) (D) Lipids:THC (95:5) (E) Lipids:CBD (95:5). (F) Lipids:Vit-E:THC (95:2.5:2.5). (G) Lipids:Vit-E:CBD (95:2.5:2.5). (H) Lipids:Vit-EAc:THC (95:2.5:2.5). (I) Lipids:Vit-EAc:CBD (95:2.5:2.5).

Pictures of the lateral organization were taken after the onset of the LC phase at 25 mN/m. The control system displays numerous tightly packed domains which leaves little room for LE phase between. DPPC forms liquid condensed domains due to its fully saturated acyl chains [96]. Cholesterol is well known to increase fluidity of tightly packed lipids [97]. This leads to formation of smaller domains seen in this system compared to the DPPC:POPG system. Additionally, cholesterol will also increase order of the unsaturated POPG component. Together, these effects result in the well-ordered domains seen in figure 38A. Addition of 5 mol% of any additive significantly alters the lateral organization. Much of the ordered domain structures are lost. In the systems with Vit-E or Vit-EAc, fewer but larger domains are present. Linactant activity by the vitamins destabilize the domain structure, resulting in a mixing of the lipid components. While linactants generally reduce domain sizes [98], the slight increase seen here may be due to loss of

cholesterol from the condensed region. Cholesterol distribution throughout the film as a result of additive action may produce similar effects seen under excess concentrations of cholesterol (≥20%). Cholesterol in the fluid phase will act to order the acyl chains of POPG, reducing the films ability to undergo high lateral compression. Loss of DPPC-cholesterol nanodomains will also impede SP adsorption to the film. While these are not able to be directly visualized with this imaging method, their formation has been reported and is akin to lipid rafts seen in membranes. These effects might account for the reduction in collapse pressure seen in the isotherm. THC and CBD systems still display numerous small domains throughout the film; however, they are less ordered due to film perturbation. There is more fluid phase visible in the films containing the cannabinoids, which reflects their ability to space out lipids increasing fluidity. The reduction in collapse pressure may be a reflection of this lost ordering.

Double additive mixtures produce more pounced effects on lateral organization as seen in the BAM images (Figure 38F-I). Demixing of the phases is apparent as clusters of large domains are spread throughout the fluid phase. Protrusions are also evident, as seen by the white spots, in the majority of the systems. The phase separation and increase of domain sizes further suggest loss of cholesterol from the condensed region, which correlates with the significant reduction of collapse pressure.

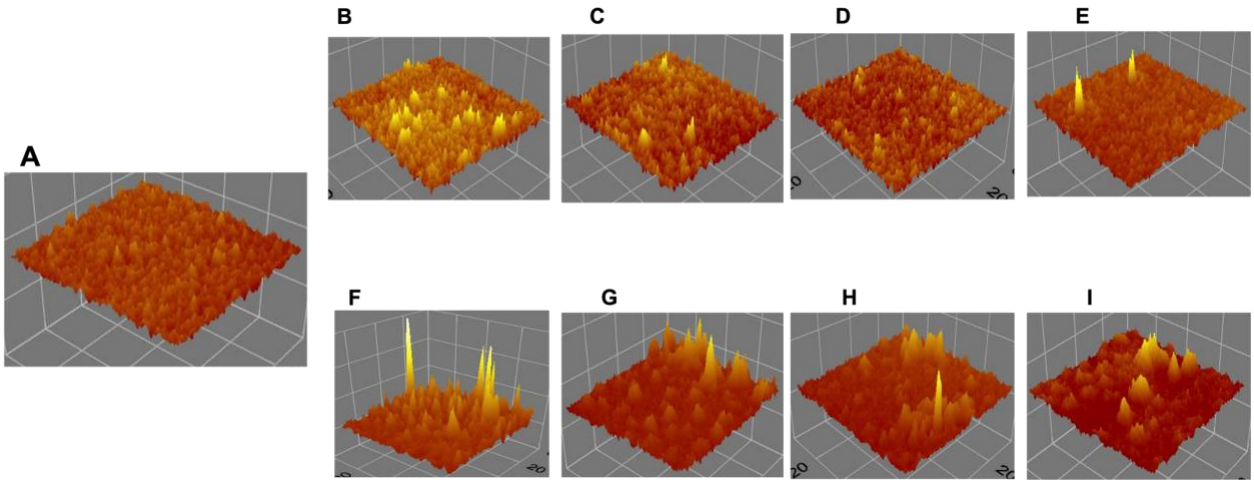

Figure 40. 3D view of BAM images of lipid systems at 25 mN/m surface pressure. (A) DPPC:POPG+cholesterol (4:1+2%). (B) Lipids:Vit-E (95:5). (C) Lipids:Vit-EAc(95:5) (D) Lipids:THC (95:5) (E) Lipids:CBD (95:5). (F) Lipids:Vit-E:THC (95:2.5:2.5). (G) Lipids:Vit-E:CBD (95:2.5:2.5). (H) Lipids:Vit-EAc:THC (95:2.5:2.5). (I) Lipids:Vit-EAc:CBD (95:2.5:2.5).

Looking further at the 3D analysis, the control system displays an orderly arrangement of domains, with little fluctuations throughout (Figure 39A). Alteration to lateral organization in the presence of the additives is exemplified in this 3D analysis. Distortions throughout the film are evident in single additive systems (Figure 39B-E). These small peaks present demixing of the monolayer material in a disordered fashion which does support a stable film.

Comparing these images to the BAM without cholesterol, single systems deplete domain formation to a higher degree. As cholesterol is localized to the condensed region, additive-cholesterol interactions will occur here where the greatest effect on domain formation can occur. While the DPPC/POPG additive systems displayed smaller, but sill ordered domains, these systems result in a disordered lateral organization.

Double additive systems display larger clusters throughout the film, as well as protrusions signified by the bright peaks.

6.4 Summary

Cholesterol at low amounts (2-10%) support a stable film capable of achieving low surface tensions. The formation of a Lo phase with DPPC contributes to this by allowing for higher lateral compression compared to the DPPC/POPG system alone. Single additive systems at 5 mol% begin to reduce the LE-LC phase transition and reduce film stability. There is a general fluidizing effect seen with all additives, as they act to space-out lipids, decreasing acyl chain ordering. The cannabinoids were shown to have the greatest effect in this regard, as their bulky rings localize near the phosphate group of lipids, allowing for more acyl chain mobility. This is enhanced by the presence of cholesterol, which assists in anchoring the cannabinoids in this region. Double additive systems resulted in an increased reduction of collapse pressure as association between the vitamins and cannabinoids act to perturb the film to greater extents. The onset of a high compressibility region was seen in all systems near the collapse point. This is likely due to some loss of material from the film, which will reduce attainable surface pressure, as well as mixing of cholesterol throughout. The latter point is supported by the BAM images, which show an increase in domain sizes and less ordered lateral architecture. Homogenization of cholesterol in the film has been shown to increase compressibility and reduce maximal surface pressure [11]. This has been directly seen in the surface pressure-area isotherms, as well as reflected by the BAM images which displayed demixing and loss of ordered domains throughout the film.

Chapter 7: Bovine Lung Extract Surfactant System

7.1 BLES Background

In this final system bovine lung extract surfactant (BLES) was used for assessing the impact of vape additives on the film functionality of a biological surfactant. BLES is a natural surfactant, containing all lipid components as well as the hydrophobic proteins SP-B and SP-C and is commonly used in surfactant replacement therapy [99]. It was first collected by Dr. Fred Possmayer at the University of Western Ontario in the 1970s, using an intact lung lavage process, which ensured the natural ratio of phospholipids to SP-B/C was preserved [100]. Later, alongside Dr. David Bjarneson and Dr. Harold Nigh, the surfactant was produced to rescue premature babies suffering from neonatal respiratory distress syndrome. To date, 160,000 patients have been administered BLES worldwide [100]. BLES self assembles into a highly active film when deposited at the air-water interface [60], making it an effective model for elucidating the harmful effects of vape additives on surfactant.

In this biophysical investigation, a Langmuir-Blodgett trough with BLES spread at the air-water interface was used to assess film stability and functionality at low surface tensions. Compression and expansion cycles were implemented to mimic respiration. Finally, the lateral film organization was visualized by Brewster angle microscopy (BAM) and molecular architecture by atomic force microscopy (AFM).

Effects of vape additives on BLES were assessed in terms of functionality and lateral surface architecture of the film. BLES is able to be compressed to high surface pressures, which correlates to the low surface tension achieved during respiration. In this state, lipid domains form in the film which contribute to overall stability. Namely, protein anchored bilayers which prevent buckling and collapse during the fast rate of area change which occurs under respiration.

7.2 Surface pressure-area Isotherms

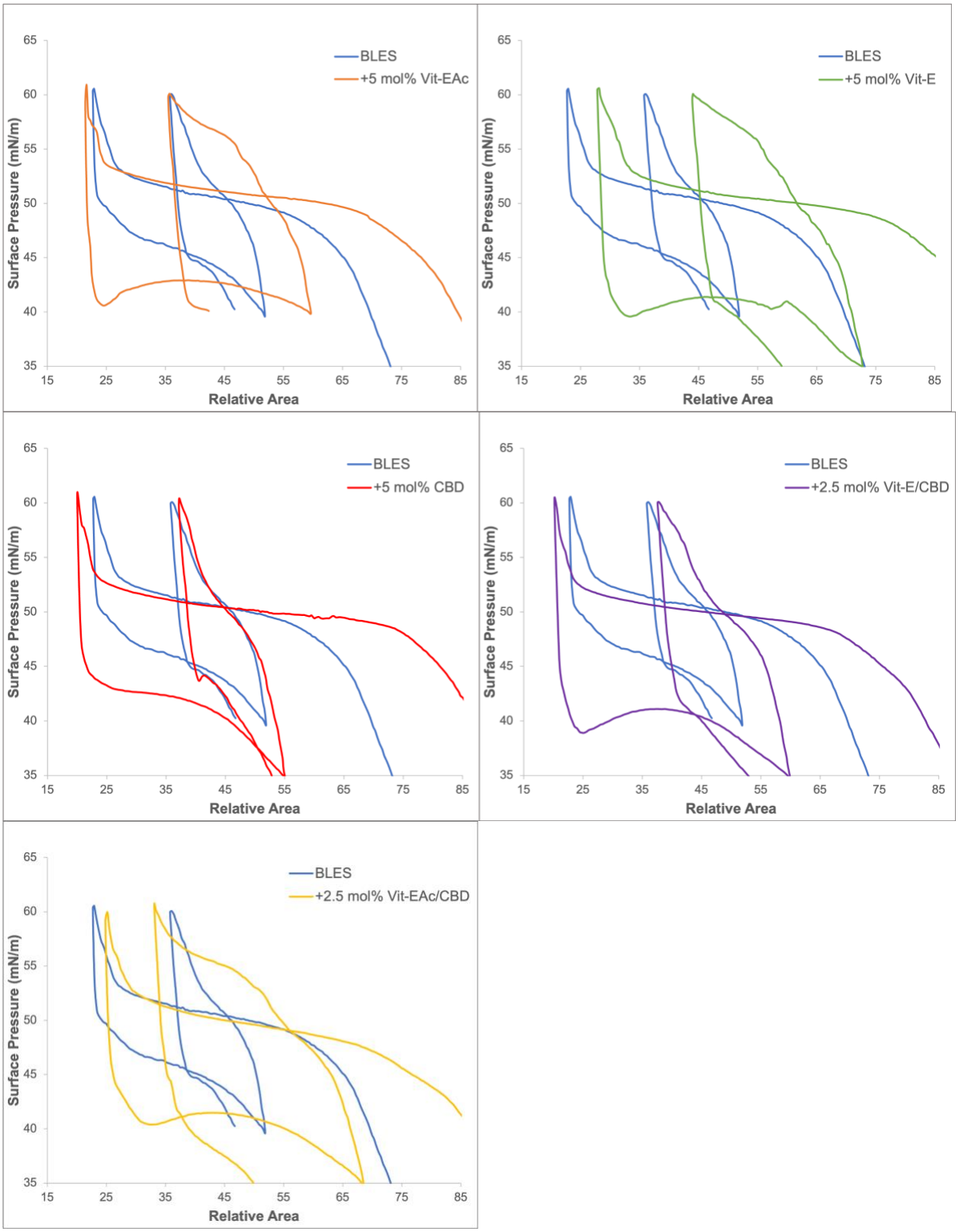

Figure 41. Surface pressure-area isotherms of **(A)** BLES cycled twice between surface pressures of 60 and 40 mN/m. **(B)** +5 mol% Vit-EAc **(C)** +5 mol% Vit-E **(D)** +5 mol% CBD **(E)** +2.5mol% Vit-E and +2.5 mol% CBD **(F)** +2.5mol% Vit-EAc and +2.5 mol% CBD.

Surface pressure-area isotherms were recorded for all systems to determine film functionality. The surface pressure reached in LS to attain near zero surface tension is ~70 mN/m [101]. Films were cycled just below this pressure, between 60 and 35 mN/m. As surfactant was deposited in excess, surface area is recorded as percent of the area compressed for ease of comparison between systems.

All isotherms displayed a steep increase in pressure up to >45 mN/m, at which point a broad shoulder formed followed by the onset of a plateau where surface pressure gradually rose, until another steep increase between 52 and 60 mN/m (Figure 40). The plateau signifies a region of high compressibility, which varied in relative compressed area size from system to system. BLES alone required the least amount of compression area (~20 % of total area) to transition back to a region of low compressibility, while CBD required the most area (~53% of total area) (Figure 40C). CBD insertion occurs at the region of the lipid phosphate and has demonstrated in the previous model films to hinder lipid packing by increasing acyl chain mobility. This may account for the extended plateau seen here. The other additive systems also increased compression area required to reach critically active surface pressures. Disruption of proper lipid packing in the film has been observed by all additives as they generally act to increase film fluidity. The vitamins may also directly influence cholesterol distribution throughout the film due to their lineactant activity. Disruption of Lo domains may mix cholesterol with fluid phases of the film, resulting in a greater relative concentration of cholesterol throughout. In films with excess cholesterol, high surface pressures are never attained, instead, a highly compressible film structure is maintained [93]. Deactivation of surfactant in this manner is largely associated with ARDS, an illness seen in EVALI patients [102].

Another shoulder became present in all of the additive systems, most prominent with 5 mol% Vit-EAc, at ~57 mN/m. This signifies another region of film reorganization, perhaps one in

which the additives are being expelled, either into the subphase or the air space, allowing the lipids to tightly pack. This may be a necessary in order for the film to achieve low surface tensions. Expulsion of material from the interface is a natural occurrence, useful for removing oxidatively damaged lipids and foreign particulates, while new lipids released from type II pneumocytes are readily incorporated by protein-mediated action [103].

Furthermore, upon expansion of BLES, surface pressure quickly declined to 50 mN/m, then gradually decreased to 40 mN/m as the film reentered a state of high compressibility. The additive systems with the vitamins alone and with CBD showed very different trends during this phase of cycling. With surface pressure decreasing close to 40 mN/m, followed by a gradual rise in surface pressure before again declining to 35 mN/m. This may indicate a disruption in the protein-assisted adsorption of lipids to the interface. One of the primary roles of SP-C is to associate with surfactant complexes in the reservoir as well as the interfacial film [104]. This facilitates quick adsorption of lipids to the respreading film during inhalation. The rapid drop in surface pressure upon expansion suggests that this process is compromised. Slow lipid reinsertion into the film may be responsible for the subsequent rise in surface pressure seen in these additive systems. This slow rate of readsorption can impede the surfactant's ability to maintain low surface tensions throughout respiration.

The negative effects of these additives, namely Vit-E, Vit-EAc, and Vit-EAc+CBD, are still evident in the second compression cycle, as numerous shoulders are present during compression from 40 mN/m to 56 mN/m which suggest packing defects. These systems also show a broad plateau is also seen from 56 mN/m to 60 mN/m, which raises concerns about proper functionality, and it is not clear if the film is still in a constant state of high compressibility. Vit-EAc+CBD displayed a sharp increase in surface pressure near the end of compression, likely a

result of the lower concentration of Vit-EAc in this system (2.5 mol%). It may be assumed that these complexes will have synergistic effects on BLES, however the results here largely show a diminished effect when compared to the vitamins alone. By complexing with CBD, characteristics of the vitamins might change. Importantly, Vit-E may lose linactant function and Vit-EAc may be situated closer to the headgroup region and interact less with SP-C, where it will not directly interfere with multilayer formation.

Overall, the films still had a degree of proper function as high surface pressures of 60 mN/m were reached. Nevertheless, the increased compression area required to reach this pressure and unusual trends during expansion and recompression raise concerns as to proper lipid organization. To reiterate similar findings from the previous chapter, this highly compressible state of the film does not allow for low surface tensions which destabilizes the lungs as a whole [94].

7.3 Brewster angle microscopy images:

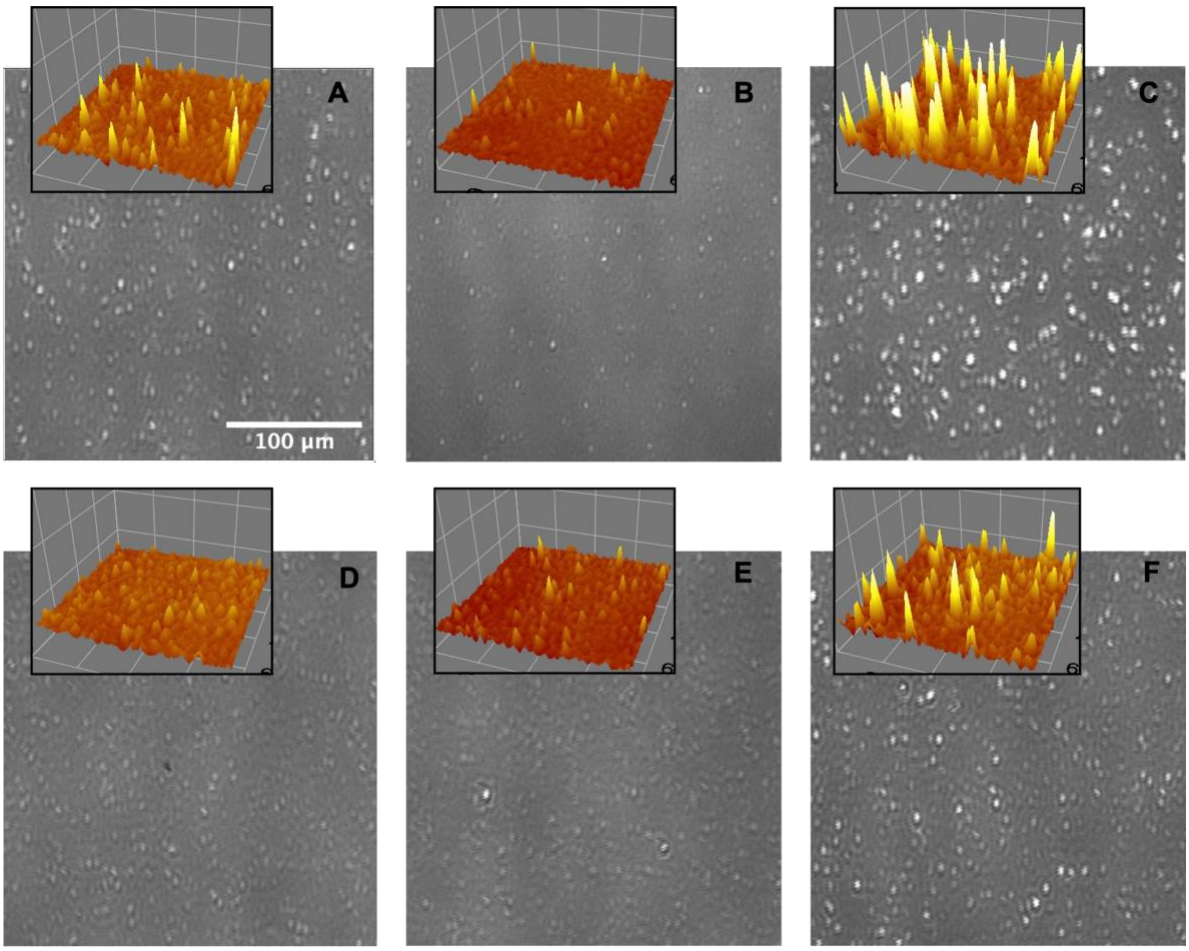

Figure 42. BAM images of BLES systems with addition of 5 mol% additives at 50 mN/m. **(A)** BLES **(B)** +Vit-E **(C)** +Vit-EAc **(D)** +CBD **(E)** +Vit-E/CBD **(F)** +Vit-EAc/CBD. Image imensions are 271x284 microns, 100 micron scale bar shown on the control for reference.

BAM images were taken at 50 mN/m during the third compression cycle to assess changes in functionally relevant domains. The lateral surface structure of BLES films characteristically displays small circular domains protruding from the film, as seen in the 3D analysis (figure 41A). These show up as brighter points in the BAM image, and are reported in films undergoing multilayer transition [105]. Their appearance here signifies an important feature of BLES that allows for maintenance low surface tensions. The multilayers act as lipid reservoirs that respread over the interface during inhalation, maintaining a low surface tension [106,107]. Their formation

is aided by SP-C as its hydrophobic ∝-helix is able to penetrate the lipid bilayer and facilitate lipid transition between a monolayer and the lamellar phase [106,107].

Domain shape is largely retained in each system, however, addition of 5 mol% Vit-E or CBD reduced the size and height of domains, while Vit-E also decreased domain count (Figure 41B,D). The loss of these domains and lack of spikes may be an indication of film failure to produce multilayers, which will reduce stability at high surface pressures. The presence of 5 mol% Vit-EAc displayed large protrusions throughout the film in lieu of regular domain formation as observed in the control (Figure 41C). These spikes may represent clusters of lipids and Vit-EAc which protrude further from the film than lipid domains. Their prominence suggests that Vit-EAc partitions to all condensed regions in the film and hinders proper multilayer formation.

Mixture of Vit-E+CBD resulted in a lateral organization that more closely reflects that of CBD, with a reduction in domain size and height but little effect on domain count (Figure 41E). Protrusions are still evident in the system with CBD+Vit-Eac, which seems to be a clear feature of Vit-EAc induction into BLES. The reduced effect in these systems is likely due to the lower concentration of vitamins used (2.5 mol%).

The SP-C-anchored lipid domains are a common feature in functional surfactant; crucial for lung stability during rapid area changes under respiration [106]. The lineactant activity of Vit-E appeared to reduce domain stability in BLES. This will directly compromise multilayer formation as anchor points for SP-C are lost.

The more hydrophobic additive, Vit-EAc, may disrupt these domains to a greater extent by directly interacting with the ∝-helix of SP-C. The spikes seen in this system may be a reflection of this interaction, in which large clusters of Vit-EAc and some lipids are associated around the peptide's helix. The loss of ordered domains will quickly lead to dysfunction of LS, as roles related

to stability and lipid adsorption are dependent on these film structures. This consequence is visible in the isotherms, as there is a quick decrease in surface pressure immediately upon expansion (60 → 40 mN/m) compared to the control (60 → 50 mN/m) due to lipids in the multilayer respreading across the interface.

7.4 Atomic Force Microscopy

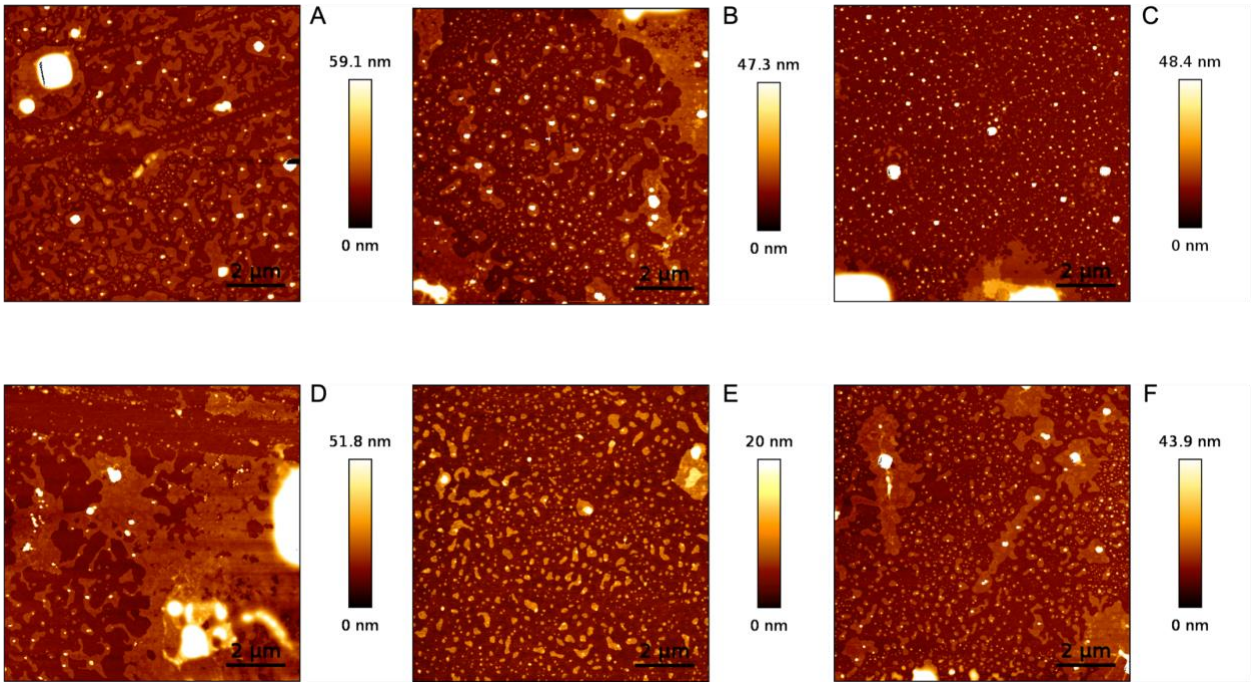

Figure 43. AFM images of BLES systems with addition of 5 mol% additives at 50 mN/m. **(A)** BLES **(B)** +Vit-E **(C)** +Vit-EAc **(D)** +CBD **(E)** +Vit-E/CBD **(F)** +Vit-EAc/CBD.

BAM provides useful information on the lateral organization of BLES and 3D analysis of domains present, however it is limited by lower resolution, and is unable to decern the presence of stacked bilayers [108]. AFM was used to resolve this key architecture of BLES and determine their fate in the presence of vape additives. Images were taken of the film compressed to 50 mN/m supported on mica plates.

AFM of BLES reveals that these bilayers are prominent throughout the film (Figure 42A), and are seen at the expected height of 5 nm for lipid bilayers [91]. After addition of Vit-E, the

bilayers noticeably shrink in surface area (Figure 42B), however, their presence suggests the film still has functioning capabilities, as also confirmed in the surface pressure-area isotherm of this system.

Vit-EAc on the other hand, shows a near depletion of all bilayers. This is cause for serious concern as the absence of stacked bilayers is a common feature of dysfunctional surfactant [91,107]. Multiple bright points seen in this image may be an indication of the additive clustering around SP-C, as discussed in the previous section. The isotherm showed that this system was still capable of reaching high surface pressures, therefore Vit-EAc may be squeezed out of the film under high compression (> 50 mN/m). The shoulder at 57 mN/m could be due to lipid reorganization into multilayers after Vit-EAc is squeezed-out.

CBD, and its mixture with Vit-E, also showed prominent bilayer architecture, signifying a relatively functional surfactant while Vit-EAc+CBD demonstrated some reduction in bilayer surface area. As seen in the isotherms, these systems were able to achieve high surface pressure, however, the steep drop in pressure upon expansion was still evident. This suggests that the presence of the additives impede fast respreading of surfactant material, regardless of multilayer formation.

The addition of Vit-EAc alone has altered the molecular architecture of BLES the most. The spikes seen in the BAM images for this system appear to be associated with an absence of bilayers. While the other additives like Vit-E reduced domain size and count, these domains were still active features of the film as reflected by the bilayer structures seen under AFM. It is worth noting that the surface areas of these bilayers are reduced, perhaps suggesting a concentration dependent effect of Vit-E. Given the low concentrations used in this study, it is possible that repeated inhalation of the additives and their accumulation in the alveolar space will produce more

significant effects on structural features of the surfactant. Nonetheless, Vit-EAc was able to deplete almost all bilayers at a concentration of only 5 mol%. As seen in the previous model system, Vit-EAc may increase cholesterol distribution throughout the film. This coupled with the additive's affinity to the hydrophobic ∝-helix of SP-C, prevents proper domain formation and the capability of multilayer assembly. This may also account for the lessened effects of the other two additives, as CBD has not demonstrated a significant ability to destabilize domain formation, and Vit-E will preferentially interact with lipids over the peptide due to its elevated hydrophilicity. Complexation between CBD and Vit-EAc may also reduce affinity towards SP-C, accounting for the increased bilayer structures seen with AFM for this system.

7.5 Summary

A fully functional surfactant must be able to stably attain high surface pressures and promote rapid lipid adsorption upon film expansion. The vape additives demonstrated a capability to hinder both these functions by altering lipid organization. Vit-EAc displayed the largest effects on proper domain and bilayer formation, while Vit-E reduced the domain count. Disruption of these domains interfere with proper protein anchoring. As SP-C plays a significant role in multilayer formation and film stability, the changes to hindrance of proper domain formation seen in the presence of the additives can lead to a dysfunctional film and many of the respiratory symptoms associated with EVALI.

Chapter 8: Conclusions and Future Directions

8.1 Summary

The aim of this thesis was to understand interactions between vape additives and primary lipid components of LS. This was done using simple model systems containing one or two physiologically relevant lipids, these being DPPC, POPC, DPPG, and POPG, then adding cholesterol and finally using a more complex biological samples, BLES, which is also used as a clinical surfactant.

In this manner, interactions with the primary lipid components could be understood before attempting to assess a more biological model. Films were formed by co-depositing lipid-additive mixtures on the surface an air-water interface, mimicking common *in-vitro* methods, in which the additives are already incorporated into the monolayer. Surface pressure-area isotherms were then recorded to assess lipid packing and film stability, while BAM images could be taken concurrently to visualize changes in lateral film organization.

The additives were found to increase fluidity of saturated lipid films, in accordance with literature results of additives in PC membranes. A fluidizing effect was demonstrated in monounsaturated lipid films, as the bulky additive rings and phytyl tails act to reduce acyl chian mobility.

Cholesterol at low amounts (2-10%) support a stable film capable of achieving low surface tensions. The formation of a Lo phase with DPPC contributes to this by allowing for higher lateral compression compared to the DPPC/POPG system alone. Single additive systems at 5 mol% begin to reduce the LE-LC phase transition and reduce film stability. There is a general fluidizing effect seen with all additives, as they act to space-out lipids, decreasing acyl chain ordering. The

cannabinoids were shown to have the greatest effect in this regard, as their bulky rings localize near the phosphate group of lipids, allowing for more acyl chain mobility.

BLES-additive films displayed an increase in required compression area to reach sufficient surface pressures for an active film. BAM and AFM imaging also revealed a depletion of protein anchored domains and multilayer formation, most notably in the presence of Vit-EAc. Cholesterol distribution throughout the film, and Vit-EAc interaction with SP-C, are the primary reasons for this. Mixing of cholesterol disallows for the formation of structural domains, impeding the films ability to maintain low surface tensions during respiration.

8.2 Conclusions

There are a number of options for vape additives to induce lung illness. Here the possible disturbance to lung surfactant as a means of EVALI development were examined. Using simple and more complex lipid systems, the interactions between vape additives and important lipid components were explored. As hindrance to LS function can result in symptoms related to EVALI, it is crucial to understand potential interactions for the purpose of safer product development. Vape additives predominantly altered lipid packing under low areas as the film packed tighter together. A fluidizing effect was generally seen in which the additives increased compressibility of the film, preventing high surface pressures from being achieved. In simple lipid systems, the reduction in collapse pressure presented a destabilized film, unable to provide the necessary reduction in surface tension required for surfactant function. In complicated systems like BLES, this presented itself as an area of high compressibility which the same effective outcome for the film. Due to the nature of the additives, they act to partition at phase boundaries, reducing domain sizes and eliminating rigidity. This effect is strongest in systems with saturated lipid components like DPPC, as this lipid primarily enters the Lc phase at low

surface areas. Alongside cholesterol, films were able to reach even higher surface pressures and displayed a uniform lateral organization populated with rigid domains. Additive introduction greatly disturbed this uniformity, resulting in loss of function. In terms of simple systems, this loss of domains is alongside destabilized films and increased compressibility. In physiologically relevant systems like BLES, the elimination of crucial multilayers prevents proper film reexpansion and robustness to achieve low surface tension. At the given level of investigation, the additives are able to partition into LS model systems and disturb lateral surface architecture. This was seen to reduced functionality in all systems tested.

8.3 Future Outlook:

The model systems studied here provide a useful application for *in vitro* analysis of potentially harmful vape additives. To better correlate results with *in vivo* the complexity of model films can be increased by implementing two PC lipids that are particularly unique. The first is palmitoylmyristoylphosphatidylcholine (PMPC) with 16:0,14:0 acyl chains. Chain length mismatch of two fully saturated tails is not common in mammalian membranes and its high amount in the PC component of lung surfactant suggests it may be important. The second lipid is palmitoylpalmitoleoylphosphatidylcholine (16:0,16:1), which differs from DPPC by a single unsaturation. This lipid makes up also makes up a large portion of the PC lipids and provides a large increase in film fluidity.

Given that the additive amounts in vape products are reported across a broad range of percentages, and the fact that accumulation may occur with prolonged vape usage, future studies should explore expanding the concentration range of vape additives implemented in the lipid systems. This will help elucidate the true extent of damage that the additives may impose on LS and lead to a clearer mechanism of vape-induced lung injury.

Another potential cause of injury is from by-products of heated vape juice. Vit-EAc in particular is reported to produce dangerous chemical emissions during aerosolization [109]. This adds another layer to potential EVALI pathology that needs to be explored further.

Lastly, instead of codepositing additives with the lipids to form the monofilm, a spray method could be used to coat the surfactant. This method moves closer to an *in vivo* scenario, as vape additives will first contact with the surfactant through the alveolar air space, interacting with the acyl tails then incorporating into the film. Tuning the methodology this way provides a better link between *in vitro* and *in vivo* studies, important for using these techniques as screening methods.

REFERENCES

1. Vatassery G, Krezowski A, Eckfeldt J. Vitamin E concentration in human blood plasma and platelets. *Am. J. Clin. Nutr.* 37, 1020–1024 (1983).
2. Mickle DAG, Weisel RD, Burton GW, Ingold KU. Effect of orally administered alpha-tocopheryl acetate on human myocardial alpha-tocopherol levels. *Cardiovasc. Drugs Ther.* 5(2 Supplement), 309–312 (1991).
3. Underwood BA, Denning CR. Blood and liver concentrations of vitamins A and E in children with cystic fibrosis of the pancreas. *Pediatr. Res.* 6(1), 26–31 (1972).
4. Azzi A, Stocker A. Vitamin E: Non-antioxidant roles. *Prog. Lipid Res.* 39(3), 231–255 (2000).
5. Machlin LJ, Vitamins EG. Kinetics of Tissue A-Tocopherol Uptake and Depletion Following Administration of High Levels of Vitamin E. *Ann. N. Y. Acad. Sci.* 393(1), 48–60 (1982).
6. DONALDSON KO, NASON A, LEHMAN IR, NICKON A. The role of lipides in electron transport. III. Purification and identification of a cytochrome c reductase lipide cofactor. *J. Biol. Chem.* [Internet]. 233(3), 566–571 (1958). Available from: http://dx.doi.org/10.1016/S0021-9258(18)64705-2.
7. Wang X, Quinn PJ. The location and function of vitamin E in membranes (Review). *Mol. Membr. Biol.* 17(3), 143–156 (2000).
8. Cohn W. Bioavailability of vitamin E. *Eur. J. Clin. Nutr.* 51(1) (1997).
9. Patel V, Rink C, Gordillo GM, *et al.* Oral tocotrienols are transported to human tissues and delay the progression of the model for end-stage liver disease score in patients. *J. Nutr.* 142(3), 513–519 (2012).
10. Kramer JKG, Biais L, Fouchard RC, Melnyk RA, Kallury KMR. A rapid method for the determination of vitamin E forms in tissues and diet by high-performance liquid chromatography using a normal-phase diol column. *Lipids*. 32(3), 323–330 (1997).
11. Xiaoyuan Wang, Peter J. Quinn. Vitamin E and its functions in biological membranes. *Prog. Lipid Res.* 38, 309–336 (1999).
12. Rief M, Pascual J, Saraste M, Gaub HE. Single Molecule Force Spectroscopy of Spectrin Repeats : Low Unfolding Forces in Helix Bundles. *J. Mol. Biol.* 286(2), 553–561 (1999).
13. Ingold KU, Bowry VW, Stocker R, Walling C. Autoxidation of lipids and antioxidation by α-tocopherol and ubiquinol in homogeneous solution and in aqueous dispersions of lipids: Unrecognized consequences of lipid particle size as exemplified by oxidation of human low density lipoprotein. *Proc. Natl. Acad. Sci. U. S. A.* 90(1), 45–49 (1993).
14. Lauridsen C, Jensen SK. α-Tocopherol incorporation in mitochondria and microsomes upon supranutritional vitamin E supplementation. *Genes Nutr.* 7(4), 475–482 (2012).
15. Evans HM, ScottBishop K. On the existence of a hitherto unrecognized dietary factor essential for reproduction1. *Science (80-.).* 1(1458), 650–651 (1922).
16. Ouahchi K, Arita M, Kayden H, *et al.* Ataxia with isolated vitamin E protein. *Nat. Genet.* 9, 141–145 (1995).
17. Traber MG, Sokol RJ, Burton GW, *et al.* Impaired ability of patients with familial isolated vitamin E deficiency to incorporate α-tocopherol into lipoproteins secreted by the liver. *J. Clin. Invest.* 85(2), 397–407 (1990).
18. Ricciarelli R, Zingg JM, Azzi A. Vitamin E 80th anniversary: A double life, not only fighting radicals. *IUBMB Life.* 52(1–2), 71–76 (2001).

19. Traber MG, Atkinson J. Vitamin E, antioxidant and nothing more. *Free Radic. Biol. Med.* 43(1), 4–15 (2007).
20. Atkinson J, Harroun T, Wassall SR, Stillwell W, Katsaras J. The location and behavior of α-Tocopherol in membranes. *Mol. Nutr. Food Res.* 54(5), 641–651 (2010).
21. Marquardt D, Williams JA, Kuc N, Wassall SR, Katsaras J, Harroun TA. Tocopherol Activity Correlates with Its Location in a Membrane: A New Perspective on the Antioxidant Vitamin E. *J. Am. Chem. Soc.* , 7523–7533 (2013).
22. Mao G, Kraus GA, Kim I, Spurlock ME, Bailey TB, Beitz DC. Effect of a mitochondria-targeted vitamin e derivative on mitochondrial alteration and systemic oxidative stress in mice. *Br. J. Nutr.* 106(1), 87–95 (2011).
23. Burton GW, Joyce A, Ingold KU. Is vitamin E the only lipid-soluble, chain-breaking antioxidant in human blood plasma and erythrocyte membranes? *Arch. Biochem. Biophys.* 221(1), 281–290 (1983).
24. Buttriss JL, Diplock AT. The relationship between α-tocopherol and phospholipid fatty acids in rat liver subcellular membrane fractions. *Biochim. Biophys. Acta (BBA)/Lipids Lipid Metab.* 962(1), 81–90 (1988).
25. Massey JB, She HS, Pownall HJ. Interaction of vitamin E with saturated phospholipid bilayers. *Biochem. Biophys. Res. Commun.* 106(3), 842–847 (1982).
26. Vieira J, Messing J. The pUC plasmids, an M13mp7-derived system for insertion mutagenesis and sequencing with synthetic universal primers. 19, 259–268 (1982).
27. KAGAN VE. Tocopherol Stabilizes Membrane against Phospholipase A, Free Fatty Acids, and Lysophospholipids. *Ann. N. Y. Acad. Sci.* 570(1), 121–135 (1989).
28. Massey JB. Interfacial properties of phosphatidylcholine bilayers containing vitamin E derivatives. *Chem. Phys. Lipids*. 109(2), 157–174 (2001).
29. Chakraborty S, Doktorova M, Molugu TR, *et al.* How cholesterol stiffens unsaturated lipid membranes. *Proc. Natl. Acad. Sci. U. S. A.* 117(36), 21896–21905 (2020).
30. Chen Z, Rand RP. The influence of cholesterol on phospholipid membrane curvature and bending elasticity. *Biophys. J.* 73(1), 267–276 (1997).
31. Bradford A, Atkinson J, Fuller N, Rand RP. The effect of vitamin E on the structure of membrane lipid assemblies. *J. Lipid Res.* [Internet]. 44(10), 1940–1945 (2003). Available from: http://dx.doi.org/10.1194/jlr.M300146-JLR200.
32. Cornell RB. Regulation of CTP : Phosphocholine Cytidylyltransferase by Lipids . 2 . Surface Curvature, Acyl Chain Length, and lipid-Phase Dependence for Activation. *Biochemistry*. 30, 5881–5888 (1991).
33. Senisterra G, Epand RM. Role of Membrane Defects in the Regulation of the Activity of Protein Kinase C. *Arch. Biochem. Biophys.* 30, 378–383 (1993).
34. Keller SL, Bezrukov SM, Gruner SM, Tate MW, Vodyanoy I, Parsegian VA. Probability of alamethicin conductance states varies with nonlamellar tendency of bilayer phospholipids. *Biophys. J.* 65(1), 23–27 (1993).
35. Cheng KH, Lepock JR, Hui SW, Yeagle PL. The role of cholesterol in the activity of reconstituted Ca-ATPase vesicles containing unsaturated phosphatidylethanolamine. *J. Biol. Chem.* 261(11), 5081–5087 (1986).
36. Koya D, Lee IK, Ishii H, Kanoh H, King GL. Prevention of Glomerular Dysfunction in Diabetic Rats by Treatment with d-α-Tocopherol. *J. Am. Soc. Nephrol.* 8(3), 426–435 (1997).
37. Tran K, Proulx PR, Chan AC. Vitamin E suppresses diacylglycerol (DAG) level in

thrombin-stimulated endothelial cells through an increase of DAG kinase activity. *Biochim. Biophys. Acta (BBA)/Lipids Lipid Metab.* 1212(2), 193–202 (1994).
38. Tran K, D'Angelo AF, Choy PC, Chan AC. Vitamin E enhances the acylation of 1-O-alkyl-sn-glycero-3-phosphocholine in human endothelial cells. *Biochem. J.* 298(1), 115–119 (1994).
39. Yamamoto I, Konto A, Handa T, Miyajima K. Regulation of phospholipase K activity by neutral lipids in egg-yolk phosphatidylcholine small unilamellar vesicles and by calcium ion in aqueous medium. *Biochim. Biophys. Acta (BBA)/Lipids Lipid Metab.* 1233, 21–26 (1995).
40. Pepper JK, Lee YO, Watson KA, Kim AE, Nonnemaker JM, Farrelly MC. Risk Factors for Youth E-Cigarette "Vape Trick" Behavior. *J. Adolesc. Heal.* [Internet]. 61(5), 599–605 (2017). Available from: https://doi.org/10.1016/j.jadohealth.2017.05.010.
41. Hajek P, Etter JF, Benowitz N, Eissenberg T, McRobbie H. Electronic cigarettes: Review of use, content, safety, effects on smokers, and ptential for harm and benefit. *Physiol. Behav.* 176(5), 139–148 (2018).
42. Boudi FB, Patel S, Boudi A, Chan C. Vitamin E Acetate as a Plausible Cause of Acute Vaping-related Illness. *Cureus*. 11(12), 10–14 (2019).
43. Blount BC, Karwowski MP, Shields PG, *et al.* Vitamin E Acetate in Bronchoalveolar-Lavage Fluid Associated with EVALI. *N. Engl. J. Med.* 382(8), 697–705 (2020).
44. Blanco O, Pérez-Gil J. Biochemical and pharmacological differences between preparations of exogenous natural surfactant used to treat Respiratory Distress Syndrome: Role of the different components in an efficient pulmonary surfactant. *Eur. J. Pharmacol.* 568(1–3), 1–15 (2007).
45. Bastacky J, Lee CYC, Goerke J, *et al.* Alveolar lining layer is thin and continuous: Low-temperature scanning electron microscopy of rat lung. *J. Appl. Physiol.* 79(5), 1615–1628 (1995).
46. Goerke J. Pulmonary surfactant: Functions and molecular composition. *Biochim. Biophys. Acta - Mol. Basis Dis.* 1408(2–3), 79–89 (1998).
47. Honda Y, Tsunematsu K, Suzuki A, Akino T. Changes in phospholipids in bronchoalveolar lavage fluid of patients with interstitial lung diseases. *Lung*. 166(1), 293–301 (1988).
48. Creuwels LAJM, Van Golde LMG, Haagsman HP. The pulmonary surfactant system: Biochemical and clinical aspects. *Lung*. 175(1), 1–39 (1997).
49. Postle AD, Heeley EL, Wilton DC. A comparison of the molecular species compositions of mammalian lung surfactant phospholipids. *Comp. Biochem. Physiol. - A Mol. Integr. Physiol.* 129(1), 65–73 (2001).
50. Fleming BD, Keough KMW. Surface respreading after collapse of monolayers containing major lipids of pulmonary surfactant. 49, 81–86 (1988).
51. Hallman M, Feldman BH, Kirkpatrick E, Gluck L. Absence of Phosphatidylglycerol (PG) in Respiratory Distress Syndrome in the Newborn. Pediatr. Res.11(6), 714–720 (1977).
52. Pérez-Gil J. Structure of pulmonary surfactant membranes and films: The role of proteins and lipid-protein interactions. *Biochim. Biophys. Acta - Biomembr.* 1778(7–8), 1676–1695 (2008).
53. Trapnell BC, Whitsett JA. GM-CSF regulates pulmonary surfactant homeostasis and alveolar macrophage-mediated innate host defense. *Annu. Rev. Physiol.* 64, 775–802 (2002).

54. Lung Injuries Associated with Use of Vaping Products | FDA. .
55. Daear W, Lai P, Anikovskiy M, Prenner EJ. Differential Interactions of Gelatin Nanoparticles with the Major Lipids of Model Lung Surfactant: Changes in the Lateral Membrane Organization. *J. Phys. Chem. B.* , 5356–5366.
56. Johansson J. Structure and properties of surfactant protein C. *Biochim. Biophys. Acta - Mol. Basis Dis.* 1408(2–3), 161–172 (1998).
57. Lopez-Rodriguez E, Pérez-Gil J. Structure-function relationships in pulmonary surfactant membranes: From biophysics to therapy. *Biochim. Biophys. Acta - Biomembr.* [Internet]. 1838(6), 1568–1585 (2014). Available from: http://dx.doi.org/10.1016/j.bbamem.2014.01.028.
58. Knebel D, Sieber M, Reichert R, Galla HJ, Amrein M. Fluorescence light microscopy of pulmonary surfactant at the air-water interface of an air bubble of adjustable size. *Biophys. J.* [Internet]. 83(1), 547–555 (2002). Available from: http://dx.doi.org/10.1016/S0006-3495(02)75190-4.
59. Baoukina S, Monticelli L, Risselada HJ, Marrink SJ, Tieleman DP. The molecular mechanism of lipid monolayer collapse. *PNAS*. 105(31), 10803–10808 (2008).
60. Sherley J, Amrein M, Leonenko Z. Pulmonary surfactant self-assembles into a functional film of defined molecular architecture irrespective of concentration and solvent of the spreading solution: A fluorescence and atomic force microscopy study. *J. Biomed. Nanotechnol.* 4(2), 210–216 (2008).
61. Cañadas O, Olmeda B, Alonso A, Pérez-Gil J. Lipid–protein and protein–protein interactions in the pulmonary surfactant system and their role in lung homeostasis. *Int. J. Mol. Sci.* 21(10) (2020).
62. Olmeda B, García-Álvarez B, Gómez MJ, Martínez-Calle M, Cruz A, Pérez-Gil J. A model for the structure and mechanism of action of pulmonary surfactant protein B. *FASEB J.* 29(10), 4236–4247 (2015).
63. Yan W, Hall SB. Rapid compressions in a captive bubble apparatus are isothermal. *J. Appl. Physiol.* 95(5), 1896–1900 (2003).
64. H Z, Wang YE, Fan Q, Zuo YY. On the Low Surface Tension of Lung Surfactant. *Langmuir* [Internet]. 21(13), 8351–8358 (2011). Available from: file:///C:/Users/Carla Carolina/Desktop/Artigos para acrescentar na qualificação/The impact of birth weight on cardiovascular disease risk in the.pdf.
65. Pusterla JM, Malfatti-Gasperini AA, Puentes-Martinez XE, Cavalcanti LP, Oliveira RG. Refractive index and thickness determination in Langmuir monolayers of myelin lipids. *Biochim. Biophys. Acta - Biomembr.* [Internet]. 1859(5), 924–930 (2017). Available from: http://dx.doi.org/10.1016/j.bbamem.2017.02.005.
66. Winsel K, Hönig D, Lunkenheimer K, Geggel K, Witt C. Quantitative Brewster angle microscopy of the surface film of human broncho-alveolar lavage fluid. *Eur. Biophys. J.* 32(6), 544–552 (2003).
67. Srivastava S, Phadke RS, Govil G, Rao CNR. Fluidity, permeability and antioxidant behaviour of model membranes incorporated with α-tocopherol and vitamin E acetate. *BBA - Biomembr.* 734(2), 353–362 (1983).
68. Hitchcock PB, Mason R, Thomas KM, Shipley GG. Structural chemistry of 1,2 dilauroyl DL phosphatidylethanolamine: molecular conformation and intermolecular packing of phospholipids. *Proc. Natl. Acad. Sci. U. S. A.* 71(8), 3036–3040 (1974).
69. Levine Y., Birdsall NJ., Lee AG, Metcalfe JC. 13C Nuclear Magnetic Resonance

Relaxation Measurements of Synthetic Lecithins and the Effect of Spin-Labeled Lipids. *Biochemistry*. 11(8), 1416 (1972).
70. Palmieri B, Yamamoto T, Brewster RC, Safran SA. Line active molecules promote inhomogeneous structures in membranes: Theory, simulations and experiments. *Adv. Colloid Interface Sci.* [Internet]. 208, 58–65 (2014). Available from: http://dx.doi.org/10.1016/j.cis.2014.02.007.
71. Muddana HS, Chiang HH, Butler PJ. Tuning membrane phase separation using nonlipid amphiphiles. *Biophys. J.* [Internet]. 102(3), 489–497 (2012). Available from: http://dx.doi.org/10.1016/j.bpj.2011.12.033.
72. DiPasquale M, Nguyen MHL, Rickeard BW, *et al.* The antioxidant vitamin E as a membrane raft modulator: Tocopherols do not abolish lipid domains. *Biochim. Biophys. Acta - Biomembr.* (2020).
73. García-Sáez AJ, Chiantia S, Schwille P. Effect of line tension on the lateral organization of lipid membranes. *J. Biol. Chem.* 282(46), 33537–33544 (2007).
74. Lee H. Vitamin E acetate as linactant in the pathophysiology of EVALI. *Med. Hypothesis*. 144 (2020).
75. Wongwailikhit K, Jiratchaya J. Comparison of the Two Common Solvents for THC and CBD Extractions. *Proc. 7th World Congr. Mech. Chem. Mater. Eng.* , 1–7 (2021).
76. Hillard CJ, Harris RA, Bloom AS. Effects of the cannabinoids on physical properties of brain membranes and phospholipid vesicles: Fluorescence studies. *J. Pharmacol. Exp. Ther.* 232(3), 579–588 (1985).
77. Mavromoustakos T, Daliani I. Effects of cannabinoids in membrane bilayers containing cholesterol. *Biochim. Biophys. Acta - Biomembr.* 1420(1–2), 252–265 (1999).
78. Mavromoustakos T, Theodoropoulou E, Papahatjis D. Studies on the thermotropic effects of cannabinoids on phosphatidylcholine bilayers using differential scanning calorimetry and small angle X-ray diffraction. *Biochim. Biophys. Acta (BBA)/Lipids Lipid Metab.* 1281, 235–244 (1996).
79. Lanzarotta A, Falconer TM, Flurer R, Wilson RA. Hydrogen Bonding between Tetrahydrocannabinol and Vitamin E Acetate in Unvaped, Aerosolized, and Condensed Aerosol e-Liquids. *Anal. Chem.* 92(3), 2374–2378 (2020).
80. Bernhard W. Lung surfactant: Function and composition in the context of development and respiratory physiology. *Ann. Anat.* [Internet]. 208, 146–150 (2016). Available from: http://dx.doi.org/10.1016/j.aanat.2016.08.003.
81. Bernhard W, Haagsman HP, Tschernig T, *et al.* Conductive Airway Surfactant: Surface-tension Function, Biochemical Composition, and Possible Alveolar Origin. *Am. J. Respir. Cell Mol. Biol.* 17(1=), 41–50 (1997).
82. Roa WH, Azarmi S, Al-Hallak MHDK, Finlay WH, Magliocco AM, Löbenberg R. Inhalable nanoparticles, a non-invasive approach to treat lung cancer in a mouse model. *J. Control. Release* [Internet]. 150(1), 49–55 (2011). Available from: http://dx.doi.org/10.1016/j.jconrel.2010.10.035.
83. Lee J, Yang S, Kiessling V, Tamm LK. The Role of Cholesterol in Viral Spike Glycoprotein-Mediated Membrane Fusion. *Biophys. J.* 112(3), 9a (2017).
84. Zhang X, Barraza KM, Beauchamp JL. Cholesterol provides nonsacrificial protection of membrane lipids from chemical damage at air–water interface. *Proc. Natl. Acad. Sci. U. S. A.* 115(13), 3255–3260 (2018).
85. Bangham AD, Morley CJ, Phillips MC. The physical properties of an effective lung

surfactant. *Biochim. Biophys. Acta (BBA)/Lipids Lipid Metab.* 573, 552–556 (1979).
86. Watkins JC. The surface properties of pure phospholipids in relation to those of lung extracts. *Biochim. Biophys. Acta (BBA)/Lipids Lipid Metab.* 152(2), 293–306 (1968).
87. Schürch S, Green FHY, Bachofen H. Formation and structure of surface films: Captive bubble surfactometry. *Biochim. Biophys. Acta - Mol. Basis Dis.* 1408(2–3), 180–202 (1998).
88. Keating E, Rahman L, Francis J, *et al.* Effect of Cholesterol on the Biophysical and Physiological Properties of a Clinical Pulmonary Surfactant. 93(August), 1391–1401 (2007).
89. Yu SH, Possmayer F. Adsorption, compression and stability of surface films from natural, lipid extract and reconstituted pulmonary surfactants. *Biochim. Biophys. Acta (BBA)/Lipids Lipid Metab.* 1167(3), 264–271 (1993).
90. Keating E, Rahman L, Francis J, *et al.* Effect of cholesterol on the biophysical and physiological properties of a clinical pulmonary surfactant. *Biophys. J.* [Internet]. 93(4), 1391–1401 (2007). Available from: http://dx.doi.org/10.1529/biophysj.106.099762.
91. Leonenko Z, Finot E, Vassiliev V, Amrein M. Effect of cholesterol on the physical properties of pulmonary surfactant films: Atomic force measurements study. *Ultramicroscopy*. 106(8–9), 687–694 (2006).
92. Slotte JP. Enzyme-Catalyzed Oxidation of Cholesterol in Mixed Phospholipid Monolayers Reveals the Stoichiometry at Which Free Cholesterol Clusters Disappear. *Biochemistry*. 31(24), 5472–5477 (1992).
93. Gunasekara L, Schürch S, Schoel WM, *et al.* Pulmonary surfactant function is abolished by an elevated proportion of cholesterol. *Biochim. Biophys. Acta - Mol. Cell Biol. Lipids*. 1737(1), 27–35 (2005).
94. Panda AK, Nag K, Harbottle RR, *et al.* Effect of acute lung injury on structure and function of pulmonary surfactant films. *Am. J. Respir. Cell Mol. Biol.* 30(5), 641–650 (2004).
95. Bhat TA, Kalathil SG, Bogner PN, Blount BC, Goniewicz ML, Thanavala YM. An Animal Model of Inhaled Vitamin E Acetate and EVALI-like Lung Injury. *N. Engl. J. Med.* 382(12), 1175–1177 (2020).
96. McConlogue CW, Vanderlick TK. A close look at domain formation in DPPC monolayers. *Langmuir*. 13(26), 7158–7164 (1997).
97. Notter RH, Tabak SA, Mavis RD. Surface properties of binary mixtures of some pulmonary surfactant components. *J. Lipid Res.* [Internet]. 21(1), 10–22 (1980). Available from: http://dx.doi.org/10.1016/S0022-2275(20)39835-7.
98. Trabelsi S, Zhang S, Lee TR, Schwartz DK. Linactants: Surfactant analogues in two dimensions. *Phys. Rev. Lett.* 100(3), 2–5 (2008).
99. Macooie AA, Fakour Z, Roanaghi P. Comparative evaluation of the effects of BLES and Survanta on treatment of respiratory distress syndrome in newborns. *J. Fam. Med. Prim. Care* [Internet]. 7(5), 1063–1067 (2018). Available from: http://www.jfmpc.com/article.asp?issn=2249-4863;year=2017;volume=6;issue=1;spage=169;epage=170;aulast=Faizi.
100. BLES Biochemicals Inc.About Us - BLES Biochemicals Inc. [Internet]. . Available from: https://blesbiochem.com/about-us/.
101. Piknova B, Schram V, Hall SB. Pulmonary surfactant: Phase behavior and function. *Curr. Opin. Struct. Biol.* 12(4), 487–494 (2002).

102. Christiani DC. Vaping-Induced Acute Lung Injury. *N. Engl. J. Med.* 382(10), 960–962 (2020).
103. Dziura M, Mansour B, Dipasquale M, Chandrasekera PC, Gauld JW, Marquardt D. Simulated breathing: Application of molecular dynamics simulations to pulmonary lung surfactant. *Symmetry (Basel).* 13(7), 1–19 (2021).
104. Rugonyi S, Biswas SC, Hall SB. The Biophysical Function of Pulmonary Surfactant. *Respir. Physiol. Neurobiol.* [Internet]. 163(1–3), 244–255 (2008). Available from: https://www.ncbi.nlm.nih.gov/pmc/articles/PMC3624763/pdf/nihms412728.pdf.
105. Sachan AK, Galla HJ. Bidirectional surface analysis of monomolecular membrane harboring nanoscale reversible collapse structures. *Nano Lett.* 13(3), 961–966 (2013).
106. Knebel D, Sieber M, Reichelt R, Galla HJ, Amrein M. Scanning force microscopy at the air-water interface of an air bubble coated with pulmonary surfactant. *Biophys. J.* [Internet]. 82(1), 474–480 (2002). Available from: http://dx.doi.org/10.1016/S0006-3495(02)75412-X.
107. Amrein M, Von Nahmen A, Sieber M. A scanning force- and fluorescence light microscopy study of the structure and function of a model pulmonary surfactant. *Eur. Biophys. J.* 26(5), 349–357 (1997).
108. Sun Z, Zheng D, Baldelli S. Distortion Correction for a Brewster Angle Microscope Using an Optical Grating. *Anal. Chem.* 89(4), 2186–2190 (2017).
109. LeBouf RF, Ranpara A, Ham J, *et al.* Chemical Emissions From Heated Vitamin E Acetate—Insights to Respiratory Risks From Electronic Cigarette Liquid Oil Diluents Used in the Aerosolization of Δ9-THC-Containing Products. *Front. Public Heal.* 9(January), 1–12 (2022).

Appendix

Copyright form:

Chapter 5: Vaping additives negatively impact the stability and lateral film organization of lung surfactant model systems